CHARACTERIZATION OF DESIGN PARAMETERS FOR A FREE FOIL ROTOR IN A PRESSURE SCREEN

By

Jaime Arturo Gonzalez

B.Sc. (Mechanical Engineering and Management), Instituto Tecnológico y de Estudios Superiores de Monterrey, 1997

A thesis submitted in partial fulfillment of
the requirements for the degree of
Master of Applied Science

in

The Faculty of Graduate Studies
Department of
Mechanical Engineering

We accept this thesis as conforming
to the required standard

THE UNIVERSITY OF BRITISH COLUMBIA

December 2002

In presenting this thesis in partial fulfilment of the requirements for an advanced degree at the University of British Columbia, I agree that the Library shall make it freely available for reference and study. I further agree that permission for extensive copying of this thesis for scholarly purposes may be granted by the head of my department or by his or her representatives. It is understood that copying or publication of this thesis for financial gain shall not be allowed without my written permission.

Department of Mechanical Engineering

The University of British Columbia
Vancouver, Canada

Date December 20, 2002

In presenting this thesis in partial fulfillment of the requirements for an advanced degree at the University of British Columbia, I agree that the Library shall make it freely available for reference and study. I further agree that permission for extensive copying of this thesis for scholarly purposes may be granted by the head of my department or by his or her representatives. It is understood that copying or publication of this thesis for financial gain shall not be allowed without my written permission.

Jaime Arturo Gonzalez
Mechanical Engineering
The University of British Columbia
2324 Main Mall
Vancouver, BC, Canada
V6T 1Z4

December 2002

ABSTRACT

This thesis experimentally examined the pressure pulses produced by a NACA foil rotor. For this purpose, an experimental apparatus representing a cross section of a small industrial pulp pressure screen was used. The Cross Sectional Screen (CSS) was fitted with high frequency pressure sensors and an optical position encoder to record the pressure pulses created by the rotor on the inside of the screen basket and the effect of foil operation and design on the pulse shape and magnitude was determined. From this study, it was shown that: (1) the magnitude of pressure increases with the square of rotor tip speed, i.e., the dimensionless pressure coefficient was independent of rotor tip speed. (2) The magnitude of the pressure pulse increased exponentially as the clearance of the foil and the screen plate decreased. (3) The magnitude of the pressure pulse decreased with increasing pulp consistency. (4) The magnitude of the positive pressure peak increases with foil thickness; this is particularly important for thicknesses greater than 12%. The magnitude of the negative pressure peak and the shape of the pulse in general do not change significantly due to foil thickness. (5) For the foils tested (0%, 4% and 8% camber) the magnitude of the suction peak increased with increasing camber at zero angle of attack. (6) Angle of attack significantly changed the shape and magnitude of the pressure peak. In particular, it was noted that the maximum negative peak occurs at angles of attack between 5^{o} and 15^{o}, depending on the type of foil and experimental conditions. For positive angles of attack, the positive pressure peak seemed to be negligible. This suggests the optimal angle of attack for a NACA0012 foil is in the vicinity of 10^{o}.

In general, it was established that the Cross Sectional Screen modified to measure pressure pulses together with CNC machining of rotor foils provide a powerful tool for designing improved foils and assessing the resulting pressure pulses.

TABLE OF CONTENTS

LIST OF FIGURES

LIST OF TABLES

ACKNOWLEDGEMENTS

To Lucy,

For her unconditional love and support.

And

To my parents and family, for their encouragement and love.

I would also like to thank, James Olson for his guidance and support through this project. There are many other people who deserve acknowledgement: Robert Gooding, Monica Feng, Petri Tuomela, Daniel Ouellet and Bruce Allison for their valuable input and discussions, Glen Jolly, Dave Pouw, Doug Yuen, Tim Paterson, Ken Wong and all the support staff at the Mechanical Engineering Department and the Pulp and Paper Centre. The students involved in the API, especially those directly involved in this project, Jordan Ko, Cam Pflueger, and Veronique Pinon, for their support and collaboration in this research. Rodolfo and Mary Dominguez, Tze Bun Wong, Roger Codo, Ester Giro, Ursula Mais, Marko and Anne Avikainen, Tim Friesen, and Jens Heymer, are thanked for their friendship through these years. Thank you all!

Chapter 1

INTRODUCTION

1.1 Pressure Screens

Pressure screens are widely used in the pulp and paper industry to improve pulp quality. Their main purpose is to remove contaminants form the pulp stream. The presence of these contaminants affects the quality of the paper being produced by reducing its strength and diminishing its optical properties. This process is essential in the production of virtually all grades of paper.

In recent years, pressure screens are also being used to separate pulp into streams with long and short fibre length distributions. This process, also known as fractionation, helps control the quality of the paper by re-blending the different pulp streams in the right proportion to produce a paper with a desired set of properties, such as strength, brightness, freeness, etc.

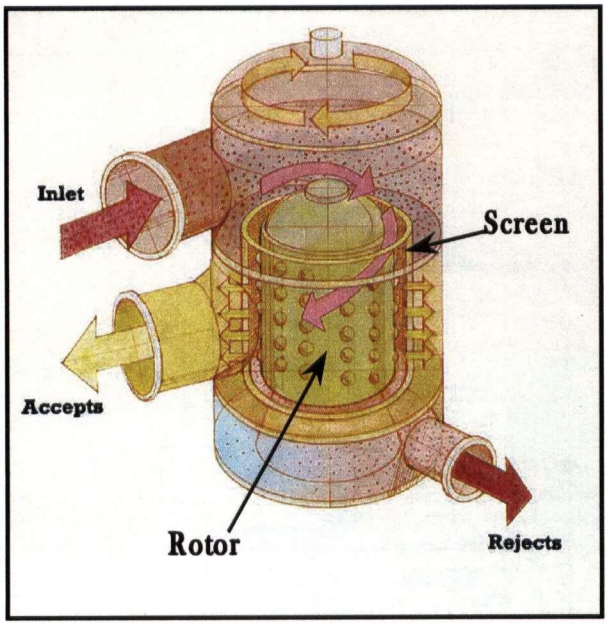

Figure 1.1 - Schematic of a typical pressure screen

The two main components of a typical pressure screen are the screen and the rotor (see Figure 1.1). The pulp suspension is fed through the gap between the rotor and the screen plate. The high velocity, at which the rotor spins, induces a high tangential velocity in the pulp suspension with respect to the screen plate. This increases the pressure inside the screen, similar to a centrifugal pump, pushing the pulp radially through the screen plate. These two effects combined cause the pulp to go through the screen apertures in "exit layers" as defined by Olson [16] (1996).

The pulp that comes into the pressure screen is known as the feed and usually enters at the top of the pressure screen. Since fibres have more difficulty passing through the screen apertures than water, the pulp stream that does not pass through the screen (rejects) has a higher consistency than the feed pulp; this is known as reject thickening. Similarly pulp that goes through the screen, or accepts, has a lower consistency than the feed. This is particularly important because as pulp flows down the pressure screen it becomes thicker and screen failure usually initiates at the bottom of the screen, where the highest consistency is found.

Pulp is usually screened at very low consistencies, generally around 2%, but can go up to approximately 4%. This range of consistencies is considered low in the pulp and paper industry. However, when it comes to screening, pulp consistencies below 2.5% are referred to as low and consistencies above 2.5% are considered high. This classification has been very important in screening as both screen baskets and rotors are generally classified in the same manner, to reflect the consistency they are suited for. This study will focus on low consistency screening; most

findings, however, are expected to be very similar at higher consistencies due to the similarity of physical and hydrodynamic properties of pulp at consistencies up to 4%.

The rotor used for this study is a foil rotor, which allows the pulp suspension to move along both sides of the foil. The solid core rotor, which is the other common rotor type, will not be analyzed in this study. Some examples of solid core rotors include the bump, lobe and S (or eccentric) rotors, all of which have an extensive variety of element shapes attached to them, as sketched in Figure 1.2.

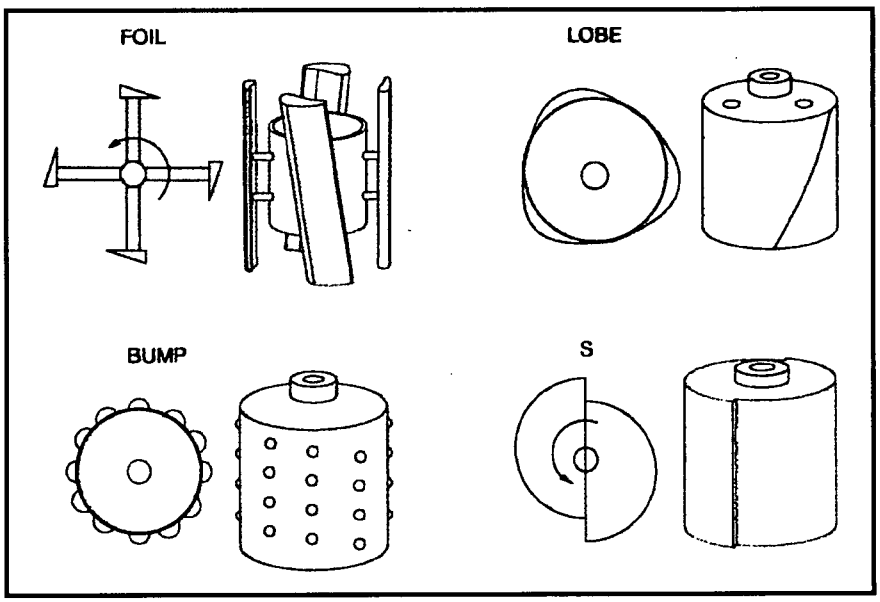

Figure 1.2 - Common types of rotors

The rotor inside the pressure screen has three functions. First, it induces a tangential velocity on the pulp suspension that allows pulp fibres align with the screen basket apertures. Secondly, it increases the pressure inside the screen basket in a way similar to a centrifugal pump due to its high angular velocity. Screen cylinders, however, would plug with fibres almost instantaneously if pulp was continuously passing through them. Therefore, the third and most important function

of the rotor is to clean and unplug the screen apertures. Rotors have hydrofoil elements attached to them, which move at high tangential speeds very near to the screen basket, typically 2-5 mm. This creates a negative pressure (suction) between the foil and the screen in a way similar to the upper surface on an airplane wing. This causes the pulp to back-flush momentarily and pull back any fibre accumulation in the apertures to prevent the screen from plugging.

This process is much more complex than one might initially think. The flow field is composed of a suspension, which is a non-Newtonian fluid whose effective viscosity changes even with rotor speed. Also, the foil travels in the wake of a previous foil at very high speeds, while the screen plate induces very distinct flow patterns due to its contoured shape and open apertures. Therefore, experiments for this research had to be simplified considerably: pressure was measured on a blank section of the wall in the pressure screen to eliminate the effect of the contour and open area. This represents the limiting case of operation where a smooth cylinder is completely plugged by fibres.

1.2 Pressure Pulses and Rotors

As one could expect these pulses (see Figure 1.3) have a direct impact on the performance and efficiency of the screen. While having pulp coming back into the screen basket reduces the amount of pulp that can be cleaned, it also increases the reliability of the screen, by ensuring it is not blocked by fibre plugs. Thus, there is no easy way to describe what a perfect pulse might look like. In fact with all the variants involved in this problem it is likely to be determined by other limitations associated with a particular mill, and its environment or resources available. For example, it is know empirically that to increase the strength of the pulses there are two easy solutions, reducing the clearance (gap) of the rotor or increasing the angle of attack of the foil.

By reducing the gap, the pulse increases dramatically, but given the fact that pulp is a suspension which contains debris, the wear of the screen basket increases in the same proportion if not more. On the other hand, by increasing the angle of attack, the foil is no longer aligned with the flow resulting in additional skin friction drag, which in turn translates to a higher energy consumption required to drive the pressure screen. The question then becomes, which is more feasible, increasing the frequency in which screen baskets must be replaced / refurbished or paying for a higher utility bill from the increased energy consumption?

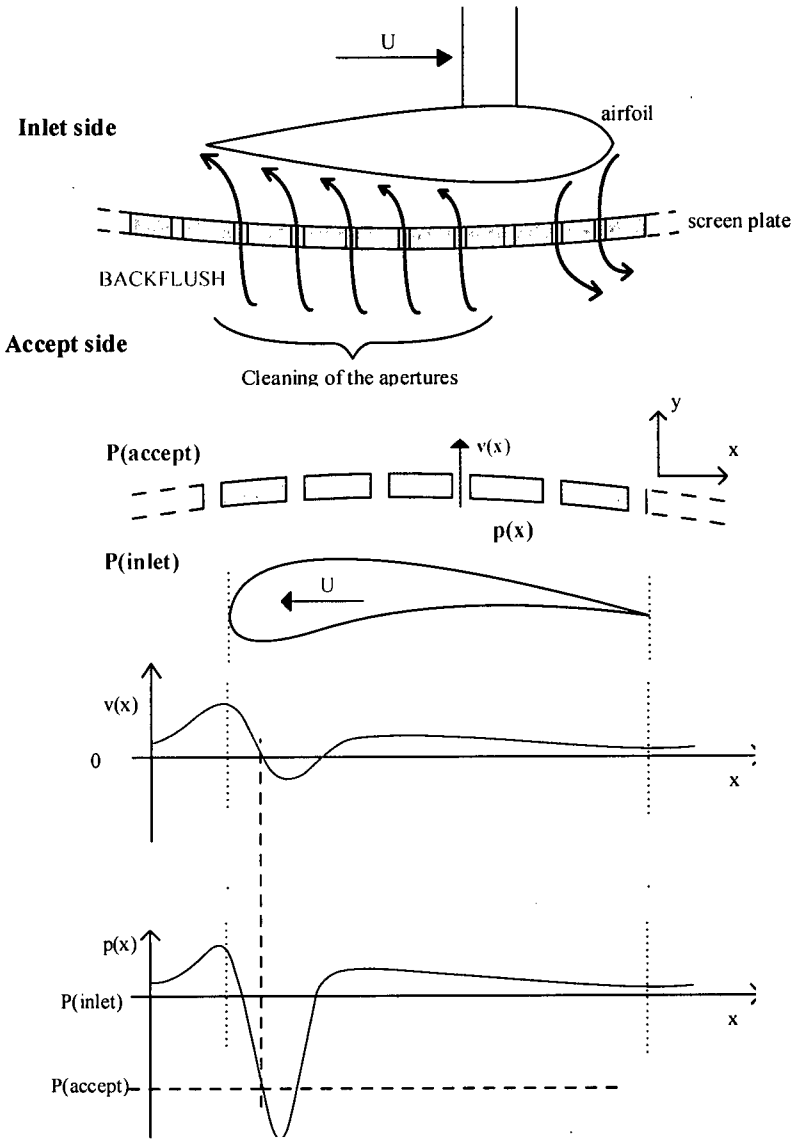

Figure 1.3 - Pressure Pulse Schematic

It is important to note that throughout this thesis, the entire pressure profile can be referred to as suction pulse, pressure pulse or simply as pulse. All three are commonly used in pulp screening, and while suction pulse is the most adequate name, it is also often referred to as pressure pulse since suction is simply another word for negative pressure, but it is most often referred to as pulse for short. When referring only to the maximum or minimum values of the pressure profile, however, they are called pressure peak or suction peak respectively.

1.3 Objectives

As there are many types of pulps and paper grades being produced, the pulse characteristics desired in the pressure screen are very different for each particular case. It is also very important to consider the effect that each parameter variation has on the pulse and how its characteristics could be compromised by performing such changes. For example, having a high turbulence intensity in the screen would help deflocculate the pulp when used upstream of a headbox resulting in a better distribution of fibres in the paper machine. However, this could result in a much higher power consumption, which might make it unfeasible economically.

The most important parameters involved in foil design are: rotor clearance, tip speed (U), and foil shape. The latter, is further divided into more quantitative characteristics, such as: camber (y/c), thickness (t), chord length (c), and angle of attack (α), as shown in Figure 1.4. These parameters were analyzed during this study independently from each other for simplicity. Nonetheless, it is important to mention that strong interactions are expected among them and although a proper analysis of such interdependencies is beyond the scope of this research, some are briefly outlined in this thesis.

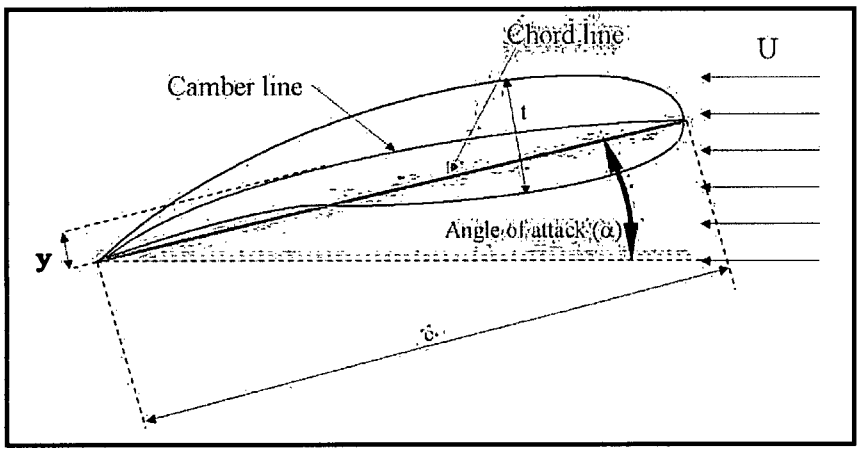

Figure 1.4 - Airfoil nomenclature

Thus the main objective of this research is to determine the effect that the various parameters involved in rotor design have on the suction pulse characteristics in the pressure screen. By better understanding these relationships, screen baskets and rotors can then be used in conjunction under the setup conditions that provide the best cleaning or fractionation performance for a particular application. This information, could then be used to validate Computational Fluid Dynamics (CFD) models or simply as a guide for future rotor designs.

By understanding how pressure pulses behave inside a pressure screen, future rotor designs can be optimized to produce high quality pulp, with the best characteristics required to produce the grade of paper it is intended for. This study is a first attempt at explaining this process in general terms, but due to its complexity much work will still have to be done to fully understand it.

Chapter 2

LITERATURE REVIEW

Previous studies relevant to this research can be grouped into three general categories:

- Screening fundamentals
- Rotor design and pulse measurements
- Airfoils and ground effect theory

2.1 Screening Fundamentals

Pulp screening has been commonly used in the past primarily as a process by which contaminants are removed from a pulp stream. Screening principles have been extensively studied and are described in great detail in a number of sources [2, 4, 6, 15, 16, 17, 21, 22, 23, 24, 25, 26]. However, most previous researchers have focused either on the basic fundamentals that govern the screening process or on the performance of screen plates in very specific applications.

Early studies on the principles of screening were based mostly in statistical and empirical analysis of screening. Tirado [22] related the relative length of a fibre to the screen apertures and the effect it has on the probability of passage through the screen. Estridge [4] analyzed the probability of fibre retention and derived a statistical model, which adequately described the few cases he analyzed experimentally. Riese *et. al.* [18] developed a numerical method to calculate the trajectory and orientation of a fibre as it approached a wire grid to determine its probability of passing through the aperture.

More recent studies have focused on explaining the physical principles governing the screening process. Yu and DeFoe [24, 25, 26] developed a qualitative analysis of the flow pattern created by a contoured screen and explained how fibres are aligned with the flow streamlines in the vicinity of the screen apertures. Olson [16] has studied the motion of fibres in a flow channel and determined that if a particular fibre was located within the "exit layer" of a slot aperture its probability of passing through the slot increased significantly. Gooding [6] focused on analyzing the flow field through screen apertures with different contours using CFD, and related their flow patterns to the orientation of fibres and determined that by modifying these contours screening performance could be improved substantially. Kumar *et. al.* [13] analyzed some common factors that can be controlled or monitored in screening, such as fibre length, stiffness and slot velocity, and explained their relation to the passage ratio for fibres of any given length.

Other important screening studies have looked into more practical applications of screening and ways of optimizing the performance of a pressure screen. Gooding and Kerekes [5] derived two equations to characterize the performance of a pulp screen; these equations relate the efficiency of the screen to reject loss in probability screening. Allison and Olson [1] studied the efficiency of several configurations for screening systems and determined that cascade-feedback systems provide the best fractionation for a wide variety of applications.

2.2 Rotor Design and Pulse Measurement

As noted above, most studies in screening have concentrated on the physics of fibre motion through apertures and screen flow patterns. However, in recent years the rotor has been considered equally important in the screening process and regarded as a major contributor to the

efficiency and performance of a pressure screen. As discussed in the previous chapter, the rotor is responsible for creating suction pulses that maintain the screen apertures unplugged. With this in mind, studies in this area have only been conducted within the last 10 years with a few notable exceptions.

Some of the earlier studies in this area date back only to the mid 1980's, with Karvinen, Halonen and Ljokki [12, 7] among the first ones to explore this field. In their research, they recognized the importance of the rotor design in increasing the performance of the pressure screen and were the first ones to characterize the shape and magnitude of the pressure pulses caused by the foil. Yu [27] later studied the pulse signature created by an S rotor, and identified some of the most important parameters that affect the shape and magnitude of the pulses, such as rotational speed and screen open area. By the end of the 90's, Saint Amand and Perrin [19, 20] measured the pressure pulse of a foil rotor in an industrial screen to analyze the mechanisms of fibre and contaminant passage through the screen apertures. Wikstrom and Fredrikson [23] looked at the turbulent flow patterns in a pressure screen and determined that energy consumption could be reduced and screening efficiency increased by modifying the foil geometry to delay or prevent flow separation.

2.3 Airfoils and Ground Effect

The principle behind the operation of the foil rotor can be better described as a combination of aerofoil theory and ground effect on wings. Even though potential flow is not the best way to describe this flow, as it is highly viscous and somewhat compressible, it is still the easiest way to initially approach this problem. With this in mind, we do not expect to obtain exact solutions to the problem from a potential flow analysis, but rather tendencies on how the pulses are modified

by the different design parameters, which is precisely what the main objective of this research is. It also helps identify the location of the pressure or suction surges with respect to the relative position of the foil, while providing an approximation of the general shape of the pulse. In addition, since the clearance between the rotor foil and the screen basket is an order of magnitude smaller than the chord length of the foil, one would expect to have a ground effect influence on the pressure field around the foil. This topic is extensively covered in a number of Fluid Mechanics and Turbulence books, two of which are by Hinze [8] and Libby [14].

Some related work that provides useful insight into the hydrodynamics of the foil rotor can be obtained from aerodynamic studies of Wings in Ground Effect (WIG). Dragos [3] developed a numerical solution for the flow field of a thin airfoil in Ground Effect. Hsiun and Chen [9, 10] used the k-e model to characterize the flow field of an airfoil in ground effect and improved a procedure to create an inverse design of an airfoil in ground effect based on its pressure distribution along the foil and the distance to the ground plane. Im and Chang [11] developed a mathematical model to solve the unsteady aerodynamics of an airfoil moving past a wavy wall, which can approximate the contour wall of a screen plate with a foil rotor passing by at high speed.

Chapter 3

EXPERIMENTAL MEASUREMENT OF PRESSURE PULSES

3.1 Introduction

Since pressure screen rotor design is a research area has just started to be explored recently, there is limited information in literature related to this study. Most experimental work in rotors so far has been conducted by rotor manufacturers to measure the overall performance and reliability of a given rotor. However, little has been published on the shape and behaviour of the suction pulses themselves. This shortage of data would make it impossible to approach this problem using Computational Fluid Dynamics (CFD) or numerical methods as the data available is not enough to validate these methods. Thus, this research is based on experimental trials, using a model that resembles the cross section of a real pressure screen, which is approximately 30 cm. in diameter. The pressure measurements obtained in this study could then be used as reference in the future to validate CFD codes, which would be a much faster and more economical way of studying the characteristics of suction pulses inside a pressure screen.

This chapter starts with a description of the experimental apparatus and flow loop used to perform the experiments. It then describes the methodology used to analyze the effect of each rotor design parameter and the effect it has on the pulsations inside a pressure screen.

3.2 Experimental Apparatus and Procedure

3.2.1 Cross Sectional Screen (CSS)

As its name suggests, the Cross Sectional Screen (Figure 3.1) is a test model of a 5-cm. span section that simulates the interior of an industrial pressure screen. The diameter of the test section is just under 30 cm. (29.2 cm.) and there is a small screen installed in the lowest part of the test section. The pulp fed into the screen comes in through 2.5-cm. PVC pipe located in the upper left quadrant of the test section; while the rejects exit the CSS through a similar pipe found in the lower right quadrant. The accepted pulp in this case passes through a small screen coupon approximately 6-cm. in length and is collected at the bottom of the CSS.

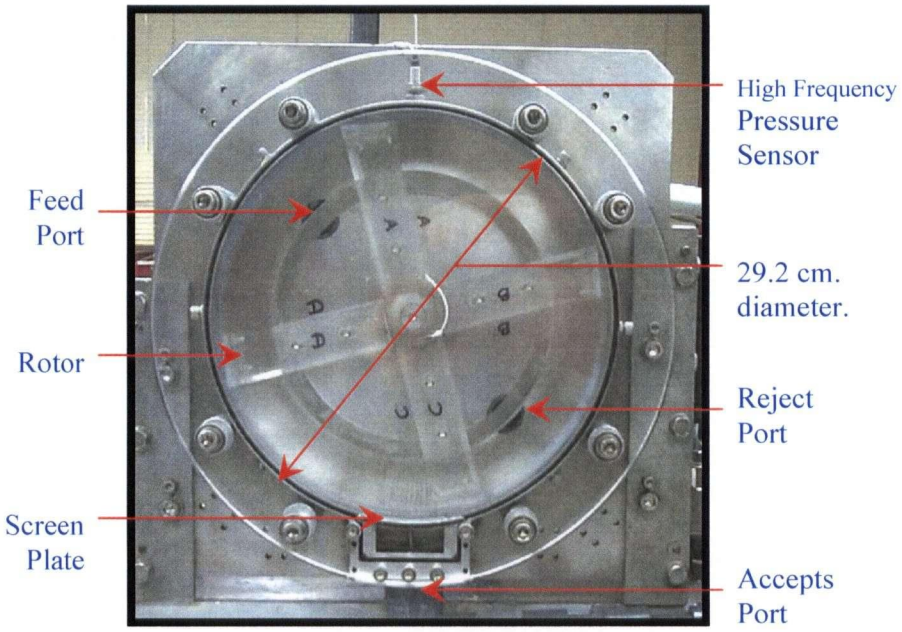

Figure 3.1 - Test Section of the Cross Sectional Screen (CSS)

The rotor of the CSS was originally made of acrylic, but due to the uncertainty on how strong the forces on the rotor arms would be, it was decided to use a new aluminium and stainless steel rotor. Since industrial rotors are also made of stainless steel, this will help ensure that any unforeseen effect the rotor material could have on the pressure pulses is eliminated. Also, since

the space between the foil and the walls of the CSS is under a millimetre, the potential effect of wing tip vortices on our measurements is assumed to be negligible.

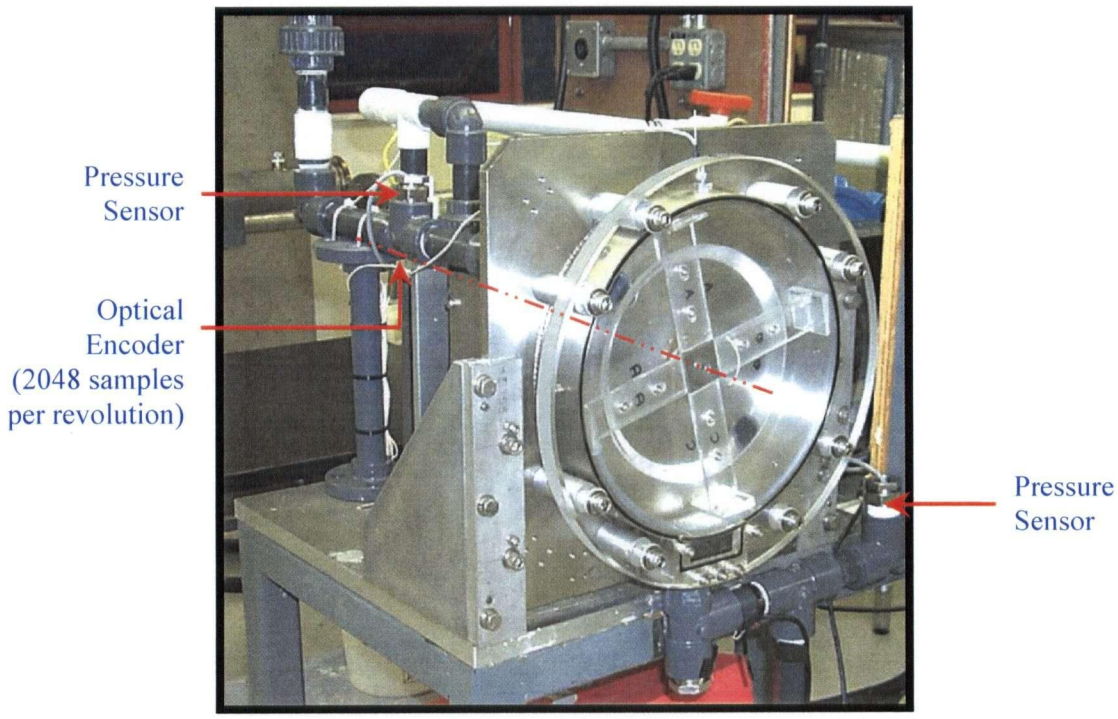

Figure 3.2 - Test Section View

For this study a high frequency pressure sensor (EPX-V01-250P by Entran Devices Inc.) was used to record the pressure at the solid wall of the test section. (Figure 3.1) The sensing diaphragm on this sensor is 3.81-mm. in diameter and was placed flush through the wall of the CSS. It is capable of sampling at a rate of up to 120-KHz, or every 8.3μs, while being subjected to a pressure of up to 250-psi. It is important to note that the sensor reads the average pressure applied in its surface, this means it is relatively more accurate for foils with larger chord lengths as its relative size is smaller. Therefore, if point measurements were taken, it would be expected that the pulse would be slightly sharper and thinner. These small inaccuracies, however, are not important in this study, as the main focus is to identify trends on how pulses are modified and after non-dimensionalizing parameters; these trends still follow the same patterns.

To synchronize the position of the rotor in the test section with the pressure measurements being recorded, it was necessary to install an optical encoder on the opposite side of the shaft to trigger the sampling process by the data acquisition system. The optical encoder used for these experiments is an HD25 by US Digital Corp., which is capable of sending two different counter signals simultaneously (see Figure 3.2). The first channel, also known as the index mark, sends a signal every revolution and can be used both to count the number of revolutions or cycles and to identify the starting point of the sampling cycle to record the pulses. The second signal is sent at equal degree increments, the model used for this research HD25-2048-O-LV-AB-I-CA7, is capable of sending 2048 signals every revolution. This means the pressure sensor would take a pressure reading every 0.1758 degrees approximately.

Thus the pressure pulses were always recorded when the rotor was at a set location and not at fixed time intervals. Therefore, pressure pulses will be plotted against non-dimensional chord length (x/c), as is often done in aerodynamics, and not against time as in most of the previous work in this field.

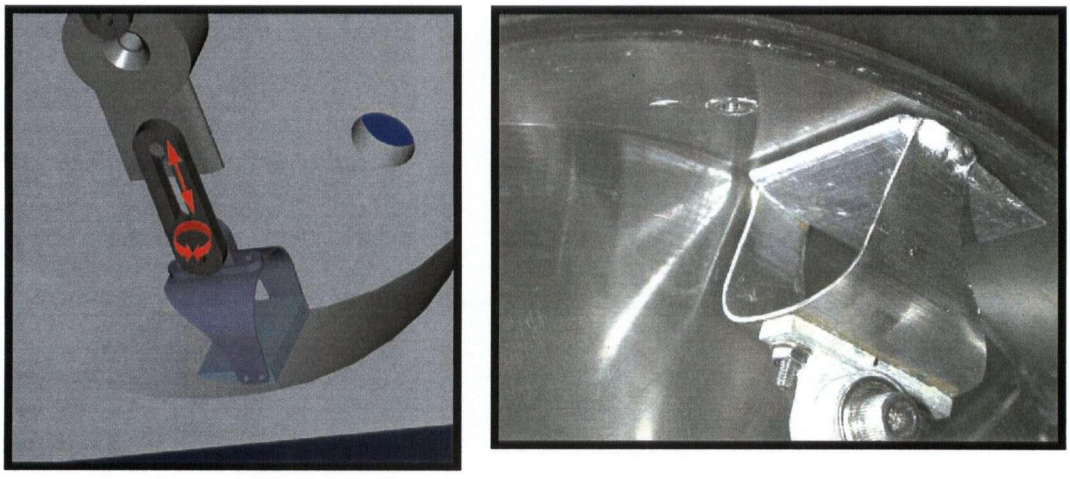

Figure 3.3 – New foil rotor design

Some changes were needed for the rotor assembly as well. (Figure 3.3) First, since the pressure sensor was mounted exactly half-way through the cress section of the CSS, it was important to reduce the turbulence created by the arm of the old rotor (shown in figures 3.1 and 3.2). This resulted in creating a new bracket to hold the foil by its sides and not from the top as before. Also, the bracket was designed to pivot so angles of attack of the foil could be modified and can be set to angles as large as +/- 85°, if necessary depending on the type, length and thickness of the foil being tested. Finally, the adjustment for the foil clearance to the wall was increased and can now be tested for gaps ranging from 1 to close to 15-mm.

While conducting the experiments, the angle of attack was adjusted by manually measuring the distance from the leading edge to the wall of the test section, and comparing it to the distance of the trailing edge to the wall. Therefore, it is expected that an error of +/- 1 degree can be present in this adjustment. Also, the gap between the foil and the CSS wall was adjusted by using a filler gauge at the closest point between the foil and the screen wall with a thickness equal to the desired clearance and tightened in place. The error present in this adjustment is approximately +/- 0.05mm, mostly due to the curvature of the wall.

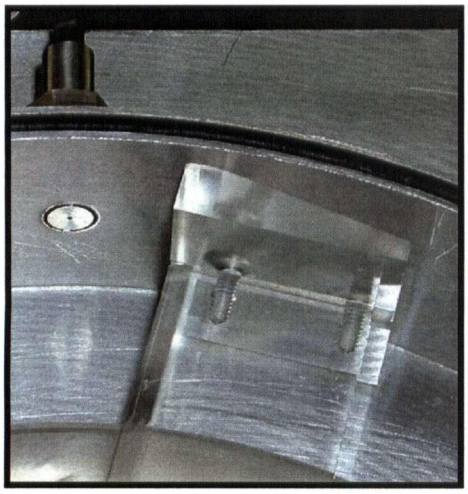

Figure 3.4 – Hooper Foil

Even though most industrial foils are not streamlined, such as the Hooper foil in figure 3.4, a NACA series foil was used to conduct this research. This was necessary to easily modify design parameters such as thickness and camber, while being able to compare the results with

those of previous studies in aerodynamics. The foils were designed using Pro/Engineer software and produced with a CNC machine in order to achieve the desired shapes.

3.2.2 Flow Loop Components and Specifications

The complete flow loop for the CSS (Figure 3.5) has been used in the past for screening studies, mostly looking at capacity issues and flow patterns through the slotted contours. Therefore, some of the equipment installed was not used in this study to record any data, but only to ensure that the experimental conditions were the same throughout the study.

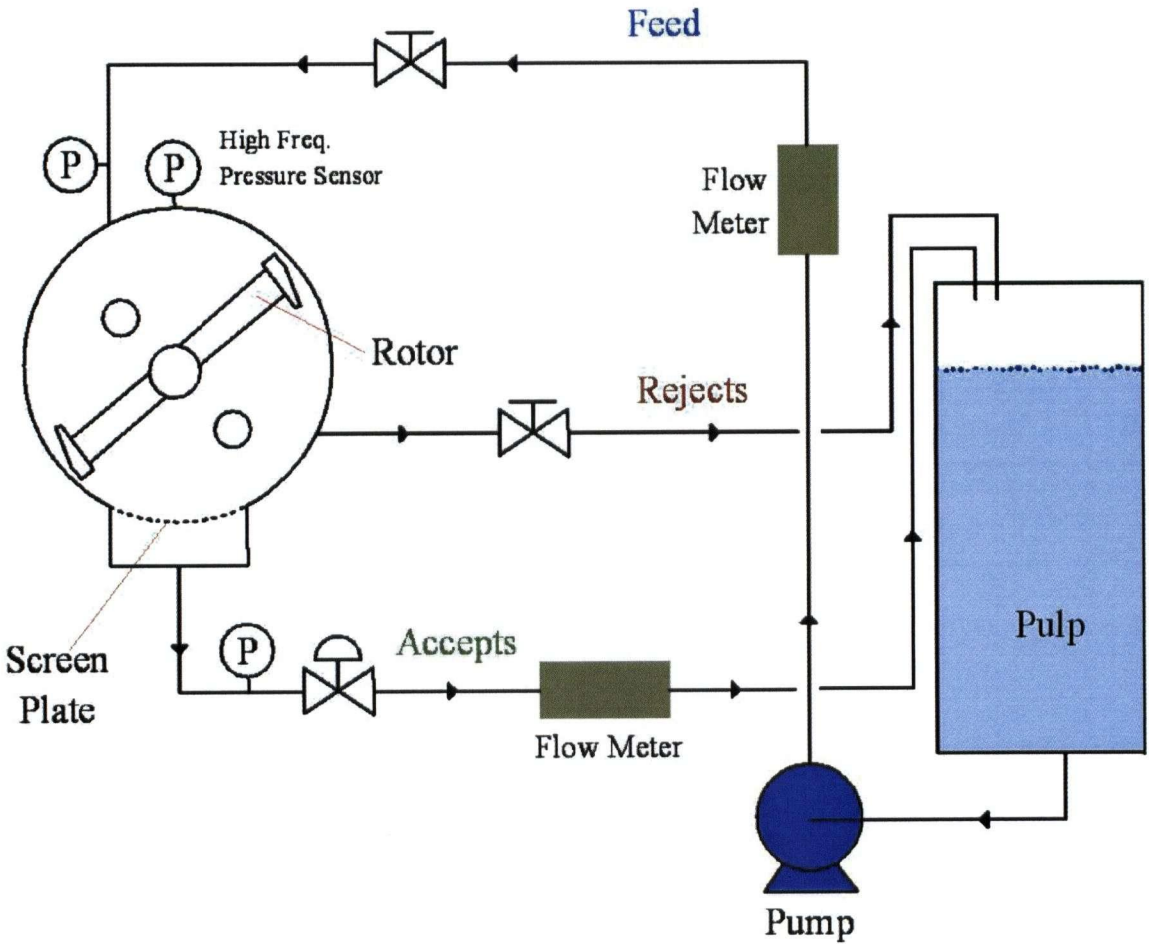

Figure 3.5 – Flow Loop Diagram

The flow loop consists of a 150 L tank, a mixer, a pump, two flow meters, two pressure transducers and PVC piping. The loop starts with the tank, which holds the pulp suspension while being agitated by the variable speed mixer. The pump then takes pulp from the bottom of the tank and pressurizes the entire loop. The pulp then enters the test section through the feed line, which has a flow meter and pressure sensor, to monitor the average flow rate and pressure respectively. The rotor in the test section is driven by a 10-hp. electric motor, which is controlled by a frequency inverter driver to ensure that speed is constant at all times. Pulp that passes through the screen plate exits the test section through the accepts line, which also has a flow meter and pressure transducer to record the conditions on this line. Finally, the remainder of the pulp exits the test section through the rejects line, the rejects flow rate is obtained by subtracting the accepts average flow rate from that of the feed line.

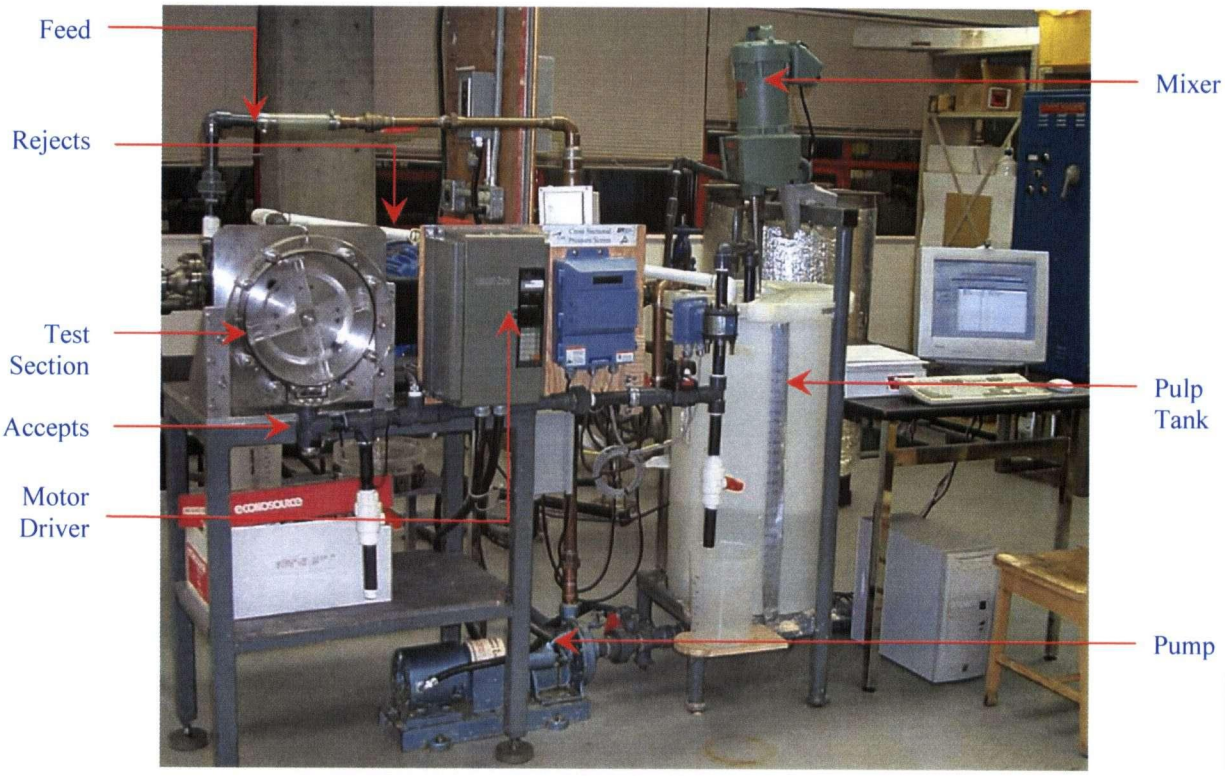

Figure 3.6 – Experimental Flow Loop

All the pressure transducers are connected to a strain gauge signal-conditioning module (DBK-43A by IOtech), while the flow meters are connected to a low pass filter module (DBK-18). These modules, as well as the optical encoder, are then connected to a data acquisition card (DaqBoard 2000) installed inside the computer. This data acquisition system is capable of sampling at a rate of 200 kHz and supports up to 256 analog channels, 40 digital I/O lines and 4 counter inputs; as well as analog, digital or software triggering. Both signal conditioning modules were connected to the analog input channels of the DaqBoard, while the optical encoder was connected to both the digital and counter channels of the card.

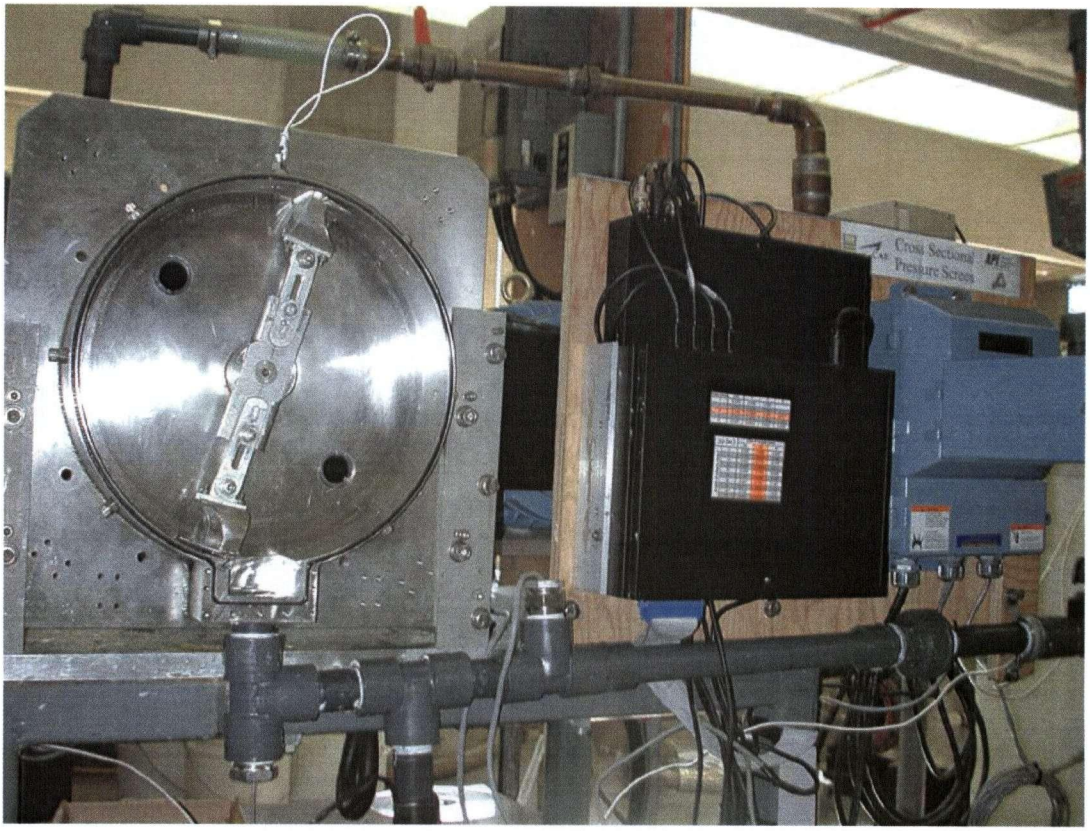

Figure 3.7 – Test Section and Data Acquisition System

3.2.3 Experimental Program

As mentioned earlier this research focuses on analyzing each one of the rotor design parameters individually. Due to the fact that the physical properties of low consistency pulp are very similar to those of water, most of the experiments were conducted using water and not pulp. Besides significantly reducing the time it would take to conduct all experiments using pulp, it also eliminated an additional variable as mechanical pulp can only be kept for approximately one week as a suspension without being refrigerated before it starts decomposing. This would mean that as new pulp had to be prepared its consistency would vary significantly between experiment batches.

A rotor with two foils was used in these experiments. Partly, because this is the minimum number of foils that can be used to maintain the rotor balanced. But most importantly, it allows more space between each foil and thus the interaction of one pulse with the next is minimized.

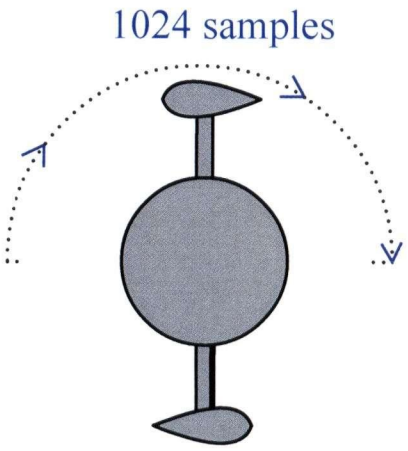

Figure 3.8 – Location of Samples

Data was read using the same foil at all times to reduce the effect of any variation in the setup of the two foils. Sampling was triggered by the index mark of the optical encoder, which was set up at 90° with respect to the rotor arm. After initiating the sampling cycle, the digital signal sent by the encoder to the data acquisition system was used to synchronize the data with the position of the rotor. The computer then logged the next 1024 samples (Figure 3.8), which are equivalent to 180°, and stopped.

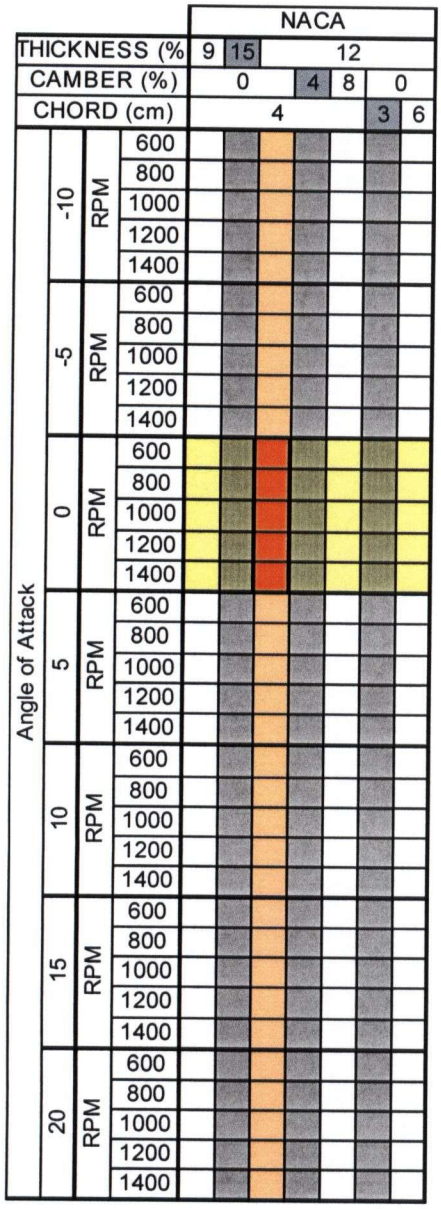

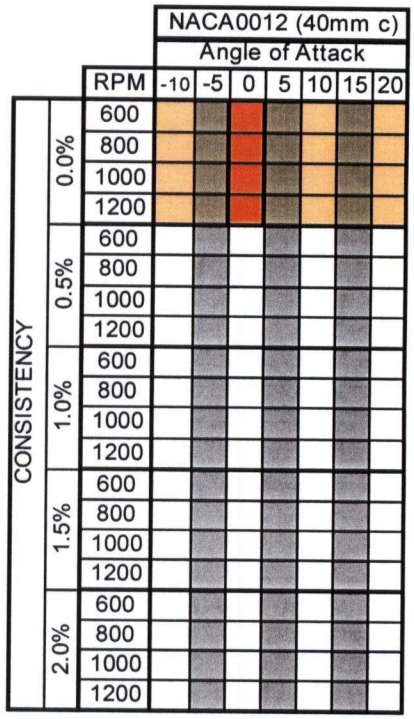

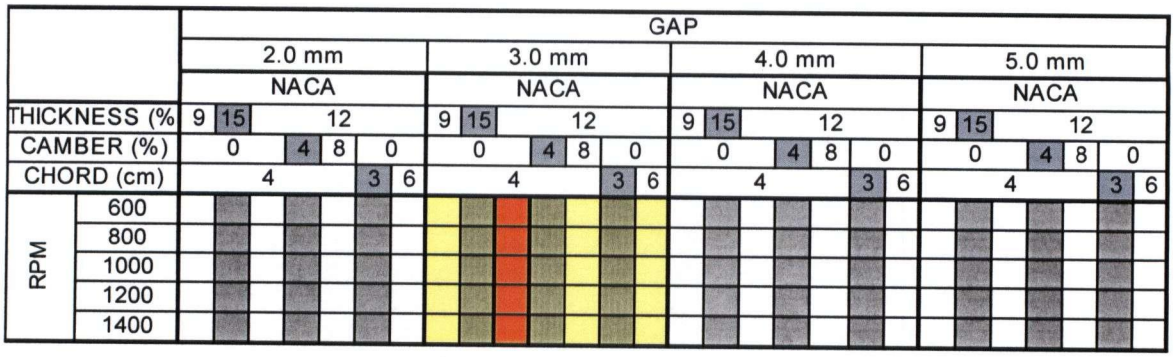

Figure 3.9 – Experimental Matrix

The experimental matrix used in this research is shown in figure 3.9, the base case is a NACA0012 foil with a chord length of 4-cm., it has a 3-mm. clearance to the CSS wall, the angle of attack is 0^o and the consistency is 0%. Rotor tip speed is also varied from 600 RPM (9.17 m/s) to 1400 RPM (21.4 m/s). Even though higher speeds will create stronger pulses, the pressure is normalized by the dynamic pressure so that speed is not expected to make a difference to the pressure coefficient (c_p).

For these experiments, the accepts line was closed, thus the reject ratio was equal to 1. This is due to the fact that flow rate through the screen does not affect the shape and magnitude of the pulses. This was confirmed by running some duplicate experiments with and without any flow through the CSS and the results were virtually identical. The flow however was set to the maximum for all experiments to provide the test section with enough cooling so that experimental conditions would not de altered over time.

Each foil configuration was tested at 5 different speeds, from 600 to 1400 rpm in 200 rpm increments, since this adjustment does not require any changes to the setup of the foil. Each of these sets of experiments at 5 different speeds, without changing the configuration or setup of the foil is referred to as an experimental run. The first set of experiments were done in water (0% consistency). These experiments were performed using 7 different foils, the first being the base case described above. The rest of the foils can be divided into three pairs, the first varying the thickness of the foil, the second pair had different camber and the third were scale versions of the NACA0012 to obtain different chord lengths.

The foils used to show the effect of thickness were a NACA0009 and a NACA0015, which have thicknesses of 9% and 15% respectively (Figure 3.10). It is also important to note that foils are conventionally divided into thick and thin foils, where this division occurs at 12% thickness. Thus, the base case was chosen to be a NACA0012 and compared to a foil in the thin foil category and another one considered a thick foil.

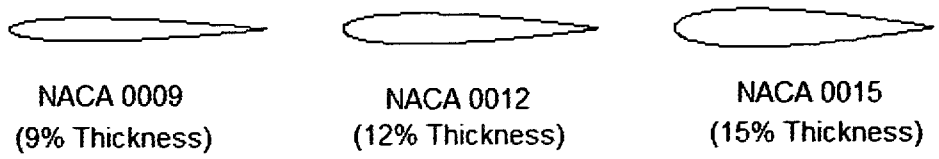

Figure 3.10 – Foils with varying thickness

Similarly, the effect of camber was tested using two foils with higher cambers than that of the base case which is an un-cambered or symmetric foil. The foils chosen were a NACA4312 and a NACA8312, with a camber of 4% and 8% respectively, but with 12% thickness in all cases. (Figure 3.11)

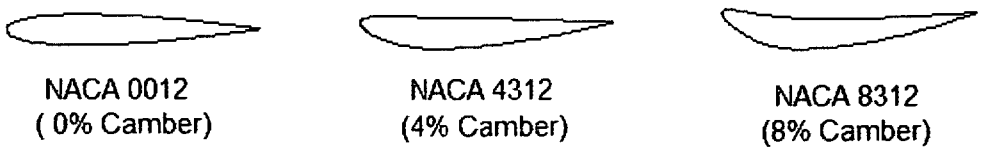

Figure 3.11 – Foils with varying camber

Even though according to airfoil theory, foils with different chord lengths are expected to produce identical pulse shapes, when normalized by its chord length, due to the fact that the screen wall is curved, the ratio of screen radius to chord length might have an effect on the

"effective camber" of the foil, as shown in Figure 3.12. Effective camber is defined as the camber a foil would have if the geometries of both the wall and the foil were mapped, such that the curved wall was converted to a straight line.

Determining the effect of effective camber is particularly important to this research, because in practice rotor foils are manufactured in a uniform size. Pressure screens, however, can be found in a great variety of sizes, which can range from about 50-cm. to over 3-m. in diameter. Thus, if this ratio has an important effect on the shape or magnitude of the pressure pulses it can greatly affect the performance of a pressure screen. Since the CSS has a fixed test section, instead of testing screens of different sizes, this ratio was modified by changing the chord length of the foils. The alternate chord lengths chosen for the experiments were 3 and 6-cm. in addition to the base case which was 4-cm.

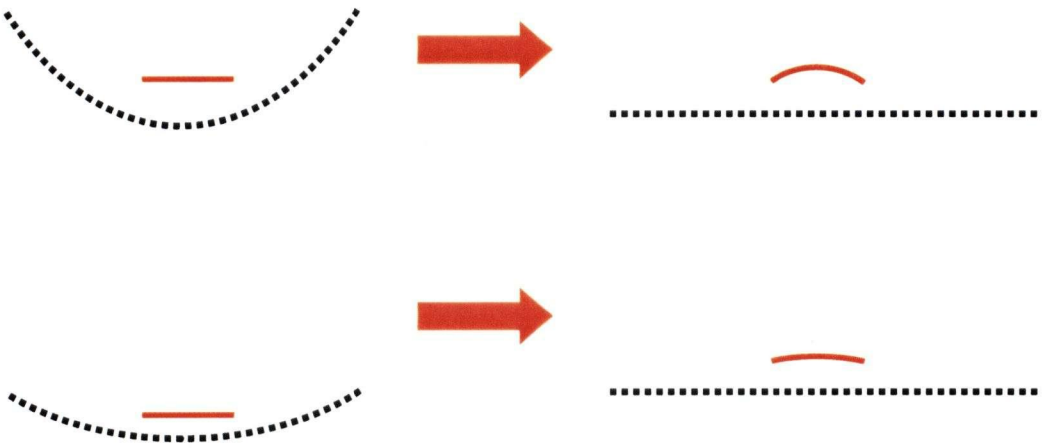

Figure 3.12 – Schematic of the variation in effective camber caused by changing the screen radius to chord length ratio.

All of these foils, were tested by varying two of the design parameters, while keeping the same kind of foil in the CSS. First, the foil was set to 0 ° angle of attack, and the gap was varied starting at 5-mm, and reducing it 1-mm at a time down to 2-mm. Then, the angle of attack was

changed, from -10° to +20° in 5° increments, always maintaining a 3-mm rotor clearance (gap) from the wall to the closest point on the rotor foil.

Finally, using the NACA0012 foil, additional tests were conducted using TMP pulp at different consistencies, which ranged from 0.477% to 1.707%, as shown in table 3.1. Originally, the target consistencies were 0.5, 1.0, 1.5 and 2.0%, but due to pulp lost during the experiments, the actual consistencies measured while running the experiments were somewhat different. However, the real consistency was always used for any calculations in this research. These tests were also conducted at different angles of attack, and the gap was always kept constant at 3-mm.

Target Consistency	Sample	Filter Wt. (g)	Wet Sample (g)	Dry Sample (g)	Real Consistency	
0.5%	A	1.227	289.49	2.626	0.483%	**0.477%**
	B	1.221	308.27	2.675	0.472%	
1.0%	A	1.194	303.02	3.992	0.923%	**0.924%**
	B	1.219	277.80	3.786	0.924%	
1.5%	A	1.222	294.52	4.967	1.272%	**1.275%**
	B	1.230	305.60	5.135	1.278%	
2.0%	A	1.198	167.37	4.061	1.711%	**1.707%**
	B	1.195	186.13	4.365	1.703%	

Table 3.1 – Consistency test results

A software program using LabVIEW, was used to record all the experimental information acquired during these trials. A picture of the main control screen is shown in figure 3.13. The program logs all the experimental conditions and pressure pulse data in three separate cycles. First, the program records information on the experimental conditions, such as average pressure in the accept and feed lines, average flow rates and rotor mean speed. All of these quantities are not particularly useful for this research, except to ensure that the conditions under which the experiments took place were identical. Also, as pressure, distance, speed, etc. are always non-

dimensional through-out this thesis, the actual quantitative values of the conditions are irrelevant. This information is recorded for 20 seconds in intervals of 10-ms and averaged, and only the mean value of the conditions is recorded in the data file.

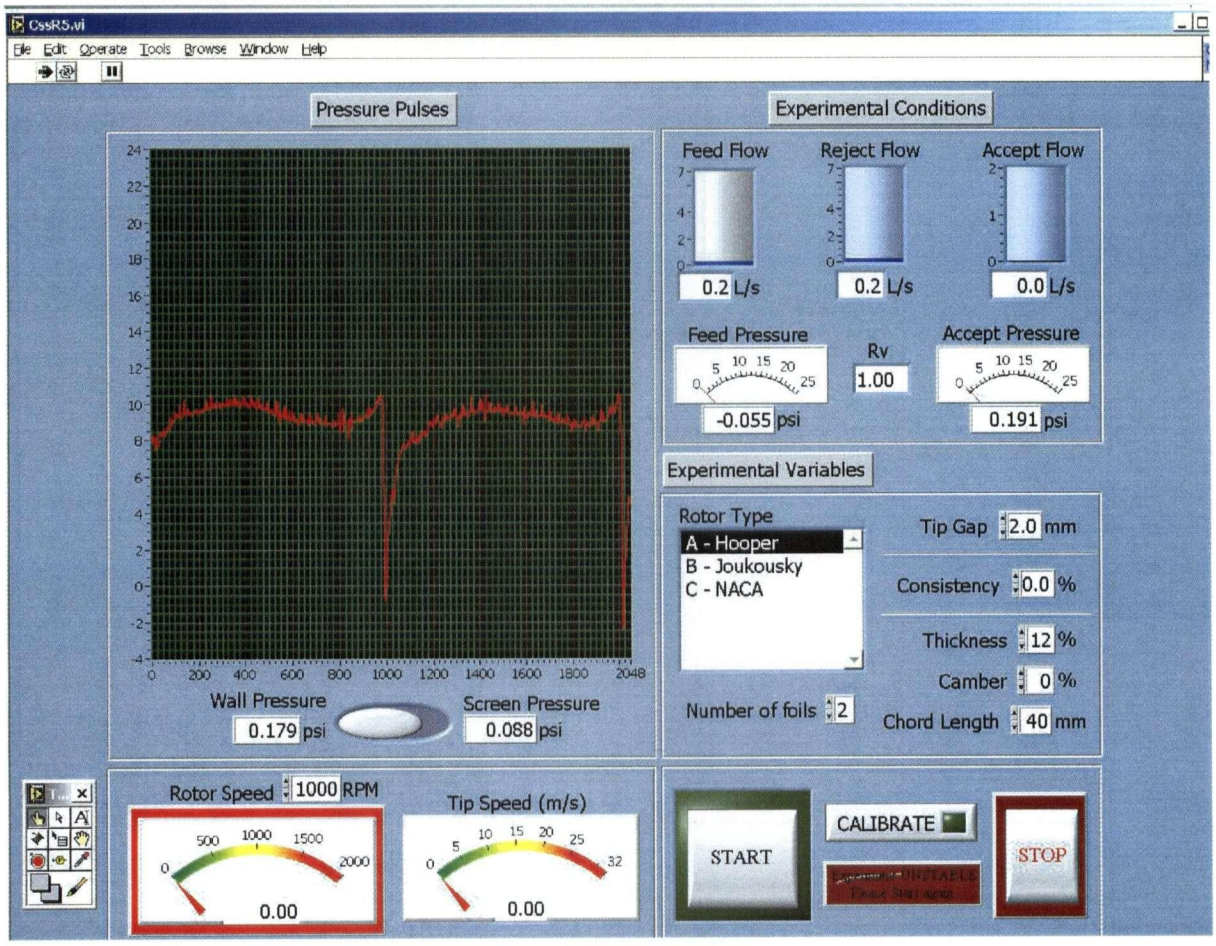

Figure 3.13 – LabVIEW Software Screenshot

The next stage of the cycle was the actual recording of pressure pulses, which consisted in recording 120 individual pulses. Each pulse was recorded when the index mark of the optical encoder transmitted a signal to de software and the next 1024 points of the encoder were synchronized with the pressure reading from the high frequency pressure sensor. The software allowed a 1 sec. pause between pulses, to obtain more representative pulse samples and minimize

any temporary fluctuations in the pressure pulses. This stage took approximately 3 minutes to complete, but varied slightly depending on the speed the rotor was moving at.

The final step consisted in repeating the first stage of the program and once the new average values for the experimental conditions were obtained, they were compared to the values from the beginning. This was done with the purpose of ensuring that the experimental conditions were constant throughout the experiment. It was determined that if the error was more than 1%, between the initial and final conditions, that particular run would be repeated. However, the maximum error recorded during the entire research was just under 0.5%.

Chapter 4

EXPERIMENTAL RESULTS AND DISCUSSION

4.1 Introduction

Experimental data obtained using the LabVIEW software, was processed using a routine developed in MatLAB. The information logged for all the foil setups was averaged and a representative pulse for each configuration was obtained. These programs were designed to record data from both free foil and solid core rotors (as defined in page 3), which could have either 2 or 4 elements.

As discussed before, the pressure pulses were normalized to be expressed as a pressure coefficient (c_p) curve, plotted against a non-dimensional chord (x/c). This was done to prove that the pressure profile of a given foil configuration is independent of Reynolds number (Re), as assumed by potential flow theory and aerodynamics. Therefore, most of the analysis in this chapter is done using non-dimensional values and is a first attempt at explaining the effect that any given parameter involved in rotor design has on the shape and magnitude of the pulsation in the screen. In all the plots the foil is located along the x/c axis, with its leading edge at x/c=0 and the trailing edge at x/c=1.

The pressure coefficient by which the pressure pulses data will be expressed in the following plots is obtained form:

$$c_p = \frac{P}{\frac{1}{2}\rho U^2} \tag{4.1}$$

Where $\frac{1}{2}\rho U^2$ in the denominator is also known as the dynamic pressure, ρ is the fluid density, U is the rotor tip speed, and P is the gauge pressure measured by the sensor.

It is important to note that when c_p or pressure (P) is equal to zero in this analysis, it refers to the mean pressure in the screen and not to atmospheric (gauge) or absolute pressure. Figure 4.1 shows a schematic to help determine the point where the pulp is back-flushed in the pressure screen. P_{screen} is the mean pressure in the vessel, P_{atm} is the atmospheric pressure and $P_{accepts}$ is the mean pressure in the accept line downstream of the screen. Pulp is back-flushed whenever the pressure of the pulse is less than $P_{accepts}$ and pulp goes through the screen when the pulse is above it. Thus, $P_{accepts}$ can be regulated by throttling the valve in the accepts line and can be equal to P_{screen} if it is completely closed and P_{atm} is it is fully open

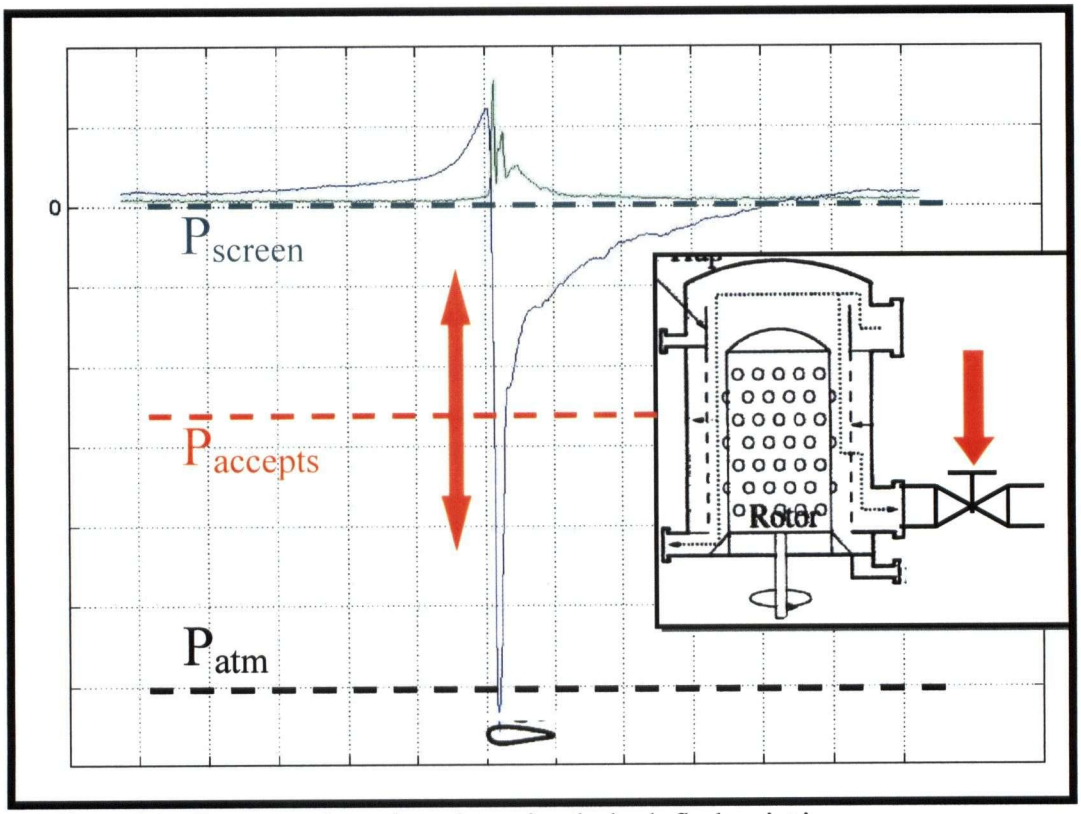

Figure 4.1 – Pressure schematic to determine the back-flush point in a pressure screen.

4.2 Effect of Design Parameters

A considerable portion of the ensuing discussion of experimental results is qualitative in nature. This is because the objective of this thesis is to serve as a general guide for future studies and designs, and it is not intended to study every design parameter in great detail. It is important to note that design parameters are only looked at individually in this thesis and that interactions between them are expected to be very strong and even difficult to separate. However, by analyzing each one separately the information can be used to validate more sophisticated computational models and simulations that can incorporate these interactions and allow a faster and more cost effective alternative to analyzing this problem.

The following discussion presents an example of each parameter analyzed in this study, which was chosen as being representative of the behaviour of the pressure pulse for that particular variable. Additional plots of the rest of the experiments performed can be found in the Appendices for comparison and review.

4.2.1 Rotor Tip Speed

As mentioned before, the general shape of the pressure pulses in not expected to be affected by the rotor tip speed. However, the magnitude of the pulse expressed in pressure units increases with the square of speed, as can be expected from rearranging equation 4.1 to:

$$P = c_p \cdot \frac{1}{2}\rho U^2 \tag{4.2}$$

Figure 4.2 shows how the magnitude of the suction peak increases, becoming more negative, as the speed of the rotor (U) increases (for more examples refer to Appendix 1). This increase

follows a quadratic relationship and is easily identified by the well defined parabola shape of the curves. This plot is shown in pressure as c_p is not expected to be affected by speed because it is normalized by the dynamic pressure, which is proportional to U^2. Also, notice that the gap between the screen basket and the rotor foil affects the magnitude of the pressure pulse, this will be discussed further in section 4.2.2.

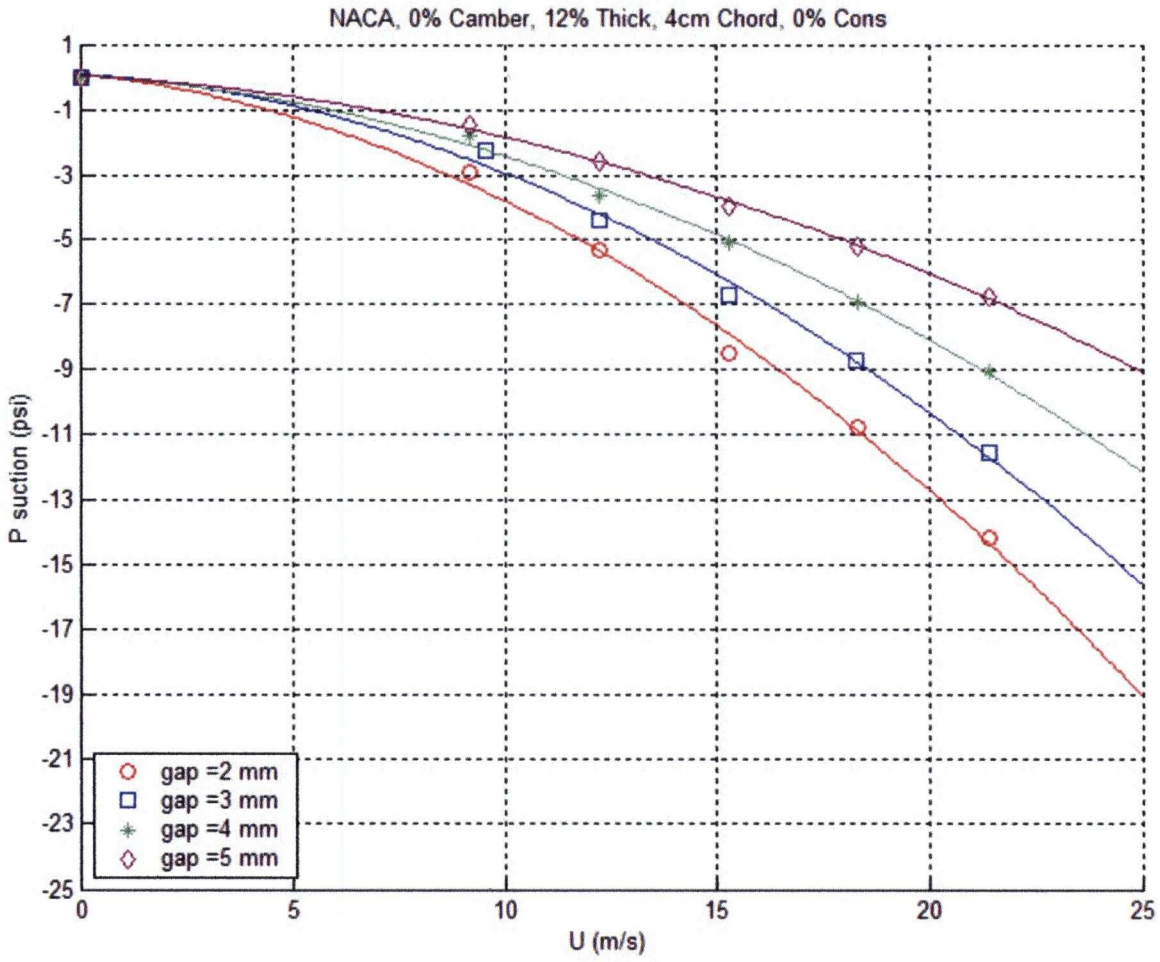

Figure 4.2 – Effect of rotor speed on pulse magnitude.

Figure 4.3 also shows that the pressure pulse retains its shape for various velocities and only the magnitude of the pulse is affected, while the general shape and the location of the pressure surges remain unchanged (see Appendix 2 for more examples).

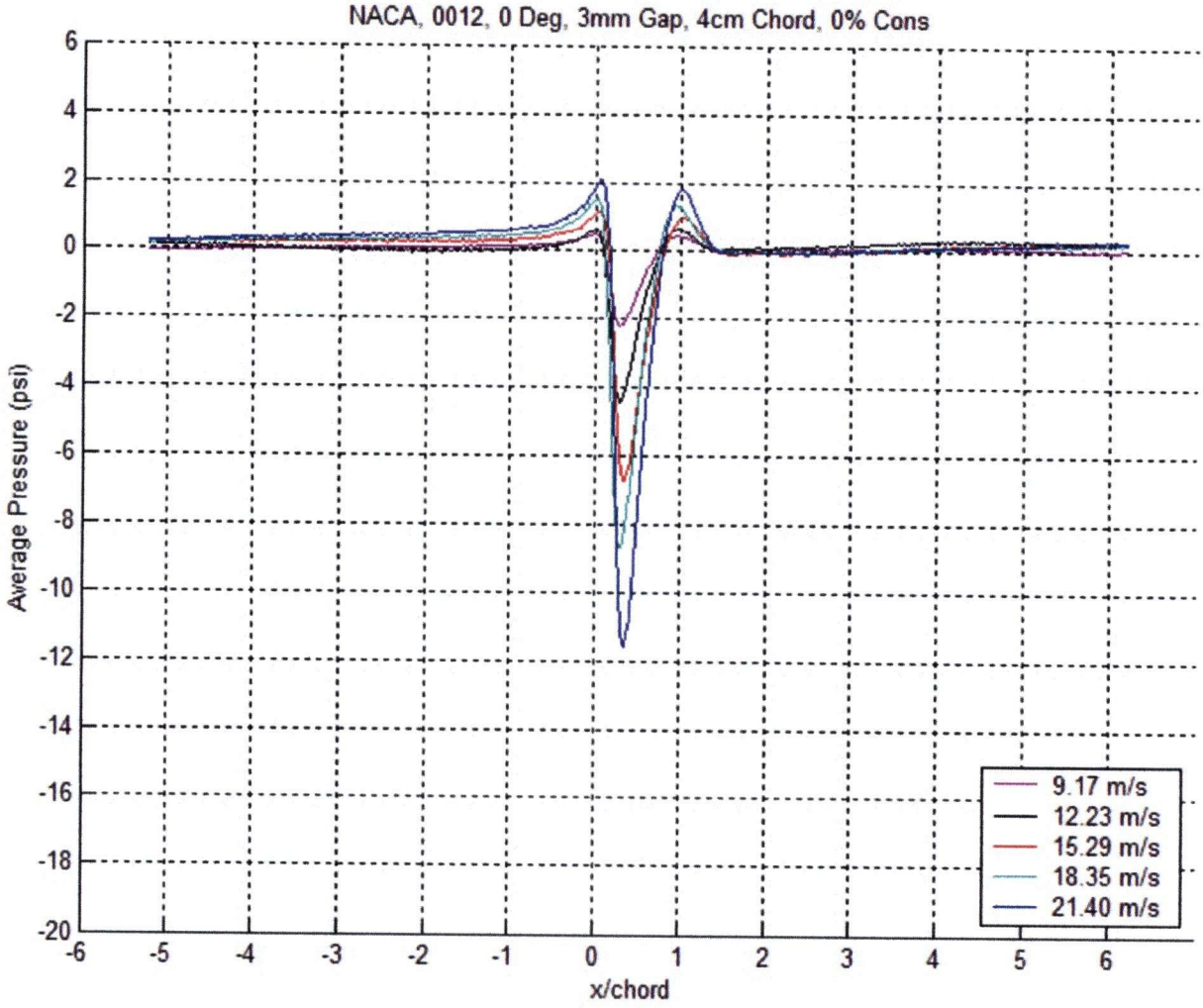

Figure 4.3 – Effect of rotor speed on pulse magnitude.

After normalizing the pressure pulses shown in figure 4.3, by the dynamic pressure created by the rotor, all the curves collapse as shown in figure 4.4. Since the dynamic pressure term has density and U^2 included in it, normalizing the pulses using their respective dynamic pressure eliminates the effect of Reynolds number. This confirms, as mentioned before, that the shape of the pressure pulse is independent of Reynolds number (Appendix 3), which implies there is no effect from rotor speed or viscosity as Reynolds number is defined as:

$$\mathrm{Re} = \frac{U \cdot t}{\nu} \tag{4.3}$$

Where, U is the rotor tip speed (m/s), t is the thickness of the foil (m), and ν is the dynamic viscosity of the fluid (m^2/s).

It is important to note that while some peaks do not seem to collapse perfectly, this is likely due to some kind of wave pattern observed throughout the experiments, which slightly modifies the pressure readings recorded. This effect was not seen in previous experiments conducted with solid core rotors, suggesting it might be due to large eddies generated by the spinning of the rotor, which could have a diameter as big as the screen radius.

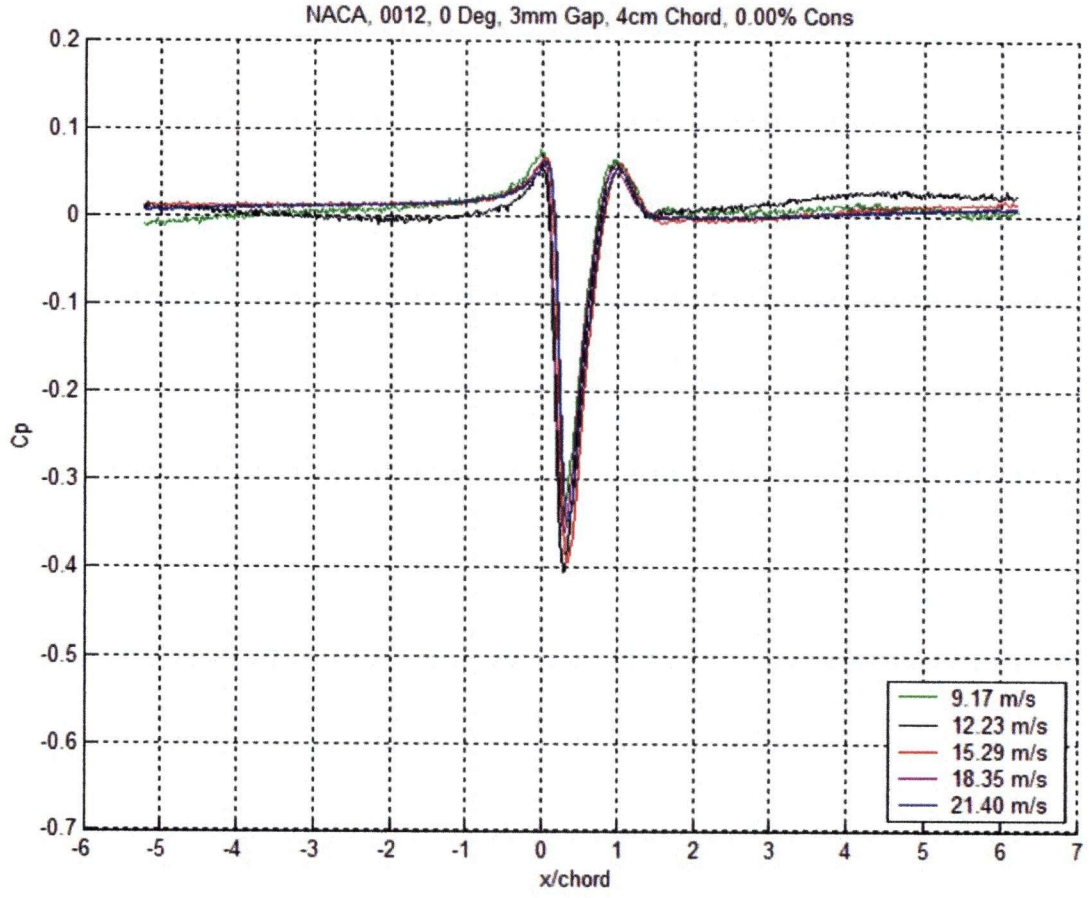

Figure 4.4 – Collapsed c_p curves for different speeds.

4.2.2 Rotor Clearance

As mentioned before, as the clearance between the rotor and the screen is reduced the magnitude of the pressure pulse increases (Figure 4.5). This is due, however to an increase in c_p, which translates into stronger pulses. As shown in aerodynamics literature, the shape and magnitude of the c_p curve is only affected by the geometry of the foil and the angle of attack. In our case however, since the domain is not only a single foil, but it also includes the screen wall the geometry is affected by the relative position even if the foil and its angle of attack are not changed (see Appendix 4).

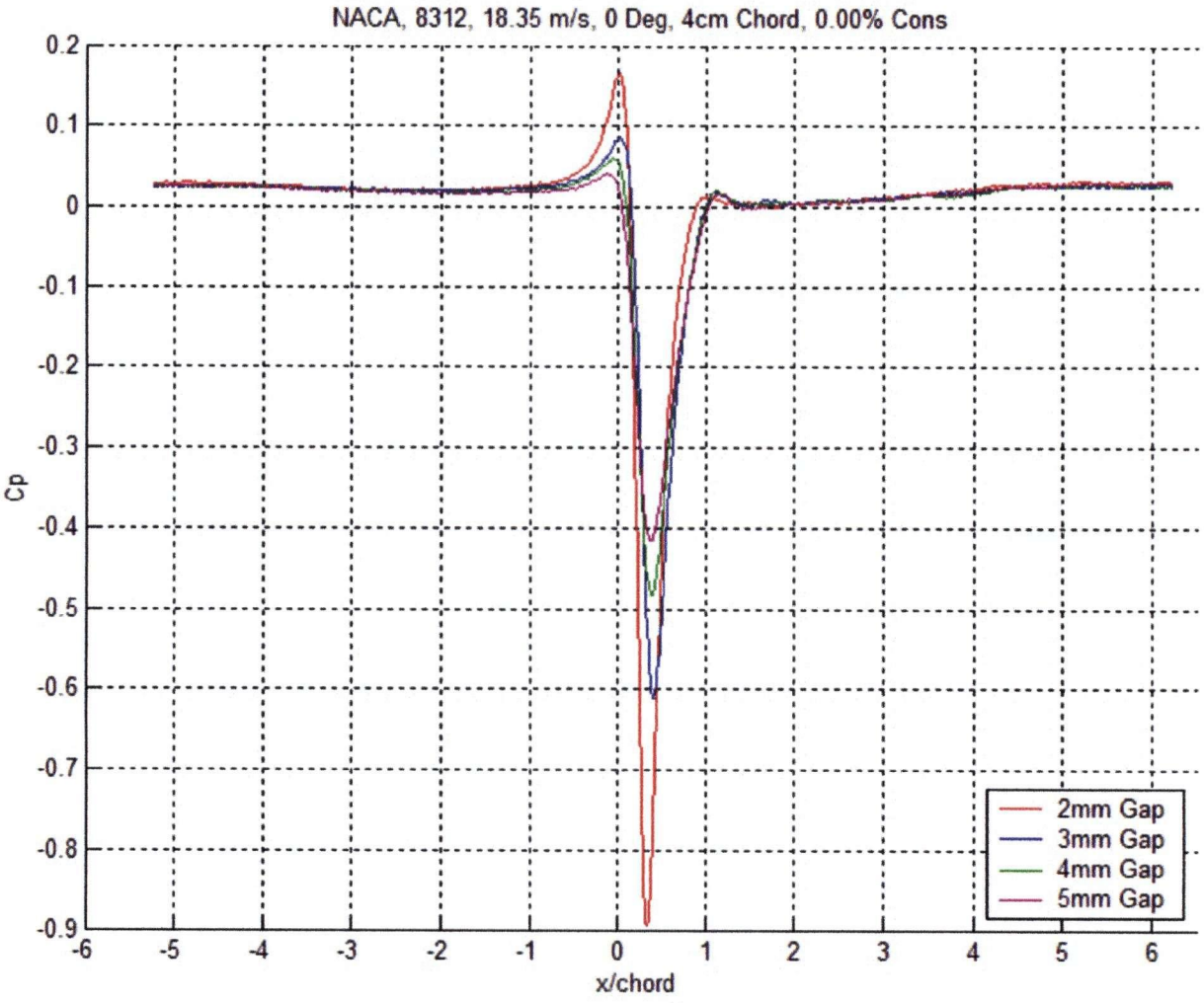

Figure 4.5 – Collapsed c_p curves for different rotor clearances.

Since we know that the pressure pulse will tend to disappear if the clearance is too great, we would expect the peaks to decrease asymptotically to zero as gap increases. The maximum c_p, would also be limited by the clearance of the foil, as it cannot be forced to rotate against the pressure screen. We would therefore expect an exponential decrease in c_p as the gap increases, as given by:

$$c_p = c_{p_o} \cdot e^{c_1(\delta - \delta_0)} \tag{4.4}$$

Where c_{po} is a reference c_p at a predetermined gap (δ_0), say 3-mm., δ is the real gap in mm. and c_1 is an experimental constant.

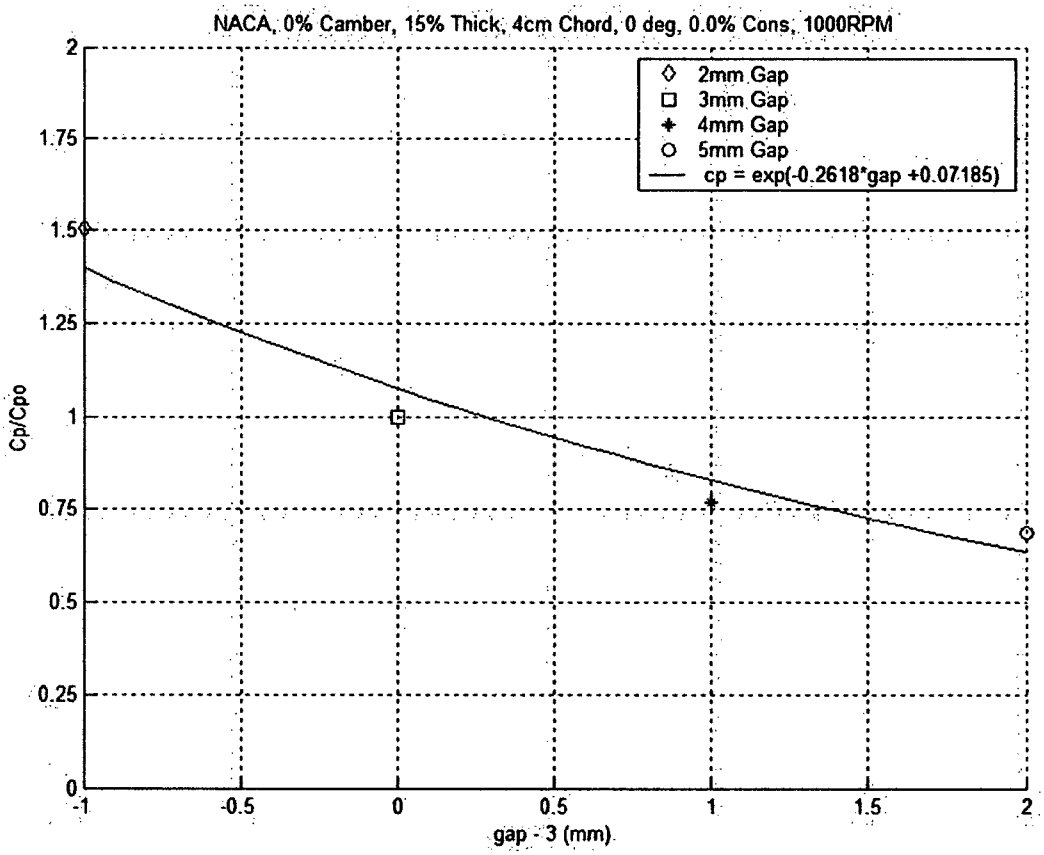

Figure 4.6 – Exponential fit of c_p.

Figure 4.6 shows and example of the exponential fit that is expected for the c_p curve when varying gap. A series of curves were fitted using the suction peak values of c_p for the experiments performed in this research and the value of c_1 was found to be -0.267.

Substituting c_p in equation 4.2 with the adjusted c_p in equation 4.4, we get:

$$P = \frac{1}{2}\rho U^2 \cdot c_{p_0} \cdot e^{-0.267(\delta - 3)} \tag{4.5}$$

It is important to note that the value of c_1, might not be the same if a different reference gap is used. Also, since the number of experiments preformed in this research is limited, it might be dependent on the specific configuration or foil shape being tested. In this case all 7 foils were tested, but always using an angle of attack equal to zero. After thoroughly analyzing the results it was determined that a more appropriate way of expressing equation 4.4, would be by non-dimensionalizing the rotor clearance by the chord length (δ_c/c) and measuring it from the chord line to the screen wall and not from the foil surface.

$$P = \frac{1}{2}\rho U^2 \cdot c_{p_0} \cdot e^{c_1\left(\frac{\delta_c - \delta_{c0}}{c}\right)} \tag{4.5}$$

4.2.3 Pulp Consistency

Since pulp is a non-Newtonian fibre suspension, consistency is expected to have a major effect on the magnitude of pressure pulse. This is due to the strong interactions among fibres in the pulp that cause the formation of bundles or flocks of fibres. Therefore, as the consistency of the

pulp increases more energy is required to move and fluidize the suspension. As a result if the rotor speed is kept constant, the speed of the pulp flow field effectively slows down, resulting in smaller pressure pulses. It is also important to note that the overall shape of the pulse is not expected to change significantly.

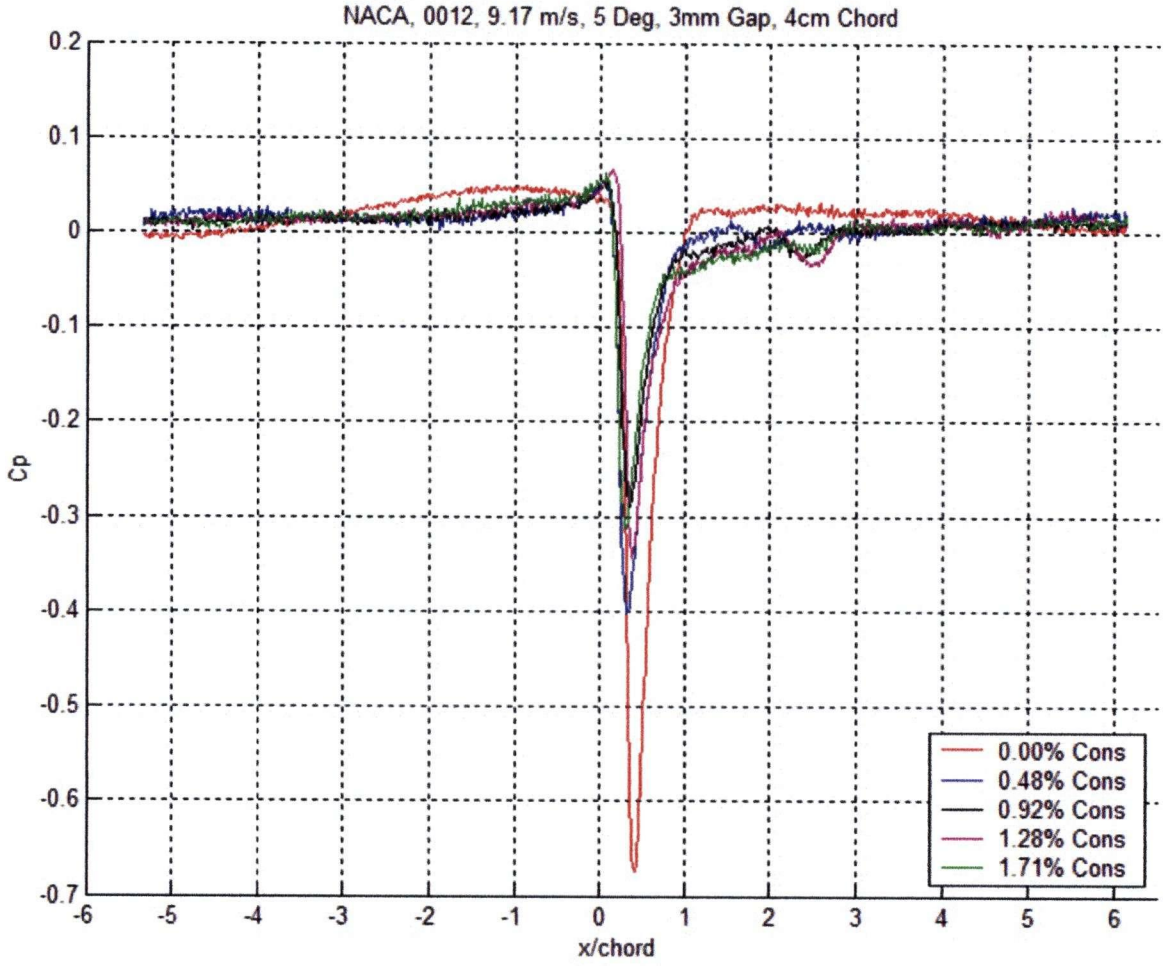

Figure 4.7 – Effect of consistency on pressure pulses.

Figure 4.7 shows that as consistency increases effective viscosity the magnitude of the suction peak decreases. This change is particularly evident when we introduced fibres to conduct experiments using a pulp suspension, compared to what was observed with water (0%

consistency). Also, as consistency increases some instability was noticed in the wake of the foil. This is likely due to fibre interaction and flocculation, which can promote the formation of eddies being shed by passing rotor foil (refer to Appendix 5 for more examples).

4.2.4 Foil Geometry

As previous aerodynamic studies have shown, foil geometry as well as the angle of attack, completely change the shape of the c_p curve, and cannot be precisely quantified. This means that only general tendencies can be identified when this group of parameters are changed. The following analysis, thus, gives some insight as to the possible causes of these changes, when geometric parameters are studied independently from one another.

4.2.4.1 Thickness

The most important finding, with respect to thicknesses in this research was the increased positive pressure surge caused by the leading edge of the foil for the 15% thickness case. This can be attributed to the fact that foils over 12% are considered thick foils and cause a more dramatic redirection on the flow towards the screen, thus creating a much higher pressure at the leading edge.

This increase in pressure upstream of the suction peak is not desirable as it might pack fibres trapped on the screen even tighter, before the suction surge has a chance to unplug the screen (Figure 4.8). This might result in the pulse not being strong enough to clear the screen, due to the tight fibre bundles accumulated on the screen.

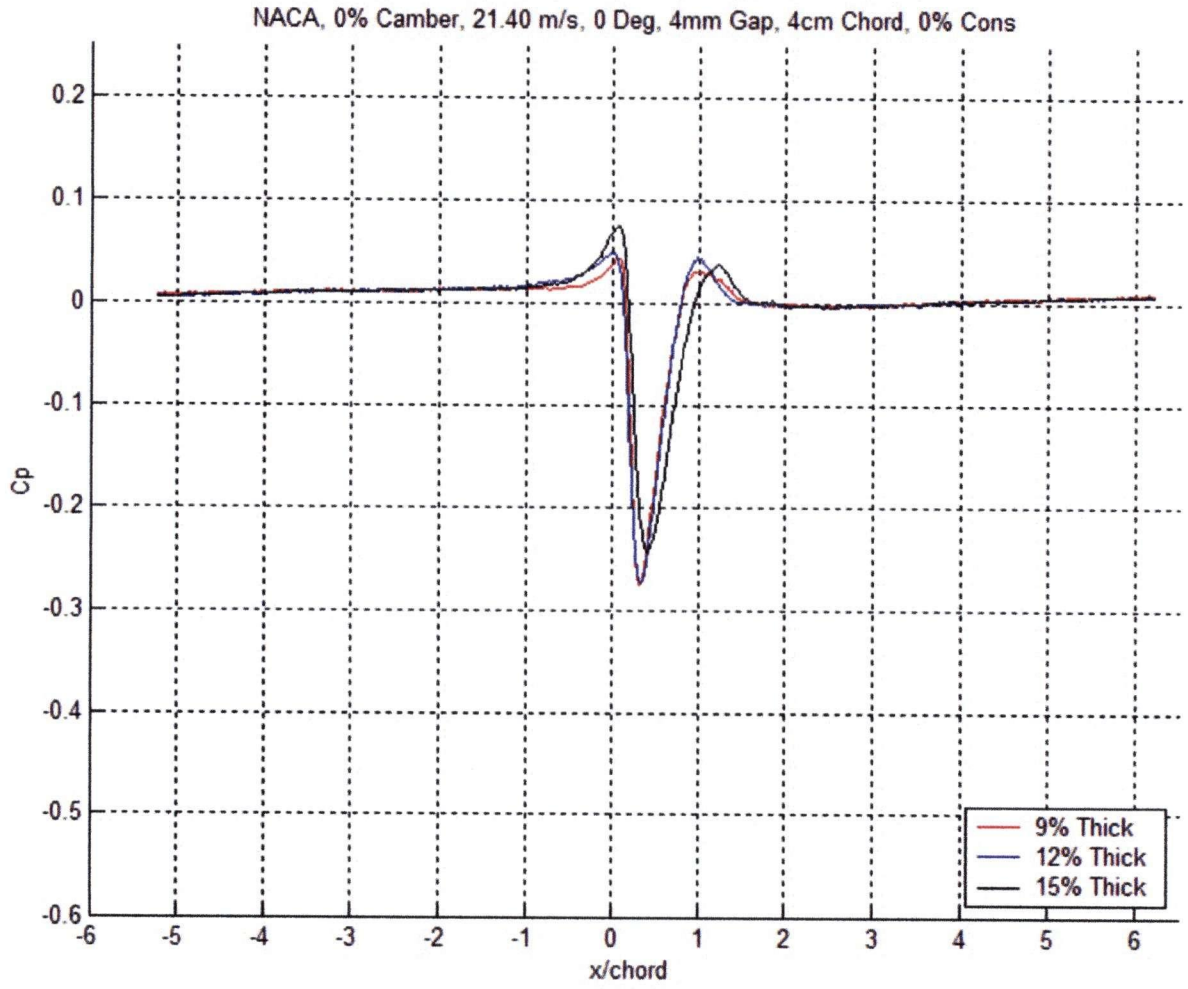

Figure 4.8 – Effect of thickness on pressure pulses

As for the suction peak, there seems to be no significant change related to the thickness of the foil, but it is expected that a very thick foil, likely over 20% thickness might cause a very high pressure surge at the leading edge and flow separation at the trailing edge. This in turn, will dramatically increase the drag on the rotor, which translates into much higher energy consumption by the pressure screen. On the other hand a very thin airfoil will not have the strength to withstand the intense pulses and would fail very easily. It is therefore expected that

the optimum range of thicknesses that combine strength and low drag is between 9% and 12% thickness (Appendix 6).

Finally, it is important to note that the gap between the screen and the surface of the foil was kept constant for these experiments. However, as discussed before on section 4.2.2, for more precise results the non-dimensional gap (δ_c/c) measured from the chord line should be kept constant. For our particular case this does not represent a significant change, but for tests involving much thicker foils or blade rotors the results may vary significantly if this is not considered.

4.2.4.2 Camber

As in high lift airfoils used in aerodynamics, camber has a very strong effect on the c_p curve of the foil. As camber increases the suction peak is much stronger; however, contrary to the constant increase caused by reducing the gap, the effect of camber is not constant throughout the entire pulse (Figure 4.9). Also, there seems to be an increase in the positive pressure at the leading edge between the uncambered and the cambered foils. This increase is likely due to a more abrupt contraction between the foil and the screen wall, which causes the fluid to slow down at the leading edge of the foil, thus increasing its stagnation pressure. The positive pressure peak, however, seems to be very similar for the two cambered foils. (Appendix 7)

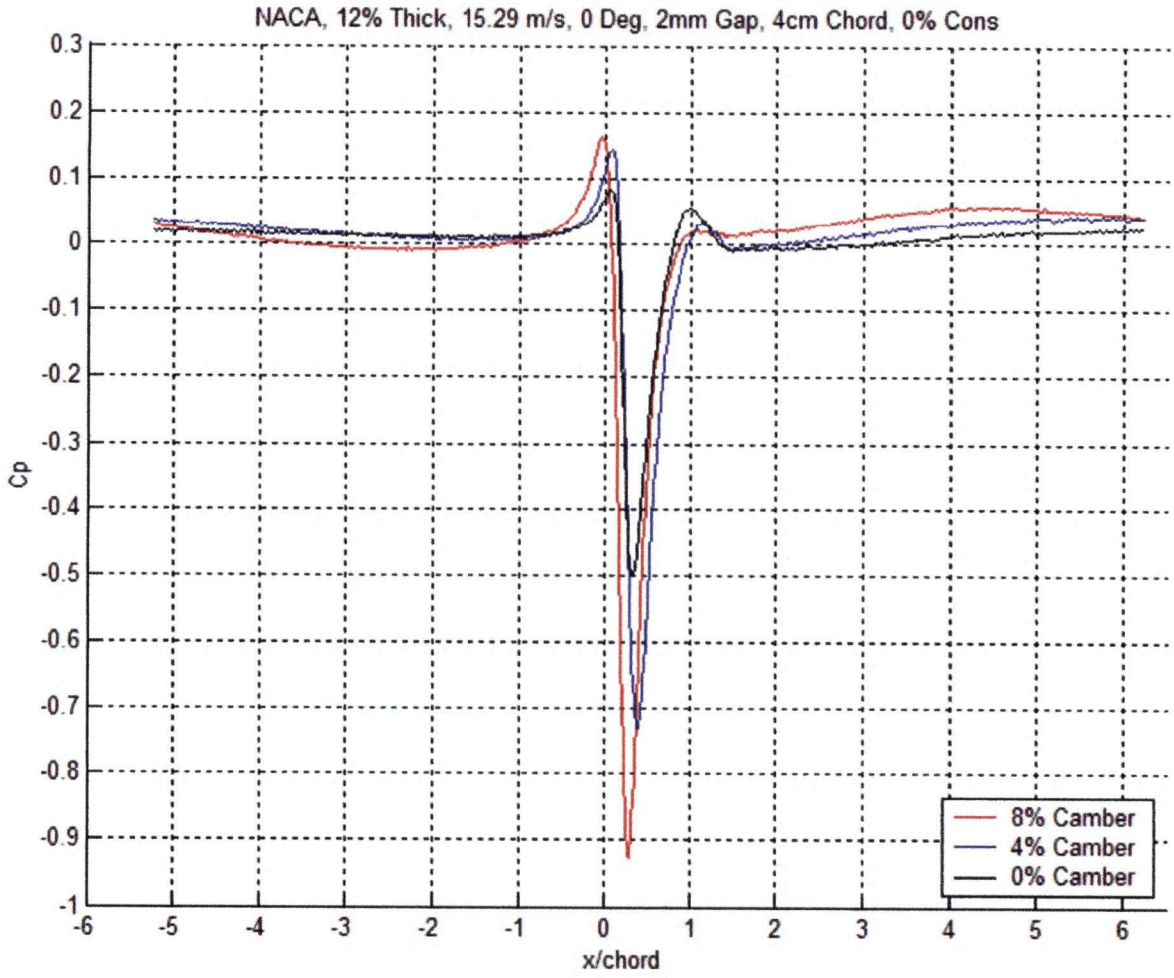

Figure 4.9 – Effect of camber on pressure pulses.

4.2.4.3 Chord Length

It is known that, from the aerodynamics point of view, a foil with a specific geometry would produce a pulse with the same c_p values regardless of its chord length. However, as discussed in Chapter 3, the fact that there are screens of different sizes would mean that if the same foil is used in different size screens, its performance would be affected due to a difference in its effective camber. Table 4.1 shows the calculated values of effective cambers tested in this experimental program.

Chord Length (cm)	Effective Camber (%)
3	- 2.5753
4	-3.4409
6	-5.1924

Table 4.1 – Effective camber for different chord lengths.

From this effective camber values and the previous analysis of camber on the magnitude of the suction pulse, one would expect to have lower c_p values for the most negative camber which would also correspond to the longest rotor foil. However, the experimental results revealed that the largest foil, with a 6-cm chord length, produced the largest values of c_p. Since all other parameters were kept constant, this suggests that the magnitude of the pulse is expected to be dependant on the ratio between chord length and the rotor clearance (δ_c/c).

The pulse shape, however, is practically the same, in that all the peaks are located in the same position with respect to the foil and the length of the pulses is almost identical (Figure 4.10). The only real difference is the magnitude of the suction peak, as even the pressure peak remains constant for different chord lengths.

Again, as discussed in section 4.2.2, in order to determine whether there is an important effect from effective camber, the non-dimensional gap (δ_c/c) should be kept constant. For these experiments, the gap was measured from the foil surface, as is commonly measured in industrial practice. This means, that while the chord length increases and the space between the foil and the wall is kept constant, the effective δ_c/c is being reduced. Thus, the resulting pulses increase in magnitude as the effective gap is decreasing. It is important to note, though, that in this case

only the suction peak increases, but the rest of the pulse is different for each chord length. This suggests that in addition to effective clearance, there is something else affecting the pulse shape, likely due to a change in effective camber. (Appendix 8)

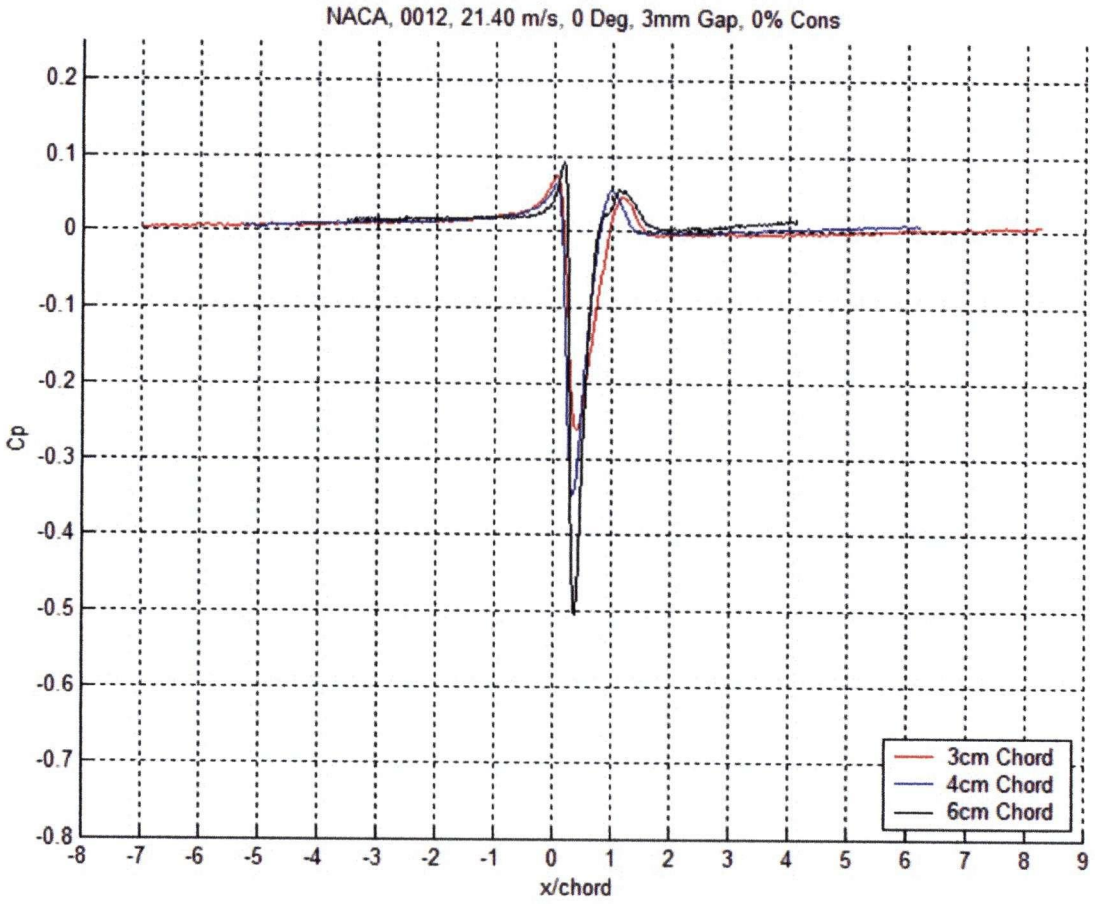

Figure 4.10 – Effect of chord length on pressure pulses.

4.2.5 Angle of Attack

From basic aerodynamics theory, one would expect the angle of attack of an airfoil to have a major impact on the entire flow field and thus completely change all the characteristics of the pressure pulses produced on the screen wall.

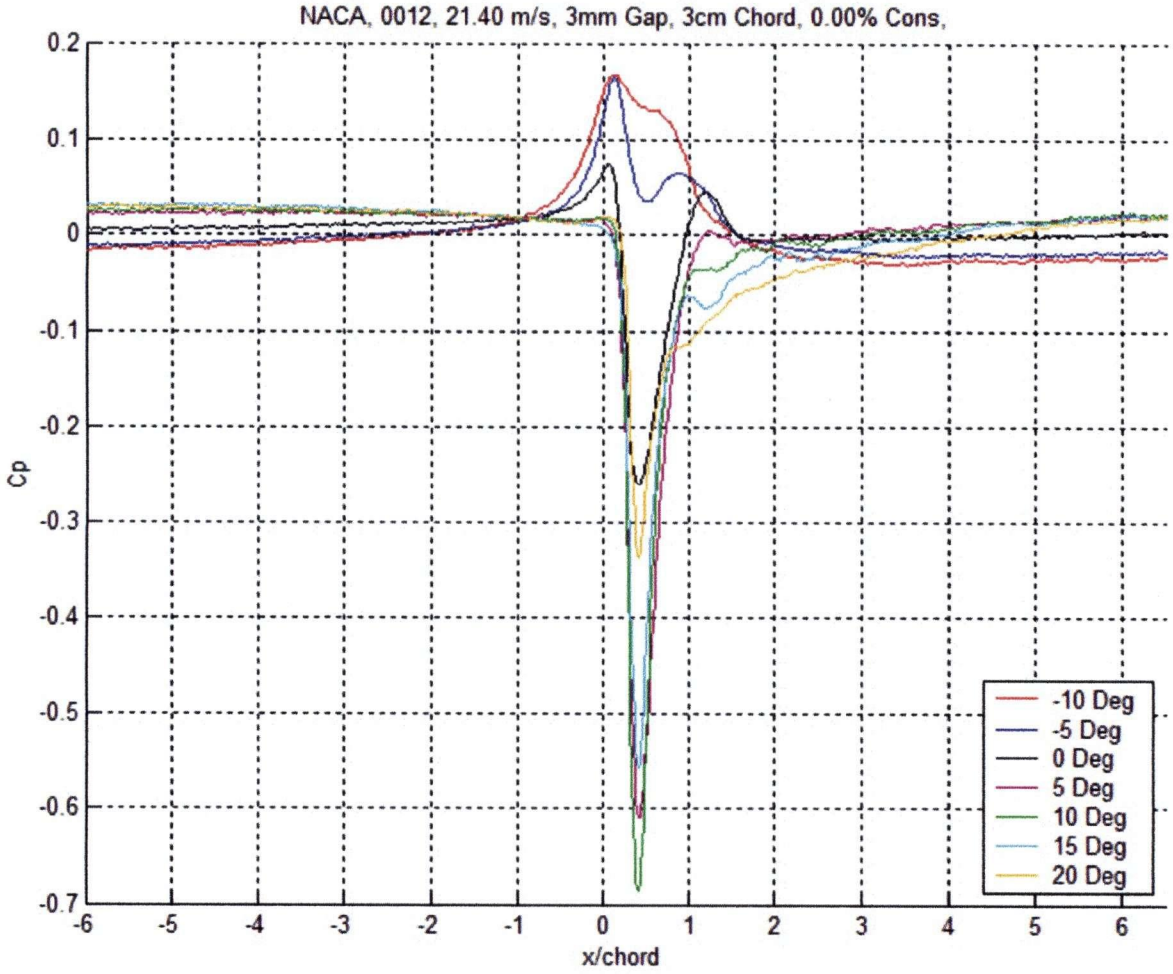

Figure 4.11 – Effect of angle of attack on pressure pulses.

The experimental data obtained for different angles of attack, showed that there is no suction pulse for negative angles and the overall shape of the pulse is completely different to the pulse obtained at zero or positive angles of attack (see Figure 4.11). It also shows that for positive angles, the positive pressure peak remains almost constant as does the overall shape of the pulse, while the most significant effect is on the suction peak and the wake of the foil. The suction peak reached its most negative values for angles of attack between 5° and 15° depending on the shape of the foil. Once the angles of attack kept increasing past its maximum peak, a highly

turbulent wake started to appear behind the foil, which suggested that there was flow separation (Appendix 9). If the drag of the rotor had been measured it would be expected that at this point it would experience a dramatic increase, thus requiring more power to drive the rotor. However, since the motor driving the CSS is a 10-hp motor and the differences in power consumption by the motor were not significant, it was not possible to measure drag. In the future the CSS will be equipped with a torque sensor on the rotor shaft to accurately measure drag on the rotor.

As a final note, the range of pressures would suggest that in some of the cases tested, cavitation might have occurred. But since the flow field was not visually analyzed and the pulses presented here is the average pulse over the sampling period, any unstable pressure readings due to cavitation are not apparent. Thus, there is no definite proof of cavitation taking place. It is important to note that two sensors were damaged during the experiments, which could be due to bubbles bursting on them caused to cavitation. This occurred when testing cambered foils at the highest speed (~21m/s) and smallest gap (2mm) settings, where the strongest pulses are expected to occur.

Chapter 5

SUMMARY AND CONSLUSIONS

This thesis experimentally examined the pressure pulses produced by a foil rotor. For this purpose an experimental apparatus representing a cross section of a real pressure screen was used. The Cross Sectional Screen (CSS) was fitted with high frequency pressure sensors to record the pulsations created by the rotor inside the screen basket. Finally, the data obtained from these experiments was analyzed to determine the effect of the most important rotor design parameters on the shape and magnitude of the pressure pulses.

From the experimental data analyzed, it was shown that:

1. The magnitude of pressure increases with the square of velocity and could be normalized by the dynamic pressure to obtain a pressure coefficient (c_p) value that represented a particular rotor foil configuration. Thus, c_p is defined as:

$$c_p = \frac{P}{\frac{1}{2}\rho U^2}$$

Where $\frac{1}{2}\rho U^2$ in the denominator is also known as the dynamic pressure, U is the rotor tip-speed, ρ is the fluid density, and P is the actual pressure measured by the sensor. This means that the shape and magnitude of the pulses are independent of Reynolds number (Re)

2. The magnitude of the pressure pulse increased as the clearance of the foil and the screen plate decreased. From these experiments the following empirical correlation was derived to estimate pressure if c_p is known at a reference clearance.

$$P = \frac{1}{2}\rho U^2 \cdot c_{p_0} \cdot e^{c_1\left(\frac{\delta_c - \delta_{c_0}}{c}\right)}$$

The overall shape of the pulse did not vary with rotor clearance, other than the magnitude of the peaks.

3. The magnitude of the pressure pulse decreased with increasing pulp consistency. It is expected that this is due to strong fibre interactions in the pulp suspension. Also, the pulse at the trailing edge of the foil appears to be less stable at higher consistencies, due perhaps to separation or vortex shedding produced by the foil; otherwise the general shape of the pulse remains constant.

4. The magnitude of the positive pressure peak increases with foil thickness; this is particularly important for thicknesses greater than 12% where the highest increase occurs. The magnitude of the negative pressure peak and the shape of the pulse in general do not change significantly due to foil thickness.

5. For the foils tested (0%, 4% and 8% camber) the magnitude of the suction increased with increasing camber at zero angle of attack.

6. The magnitude of the pressure pulses increased with chord length. This is likely due to the fact that effective rotor clearance (δ_e/c) is decreasing. If this parameter is kept constant it is expected that the magnitude of the pulse will decrease due to a more negative effective camber for foils with larger chord lengths.

7. Angle of attack significantly changed the shape and magnitude for the pressure peak as follows:
   - The maximum negative peak occurs at angles of attack between 5° and 15°, depending on the type of foil and experimental conditions.
   - For positive angles of attack the positive pressure peak seemed to be negligible.

   This suggests the optimal angle of attack for a NACA0012 foil is in the vicinity of 10°.

The Cross Sectional Screen modified to measure pressure pulses and the CNC machining of rotor foils provide a convenient tool for assessing the pressure pulse generated by different foils shapes and operating conditions. The results obtained from this type of experiment can be used in the future to develop more efficient rotor designs that are suited for a particular application.

Bibliography

[1] B. J. Allison and J. A. Olson. Optimization of Multiple Screening Stages for Fibre Length Fractionation: Two Stage Case. *Journal of Pulp and Paper Science*, 26(3): 113-119, 2000.

[2] J. N. Dewynne, S. D. Howison, J. R. Ockendon, L. C. Morland, and E. J. Watson. Slot Suction from Inviscid Channel Flow. *Journal of Fluid Mechanics*, 200: 265-282, 1989.

[3] L. Dragos. Numerical Solution of the Equation for a Thin Airfoil in Ground Effect. *AIAA Journal*, 28(12): 2132-2134, 1990.

[4] R. Estridge. The Initial Retention of Fibres by Wire Grids. *Tappi Journal*, 45(4): 285-291, 1962.

[5] R. W. Gooding and R. J. Kerekes. Derivation of Performance Equations for Solid-Solid Screens. *The Canadian Journal of Chemical Engineering.* 67(10): 801-805, 1989.

[6] R. W. Gooding. *Flow Resistance of Screen Plate Apertures.* PhD Thesis, University of British Columbia, 1996.

[7] L. Halonen and R. Ljokkoi, Improved Screening Concepts, *Tappi Proceedings, Pulping Conference*, 61-66, 1989.

[8] J. O. Hinze. *Turbulence.* McGraw-Hill Inc., 1975.

[9] C. M. Hsiun and C. K. Chen. Aerodynamic Characteristics of a Two-Dimensional Airfoil in Ground Effect. *Journal of Aircraft.* 33(2): 386-392, 1996.

[10] C. M. Hsiun and C. K. Chen. Improved Procedure for the Inverse Design of Two-Dimensional Airfoils in Ground Effect. *Journal of Aircraft.* 33(6): 1094-1100, 1996.

[11] Y. H. Im and K. S. Chang. Unsteady Aerodynamics of a Wing-in-Ground-Effect Airfoil Flying over a Wavy Wall. *Journal of Aircraft.* 37(4): 690-696, 2000.

[12] R. Karvinen and L. Halonen. The Effect of Various Factors on Pressure Pulsation of a Screen. *Paperi ja Puu.* 2: 80-83, 1984.

[13] A. Kumar, R. W. Gooding, and R. J. Kerekes. Factors Controlling the Passage of Fibres through Slots. Tappi Journal. 81(5): 247-254, 1998.

[14] P. A. Libby. *Introduction to Turbulence.* Taylor & Francis., 1996.

[15] J. Niinimaki, O. Dahl, J. Hautala and H. Kuopanportti. Effect of the Pressure Difference over the Screen Basket on the Performance of a Pressure Screen. *Tappi Journal.* 176-180, April 1999.

[16] J. A. Olson. *The Effect of Fibre Length on Passage Through Narrow Apertures.* PhD Thesis, University of British Columbia, 1996.

[17] J. A. Olson and R. J. Kerekes. The Motion of Fibres in Turbulent Flow. *Journal of Fluid Mechanics.* 377: 47-64, 1998.

[18] J. W. Riese, H. L. Spiegelberg, and S. R. Kellenberg. Mechanism of Screening; Dilute Suspensions of Stiff Fibres at Normal Incidence. *Tappi Journal.* 52(5): 895-903, 1969.

[19] F. J. Saint Amand and B. Perrin. Fundamentals of Screening: Effect of Rotor Design and Fibre Properties. *Tappi Pulping Conference*, 941-955, 1999.

[20] F. J. Saint Amand and B. Perrin. Screening: Experimental Approach and Modelling. *Tappi Pulping Conference*, 1019-1031, 1998.

[21] A. S. W. Thomas and K. C. Cornelius. Investigation of a Laminar Boundary-Layer Suction Slot. *AIAA Journal.* 20(6): 790-796, 1982.

[22] A. Tirado. Theory of Screening. *Tappi Journal*, 41(5): 237-245, 1958.

[23] T. Wikstrom and B. Fredriksson. Hydrodynamics in a Pressure Screen – Consequences on the Separation Process. *5th Research Forum on Recycling*, 197-202, 1999.

[24] C. J. Yu and R. J. DeFoe. Fundamental Study in Screening Hydraulics – Part 1: Flow Patterns at the Feed-Side Surface of Screen Baskets; Mechanism of Fibre-mat Formation and Remixing. *Tappi Journal*, 77(8): 219-226, 1994.

[25] C. J. Yu and R. J. DeFoe. Fundamental Study in Screening Hydraulics – Part 2: Fibre Orientation on the Feed Side of a Screen Basket. *Tappi Journal*, 77(9): 119-124, 1994.

[26] C. J. Yu and R. J. DeFoe. Fundamental Study in Screening Hydraulics – Part 3: Model for Calculating Effective Open Area. *Tappi Journal*, 77(9): 125-131, 1994.

[27] C. J. Yu. Pulsation Measurement in a Screen – Part 1: Pulse signature and magnitude of S-Shape Rotor. *Tappi Proceedings, Engineering Conference*. 767-782, 1994.

Appendix 1

The Effect of Rotor Tip Speed on Suction Peak Magnitude

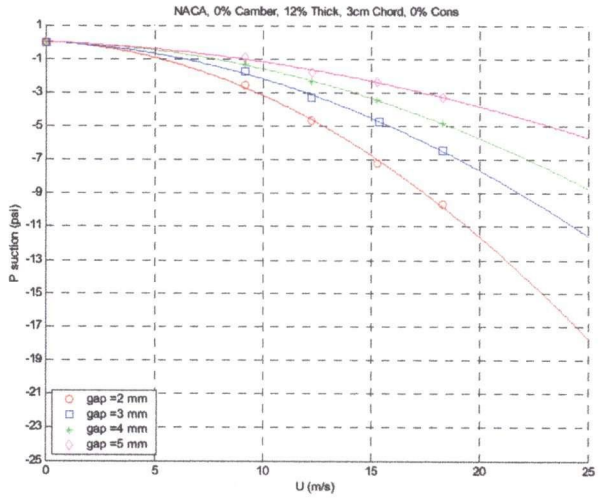
NACA, 0% Camber, 12% Thick, 3cm Chord, 0% Cons
P suction (psi)
U (m/s)
gap =2 mm
gap =3 mm
gap =4 mm
gap =5 mm

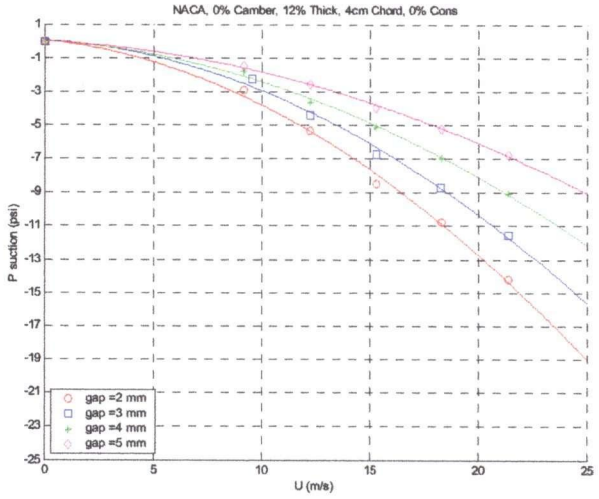
NACA, 0% Camber, 12% Thick, 4cm Chord, 0% Cons
P suction (psi)
U (m/s)
gap =2 mm
gap =3 mm
gap =4 mm
gap =5 mm

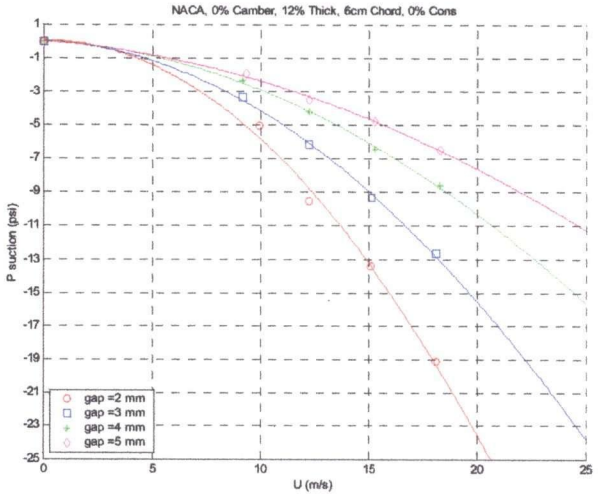
NACA, 0% Camber, 12% Thick, 6cm Chord, 0% Cons
P suction (psi)
U (m/s)
gap =2 mm
gap =3 mm
gap =4 mm
gap =5 mm

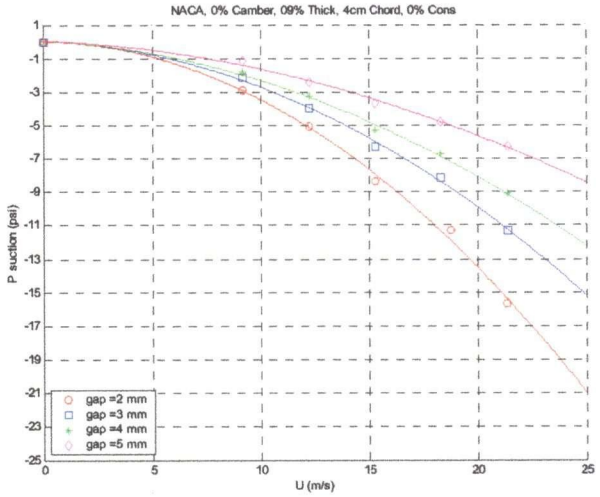
NACA, 0% Camber, 09% Thick, 4cm Chord, 0% Cons
P suction (psi)
U (m/s)
gap =2 mm
gap =3 mm
gap =4 mm
gap =5 mm

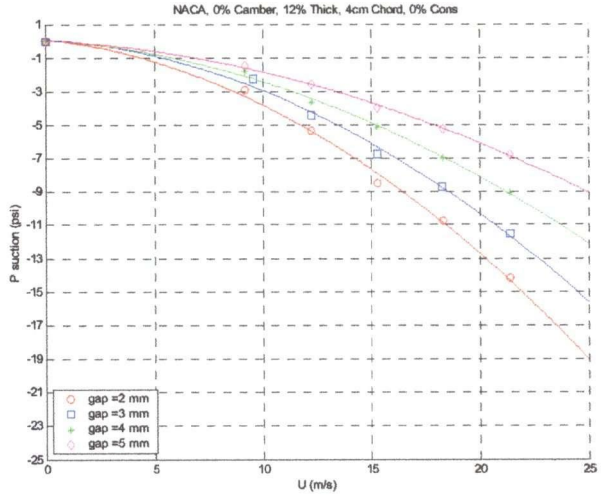
NACA, 0% Camber, 12% Thick, 4cm Chord, 0% Cons
P suction (psi)
U (m/s)
gap =2 mm
gap =3 mm
gap =4 mm
gap =5 mm

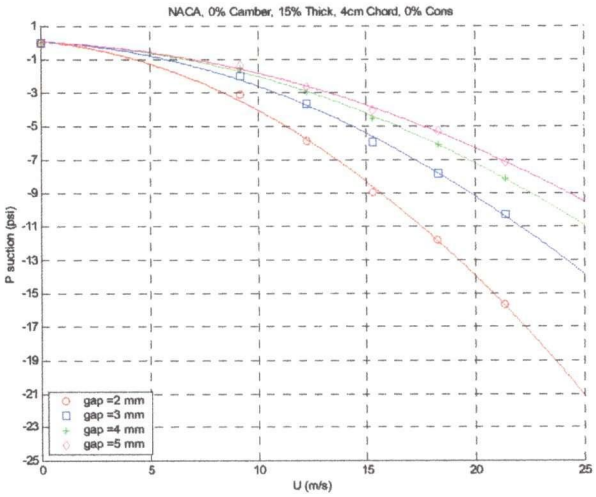
NACA, 0% Camber, 15% Thick, 4cm Chord, 0% Cons
P suction (psi)
U (m/s)
gap =2 mm
gap =3 mm
gap =4 mm
gap =5 mm

Appendix 1 – The Effect of Rotor Tip Speed on Suction Peak Magnitude

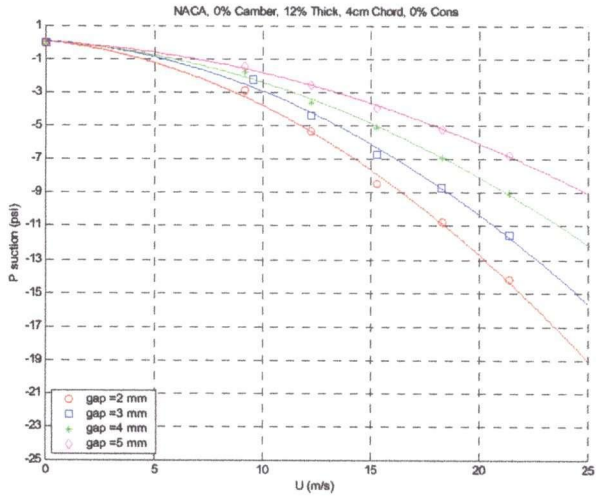

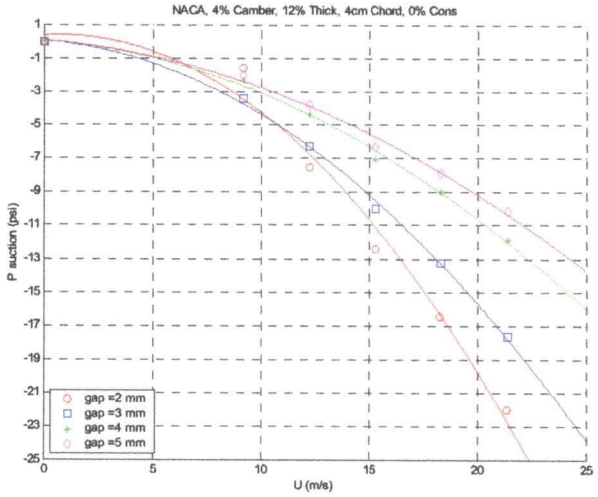

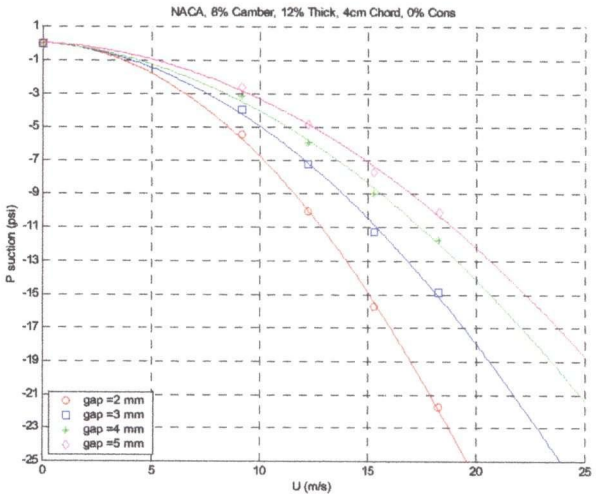

Appendix 2

The Effect of Rotor Tip Speed on Suction Pulse Magnitude

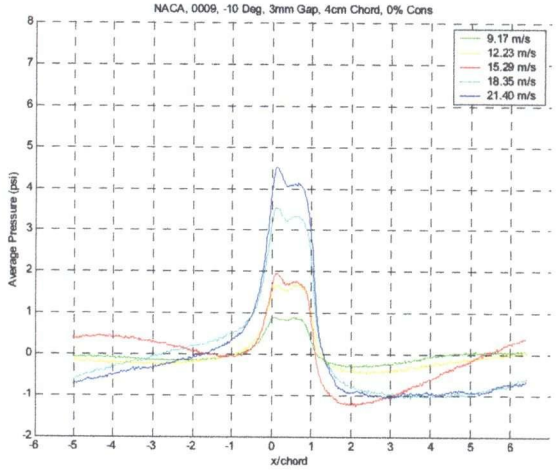
NACA, 0009, -10 Deg, 3mm Gap, 4cm Chord, 0% Cons
Average Pressure (psi)
x/chord
9.17 m/s
12.23 m/s
15.29 m/s
18.35 m/s
21.40 m/s

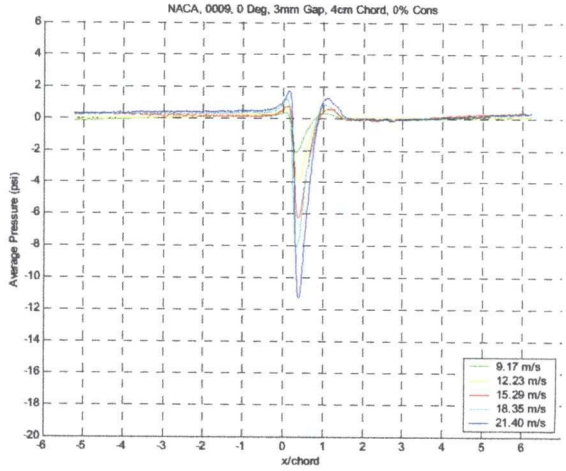
NACA, 0009, 0 Deg, 3mm Gap, 4cm Chord, 0% Cons
Average Pressure (psi)
x/chord
9.17 m/s
12.23 m/s
15.29 m/s
18.35 m/s
21.40 m/s

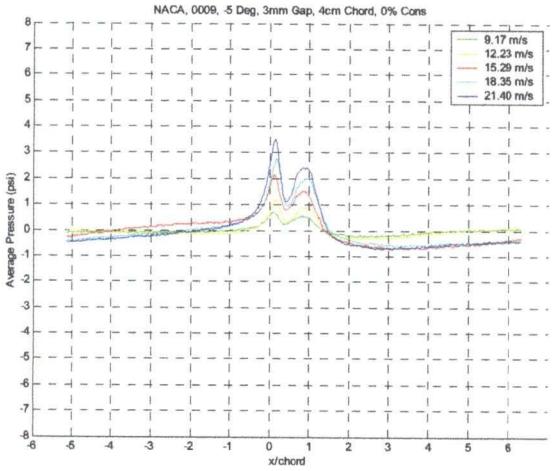
NACA, 0009, -5 Deg, 3mm Gap, 4cm Chord, 0% Cons
Average Pressure (psi)
x/chord
9.17 m/s
12.23 m/s
15.29 m/s
18.35 m/s
21.40 m/s

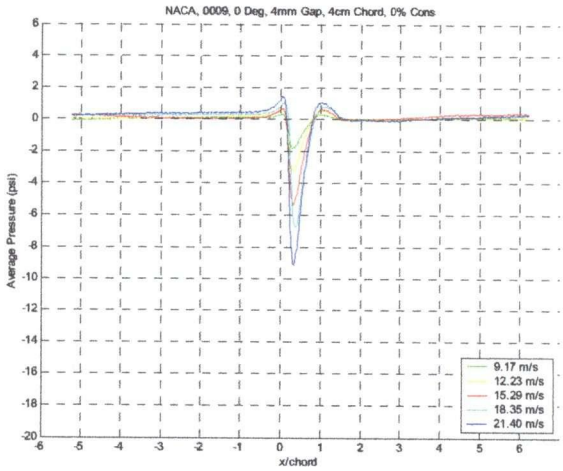
NACA, 0009, 0 Deg, 4mm Gap, 4cm Chord, 0% Cons
Average Pressure (psi)
x/chord
9.17 m/s
12.23 m/s
15.29 m/s
18.35 m/s
21.40 m/s

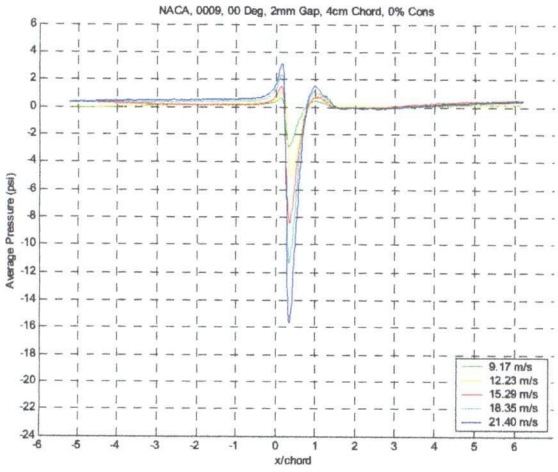
NACA, 0009, 00 Deg, 2mm Gap, 4cm Chord, 0% Cons
Average Pressure (psi)
x/chord
9.17 m/s
12.23 m/s
15.29 m/s
18.35 m/s
21.40 m/s

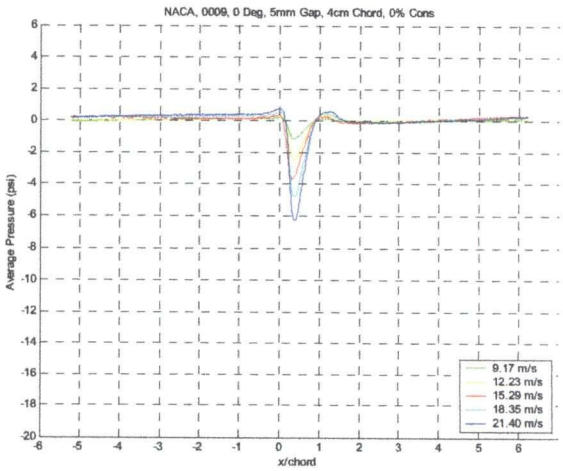
NACA, 0009, 0 Deg, 5mm Gap, 4cm Chord, 0% Cons
Average Pressure (psi)
x/chord
9.17 m/s
12.23 m/s
15.29 m/s
18.35 m/s
21.40 m/s

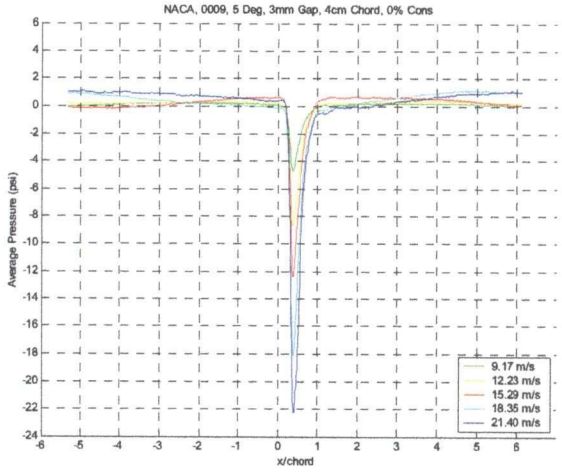
NACA, 0009, 5 Deg, 3mm Gap, 4cm Chord, 0% Cons
Average Pressure (psi)
x/chord
9.17 m/s
12.23 m/s
15.29 m/s
18.35 m/s
21.40 m/s

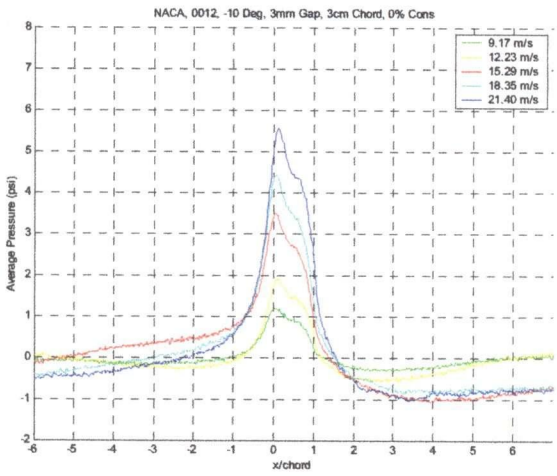
NACA, 0012, -10 Deg, 3mm Gap, 3cm Chord, 0% Cons
Average Pressure (psi)
x/chord
9.17 m/s
12.23 m/s
15.29 m/s
18.35 m/s
21.40 m/s

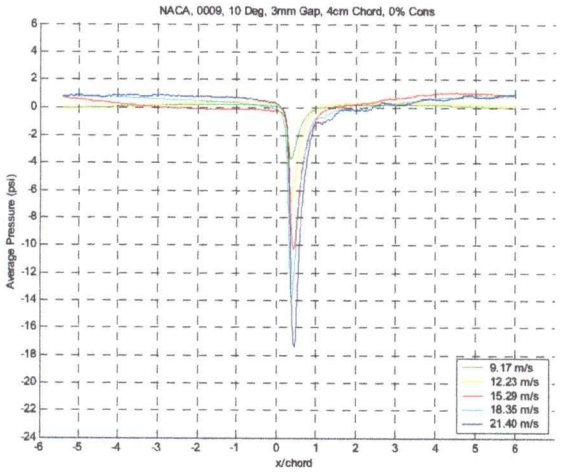
NACA, 0009, 10 Deg, 3mm Gap, 4cm Chord, 0% Cons
Average Pressure (psi)
x/chord
9.17 m/s
12.23 m/s
15.29 m/s
18.35 m/s
21.40 m/s

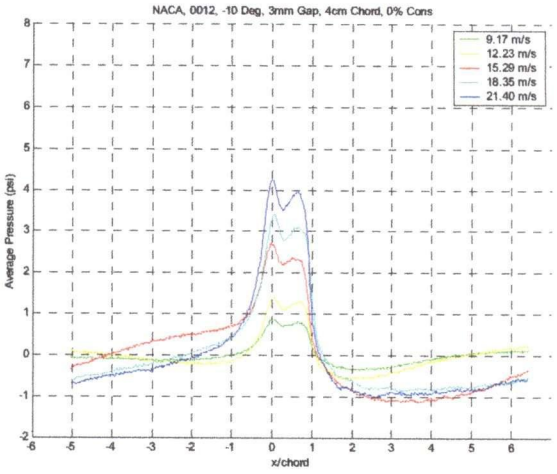
NACA, 0012, -10 Deg, 3mm Gap, 4cm Chord, 0% Cons
Average Pressure (psi)
x/chord
9.17 m/s
12.23 m/s
15.29 m/s
18.35 m/s
21.40 m/s

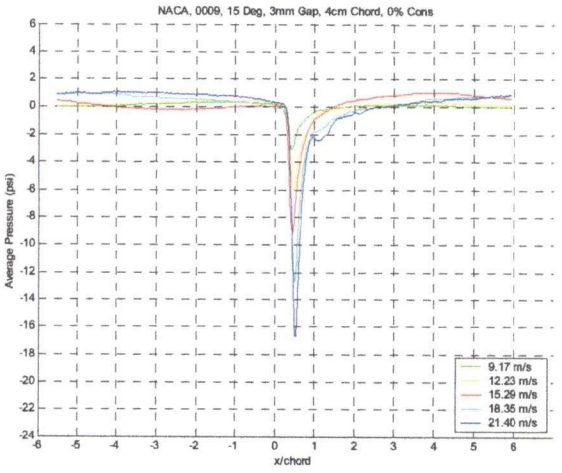
NACA, 0009, 15 Deg, 3mm Gap, 4cm Chord, 0% Cons
Average Pressure (psi)
x/chord
9.17 m/s
12.23 m/s
15.29 m/s
18.35 m/s
21.40 m/s

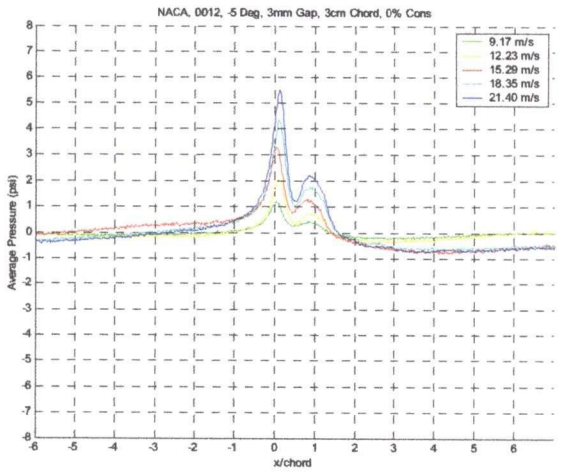
NACA, 0012, -5 Deg, 3mm Gap, 3cm Chord, 0% Cons
Average Pressure (psi)
x/chord
9.17 m/s
12.23 m/s
15.29 m/s
18.35 m/s
21.40 m/s

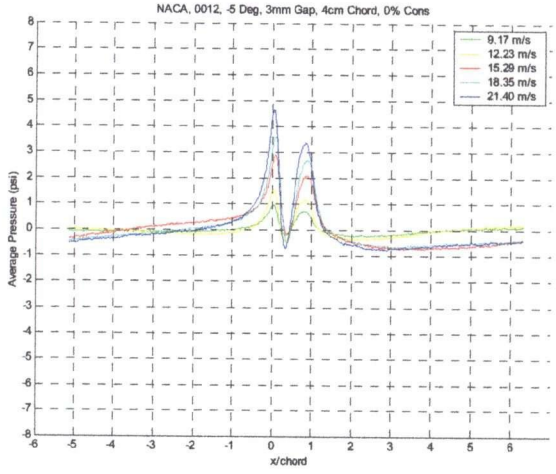
NACA, 0012, -5 Deg, 3mm Gap, 4cm Chord, 0% Cons
9.17 m/s
12.23 m/s
15.29 m/s
18.35 m/s
21.40 m/s
Average Pressure (psi)
x/chord

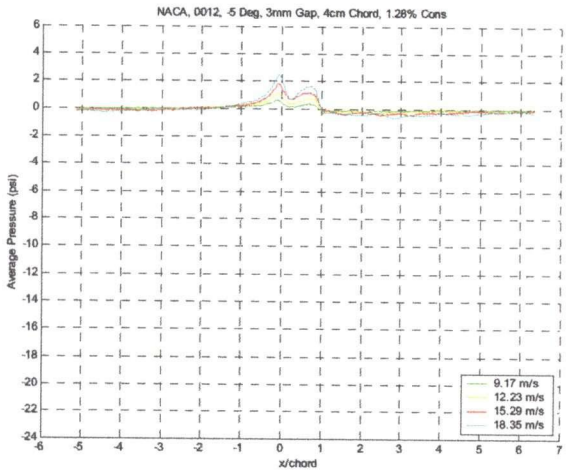
NACA, 0012, -5 Deg, 3mm Gap, 4cm Chord, 1.28% Cons
9.17 m/s
12.23 m/s
15.29 m/s
18.35 m/s
Average Pressure (psi)
x/chord

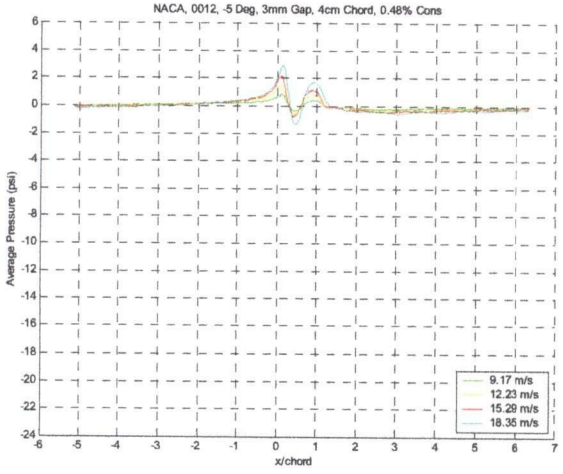
NACA, 0012, -5 Deg, 3mm Gap, 4cm Chord, 0.48% Cons
9.17 m/s
12.23 m/s
15.29 m/s
18.35 m/s
Average Pressure (psi)
x/chord

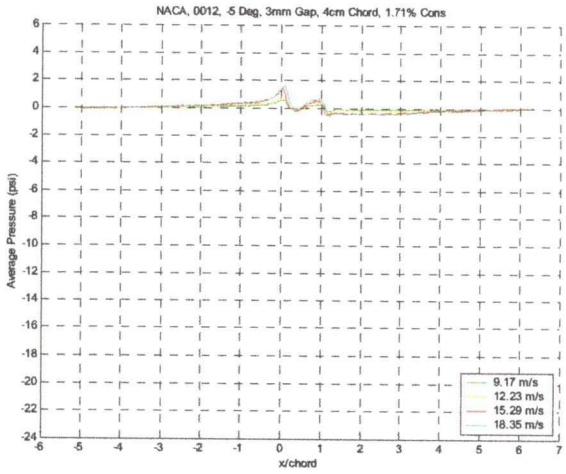
NACA, 0012, -5 Deg, 3mm Gap, 4cm Chord, 1.71% Cons
9.17 m/s
12.23 m/s
15.29 m/s
18.35 m/s
Average Pressure (psi)
x/chord

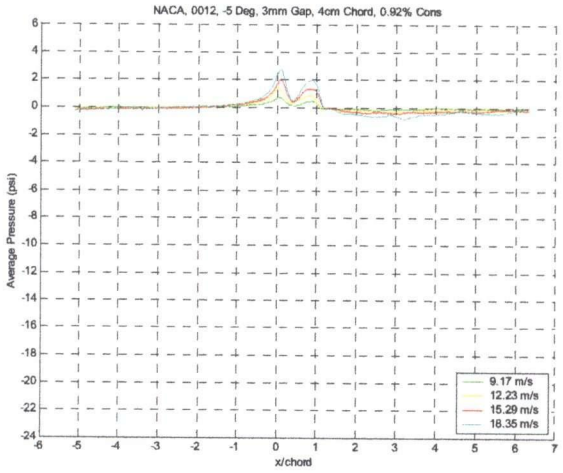
NACA, 0012, -5 Deg, 3mm Gap, 4cm Chord, 0.92% Cons
9.17 m/s
12.23 m/s
15.29 m/s
18.35 m/s
Average Pressure (psi)
x/chord

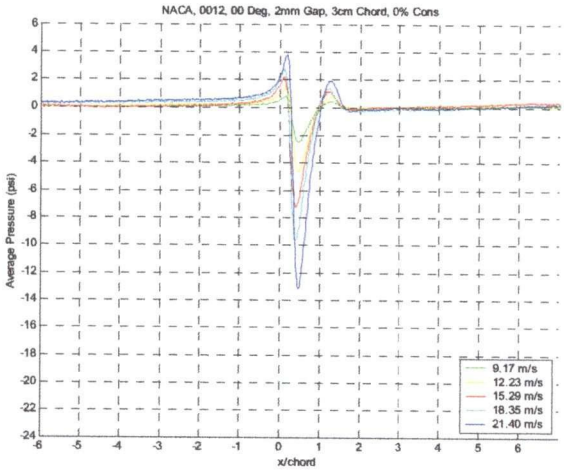
NACA, 0012, 00 Deg, 2mm Gap, 3cm Chord, 0% Cons
9.17 m/s
12.23 m/s
15.29 m/s
18.35 m/s
21.40 m/s
Average Pressure (psi)
x/chord

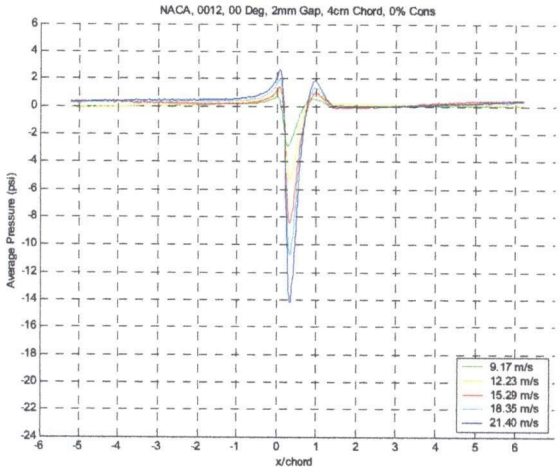
NACA, 0012, 00 Deg, 2mm Gap, 4cm Chord, 0% Cons
Average Pressure (psi)
x/chord
9.17 m/s
12.23 m/s
15.29 m/s
18.35 m/s
21.40 m/s

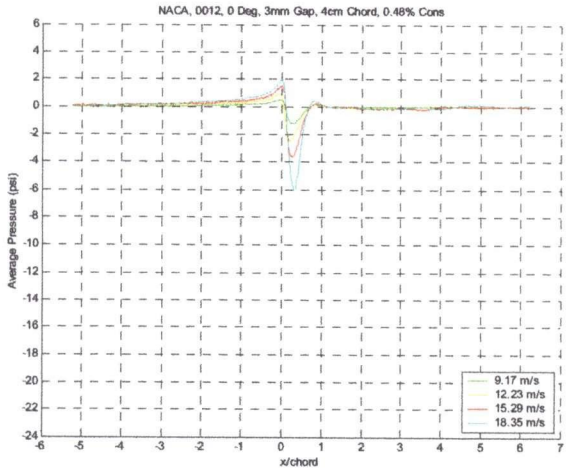
NACA, 0012, 0 Deg, 3mm Gap, 4cm Chord, 0.48% Cons
Average Pressure (psi)
x/chord
9.17 m/s
12.23 m/s
15.29 m/s
18.35 m/s

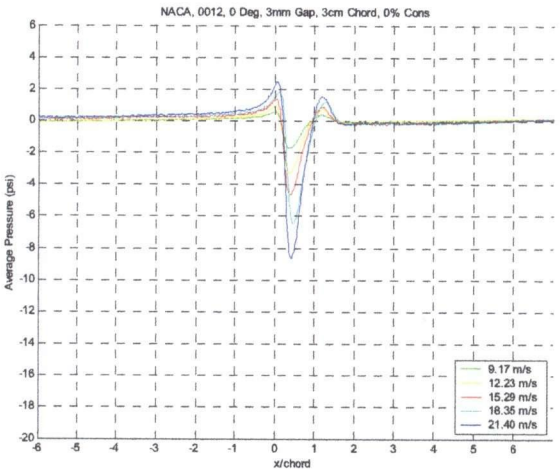
NACA, 0012, 0 Deg, 3mm Gap, 3cm Chord, 0% Cons
Average Pressure (psi)
x/chord
9.17 m/s
12.23 m/s
15.29 m/s
18.35 m/s
21.40 m/s

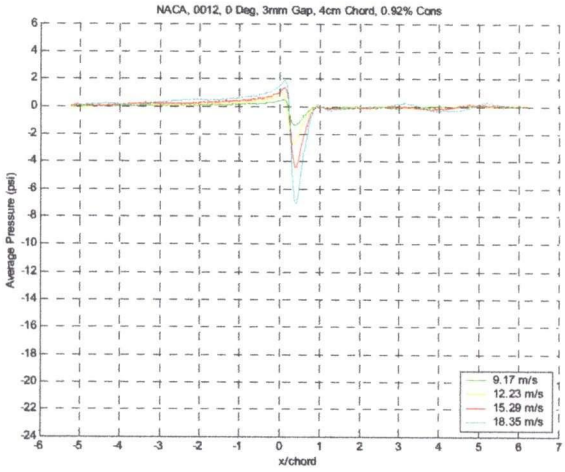
NACA, 0012, 0 Deg, 3mm Gap, 4cm Chord, 0.92% Cons
Average Pressure (psi)
x/chord
9.17 m/s
12.23 m/s
15.29 m/s
18.35 m/s

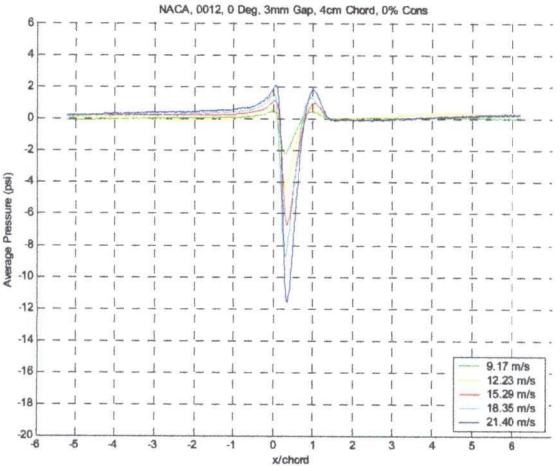
NACA, 0012, 0 Deg, 3mm Gap, 4cm Chord, 0% Cons
Average Pressure (psi)
x/chord
9.17 m/s
12.23 m/s
15.29 m/s
18.35 m/s
21.40 m/s

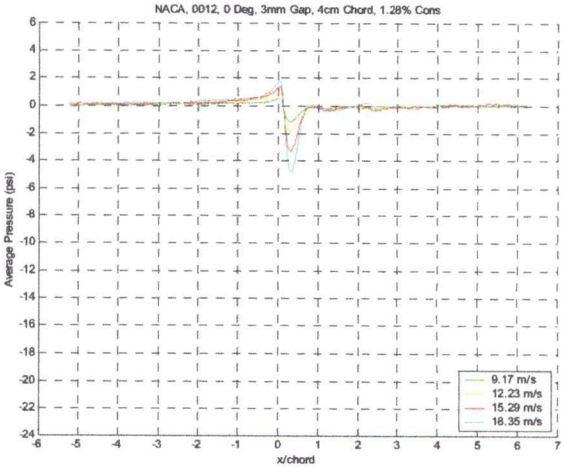
NACA, 0012, 0 Deg, 3mm Gap, 4cm Chord, 1.28% Cons
Average Pressure (psi)
x/chord
9.17 m/s
12.23 m/s
15.29 m/s
18.35 m/s

Appendix 2 – The Effect of Rotor Tip Speed on Suction Pulse Magnitude

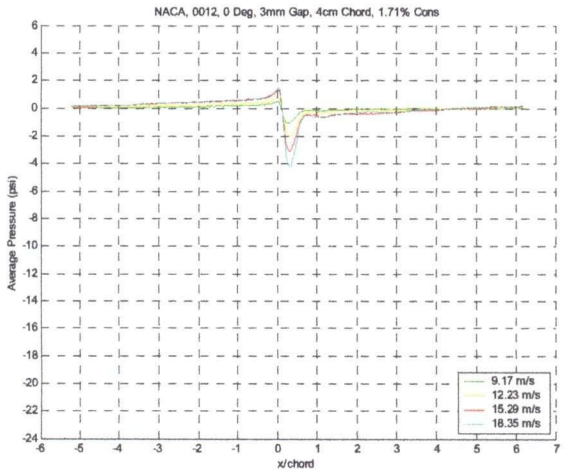

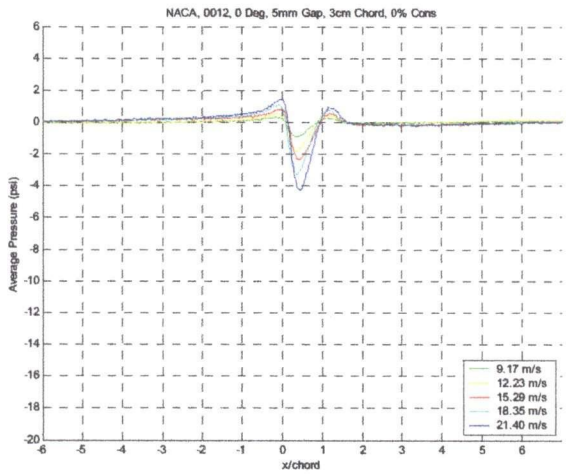

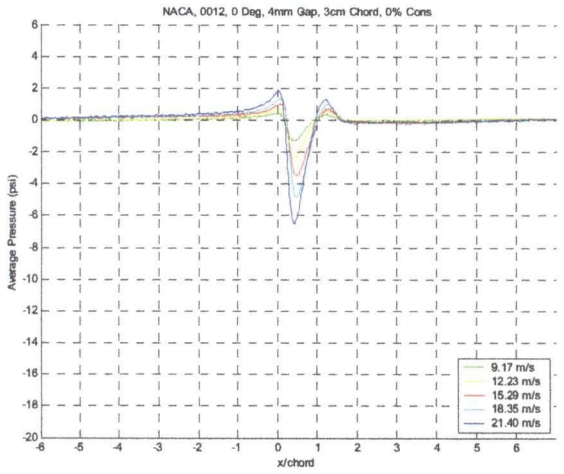

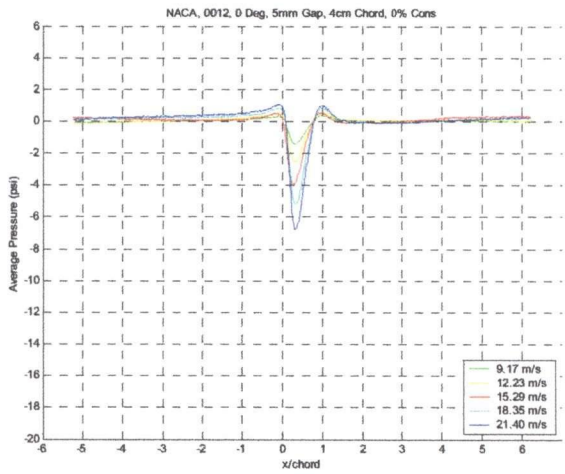

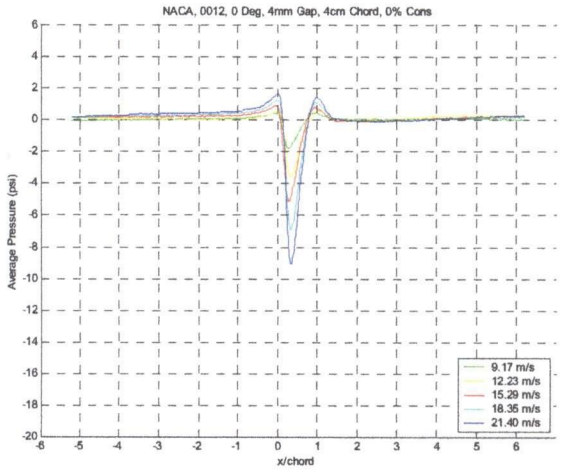

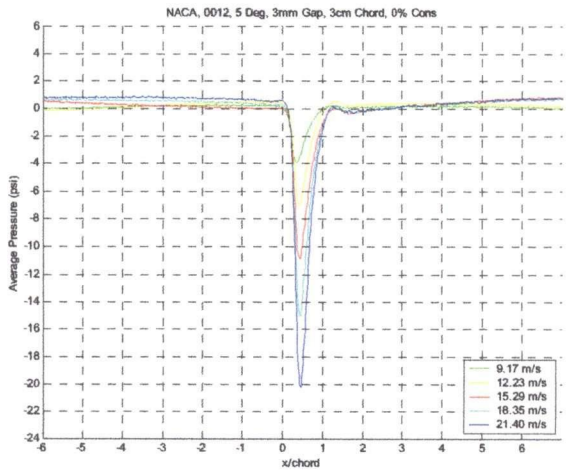

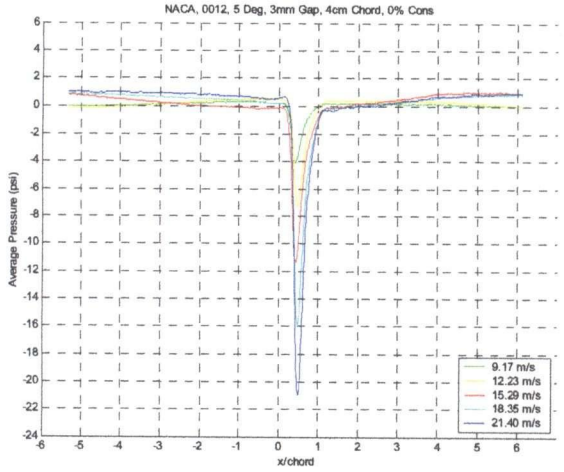
NACA, 0012, 5 Deg, 3mm Gap, 4cm Chord, 0% Cons
Average Pressure (psi)
x/chord
9.17 m/s
12.23 m/s
15.29 m/s
18.35 m/s
21.40 m/s

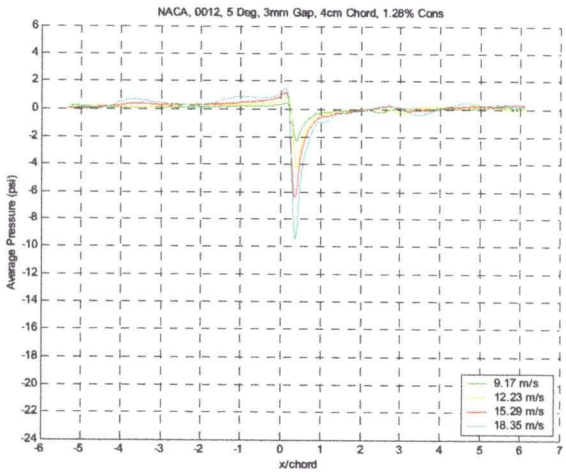
NACA, 0012, 5 Deg, 3mm Gap, 4cm Chord, 1.28% Cons
Average Pressure (psi)
x/chord
9.17 m/s
12.23 m/s
15.29 m/s
18.35 m/s

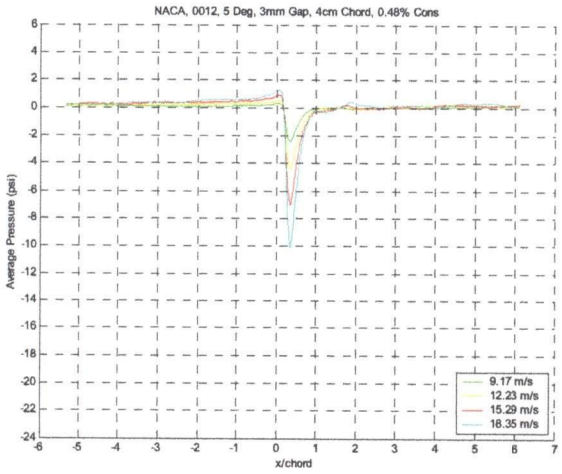
NACA, 0012, 5 Deg, 3mm Gap, 4cm Chord, 0.48% Cons
Average Pressure (psi)
x/chord
9.17 m/s
12.23 m/s
15.29 m/s
18.35 m/s

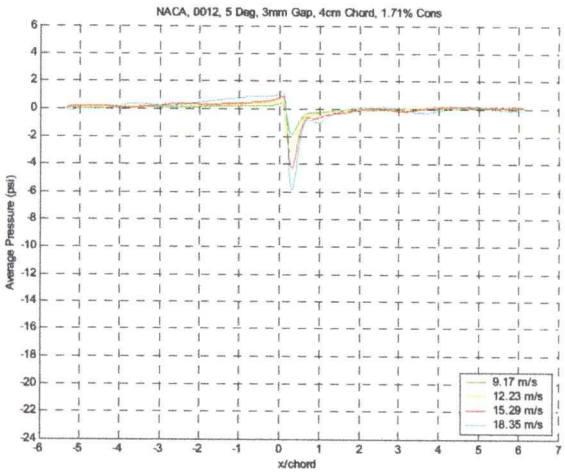
NACA, 0012, 5 Deg, 3mm Gap, 4cm Chord, 1.71% Cons
Average Pressure (psi)
x/chord
9.17 m/s
12.23 m/s
15.29 m/s
18.35 m/s

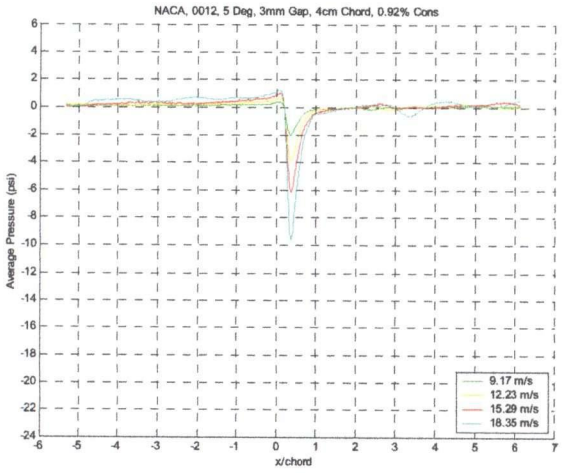
NACA, 0012, 5 Deg, 3mm Gap, 4cm Chord, 0.92% Cons
Average Pressure (psi)
x/chord
9.17 m/s
12.23 m/s
15.29 m/s
18.35 m/s

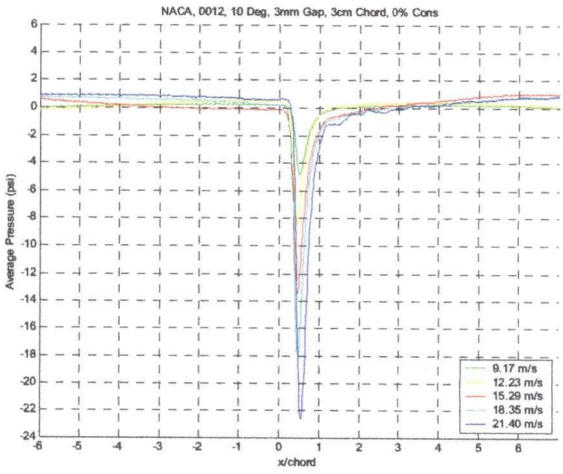
NACA, 0012, 10 Deg, 3mm Gap, 3cm Chord, 0% Cons
Average Pressure (psi)
x/chord
9.17 m/s
12.23 m/s
15.29 m/s
18.35 m/s
21.40 m/s

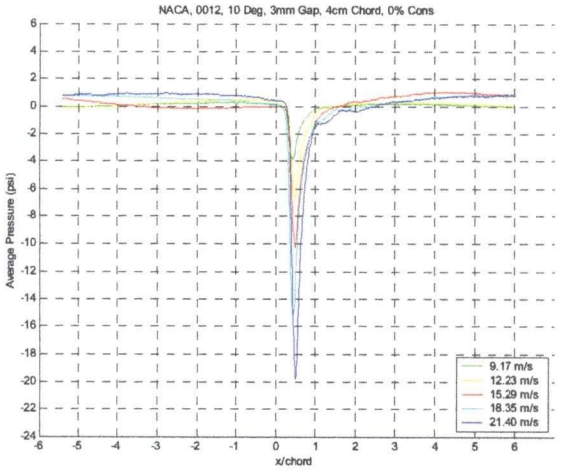
NACA, 0012, 10 Deg, 3mm Gap, 4cm Chord, 0% Cons
Average Pressure (psi)
x/chord
9.17 m/s
12.23 m/s
15.29 m/s
18.35 m/s
21.40 m/s

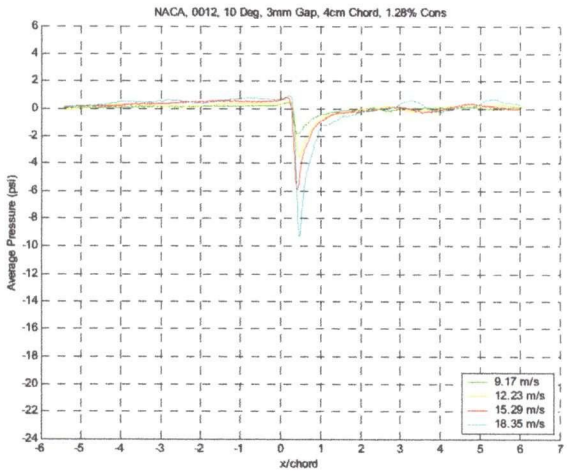
NACA, 0012, 10 Deg, 3mm Gap, 4cm Chord, 1.28% Cons
Average Pressure (psi)
x/chord
9.17 m/s
12.23 m/s
15.29 m/s
18.35 m/s

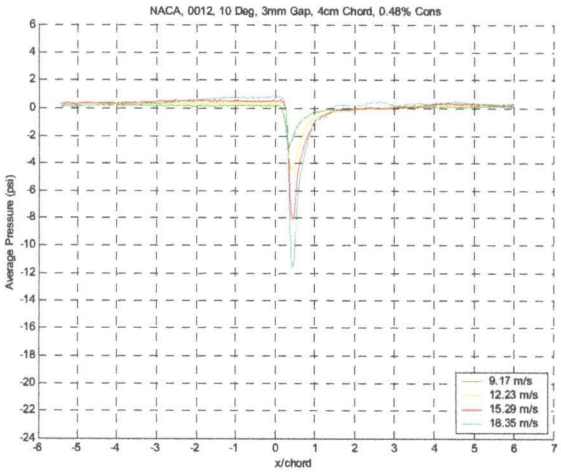
NACA, 0012, 10 Deg, 3mm Gap, 4cm Chord, 0.48% Cons
Average Pressure (psi)
x/chord
9.17 m/s
12.23 m/s
15.29 m/s
18.35 m/s

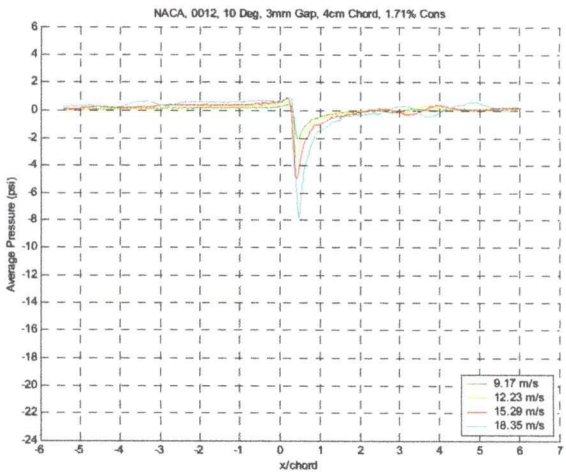
NACA, 0012, 10 Deg, 3mm Gap, 4cm Chord, 1.71% Cons
Average Pressure (psi)
x/chord
9.17 m/s
12.23 m/s
15.29 m/s
18.35 m/s

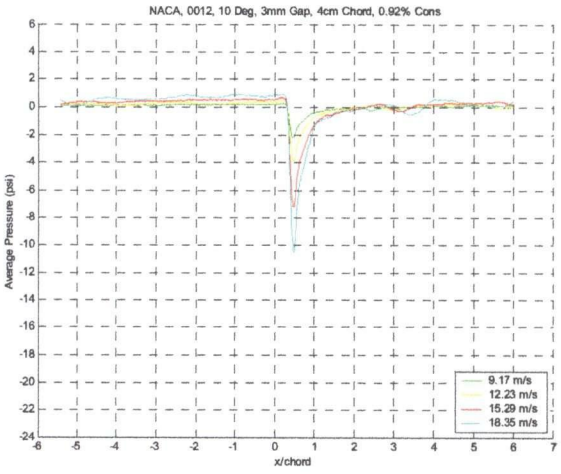
NACA, 0012, 10 Deg, 3mm Gap, 4cm Chord, 0.92% Cons
Average Pressure (psi)
x/chord
9.17 m/s
12.23 m/s
15.29 m/s
18.35 m/s

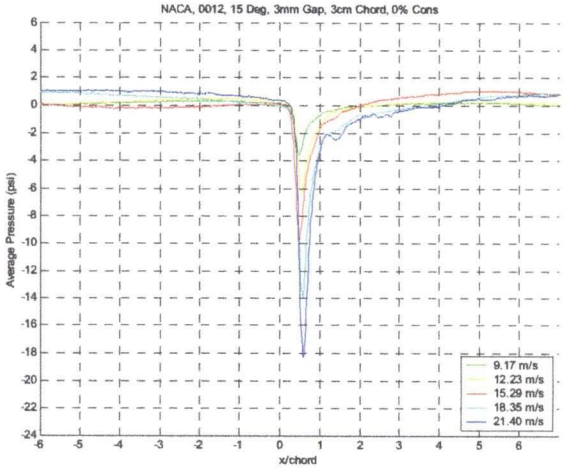
NACA, 0012, 15 Deg, 3mm Gap, 3cm Chord, 0% Cons
Average Pressure (psi)
x/chord
9.17 m/s
12.23 m/s
15.29 m/s
18.35 m/s
21.40 m/s

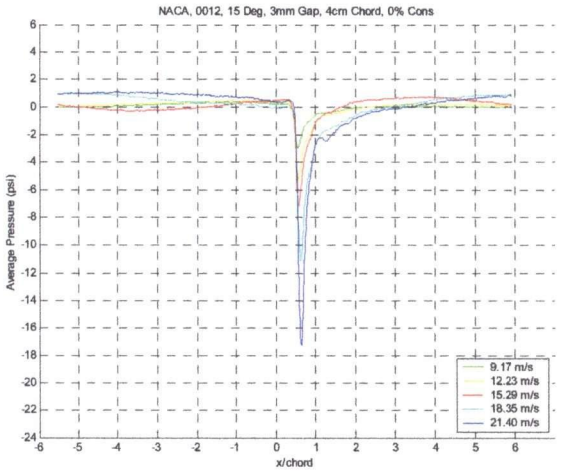
NACA, 0012, 15 Deg, 3mm Gap, 4cm Chord, 0% Cons
Average Pressure (psi)
x/chord
9.17 m/s
12.23 m/s
15.29 m/s
18.35 m/s
21.40 m/s

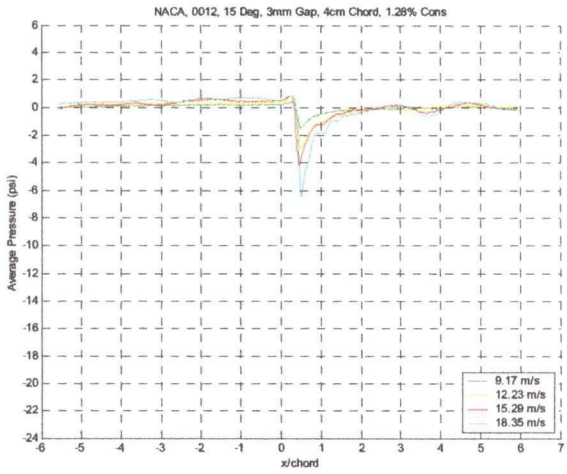
NACA, 0012, 15 Deg, 3mm Gap, 4cm Chord, 1.28% Cons
Average Pressure (psi)
x/chord
9.17 m/s
12.23 m/s
15.29 m/s
18.35 m/s

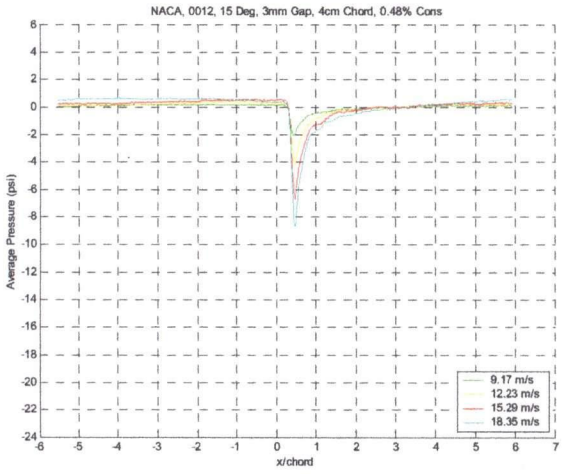
NACA, 0012, 15 Deg, 3mm Gap, 4cm Chord, 0.48% Cons
Average Pressure (psi)
x/chord
9.17 m/s
12.23 m/s
15.29 m/s
18.35 m/s

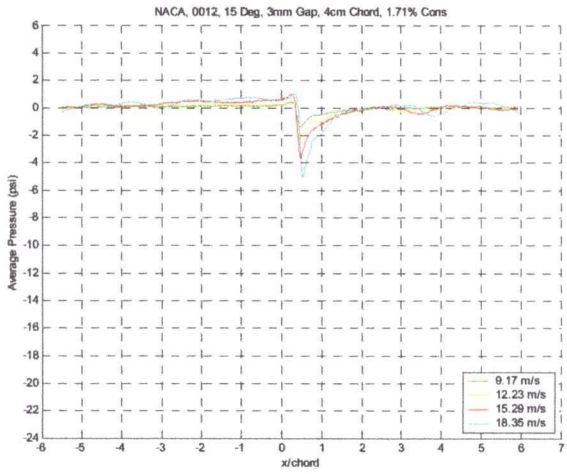
NACA, 0012, 15 Deg, 3mm Gap, 4cm Chord, 1.71% Cons
Average Pressure (psi)
x/chord
9.17 m/s
12.23 m/s
15.29 m/s
18.35 m/s

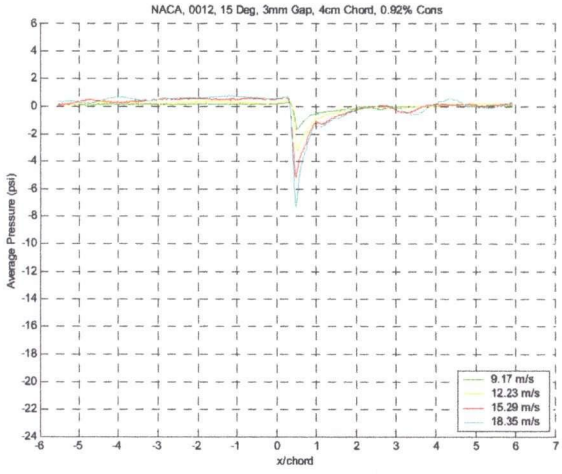
NACA, 0012, 15 Deg, 3mm Gap, 4cm Chord, 0.92% Cons
Average Pressure (psi)
x/chord
9.17 m/s
12.23 m/s
15.29 m/s
18.35 m/s

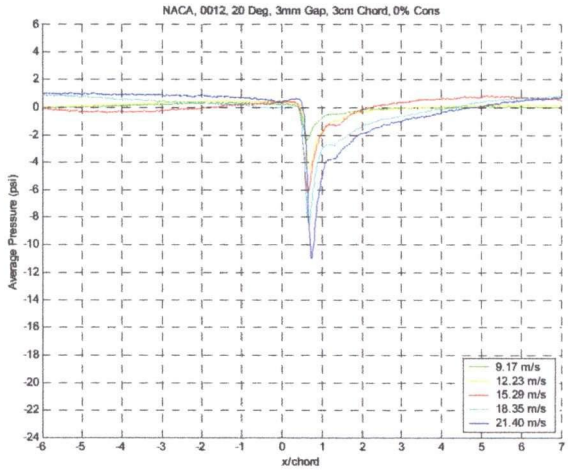
NACA, 0012, 20 Deg, 3mm Gap, 3cm Chord, 0% Cons
Average Pressure (psi)
x/chord
9.17 m/s
12.23 m/s
15.29 m/s
18.35 m/s
21.40 m/s

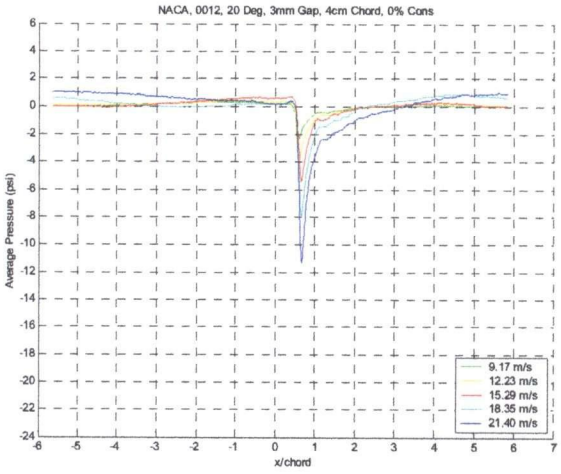
NACA, 0012, 20 Deg, 3mm Gap, 4cm Chord, 0% Cons
Average Pressure (psi)
x/chord
9.17 m/s
12.23 m/s
15.29 m/s
18.35 m/s
21.40 m/s

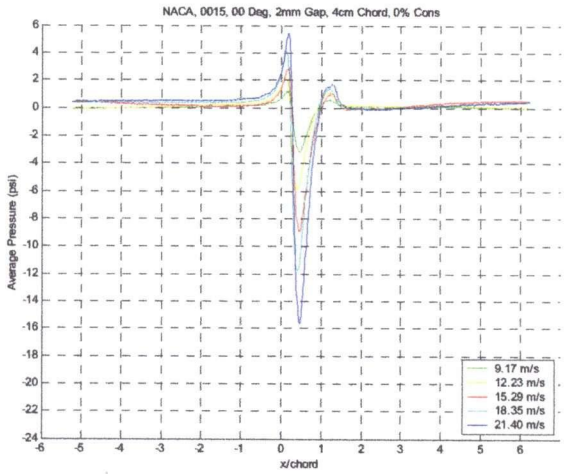
NACA, 0015, 00 Deg, 2mm Gap, 4cm Chord, 0% Cons
Average Pressure (psi)
x/chord
9.17 m/s
12.23 m/s
15.29 m/s
18.35 m/s
21.40 m/s

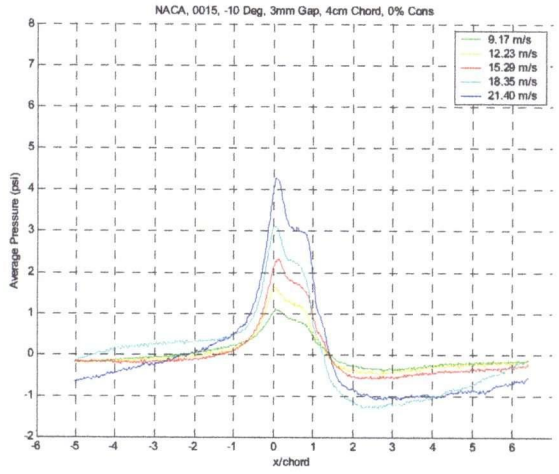
NACA, 0015, -10 Deg, 3mm Gap, 4cm Chord, 0% Cons
Average Pressure (psi)
x/chord
9.17 m/s
12.23 m/s
15.29 m/s
18.35 m/s
21.40 m/s

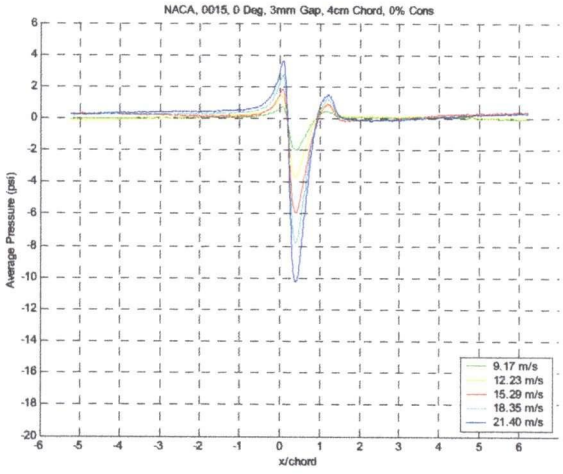
NACA, 0015, 0 Deg, 3mm Gap, 4cm Chord, 0% Cons
Average Pressure (psi)
x/chord
9.17 m/s
12.23 m/s
15.29 m/s
18.35 m/s
21.40 m/s

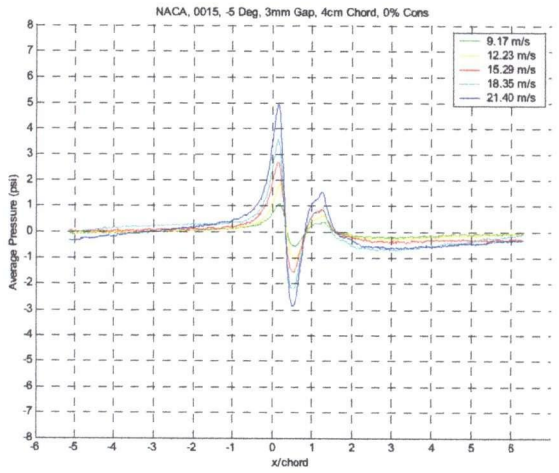
NACA, 0015, -5 Deg, 3mm Gap, 4cm Chord, 0% Cons
Average Pressure (psi)
x/chord
9.17 m/s
12.23 m/s
15.29 m/s
18.35 m/s
21.40 m/s

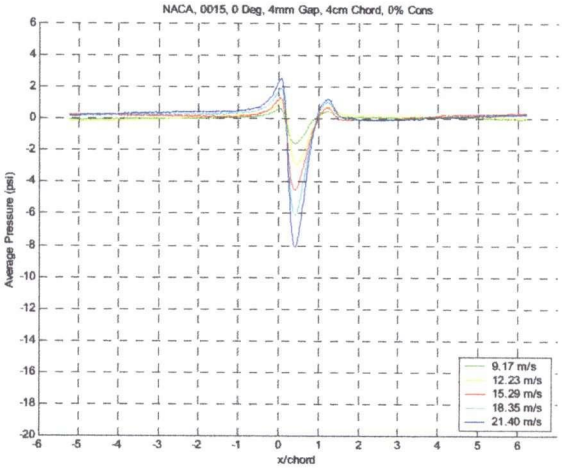
NACA, 0015, 0 Deg, 4mm Gap, 4cm Chord, 0% Cons
Average Pressure (psi)
x/chord
9.17 m/s
12.23 m/s
15.29 m/s
18.35 m/s
21.40 m/s

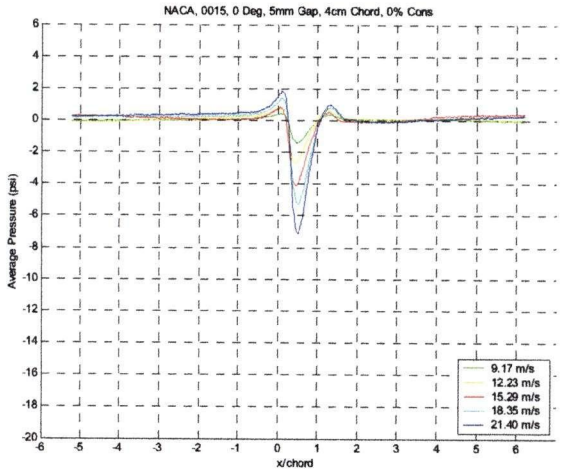
NACA, 0015, 0 Deg, 5mm Gap, 4cm Chord, 0% Cons
Average Pressure (psi)
x/chord
9.17 m/s
12.23 m/s
15.29 m/s
18.35 m/s
21.40 m/s

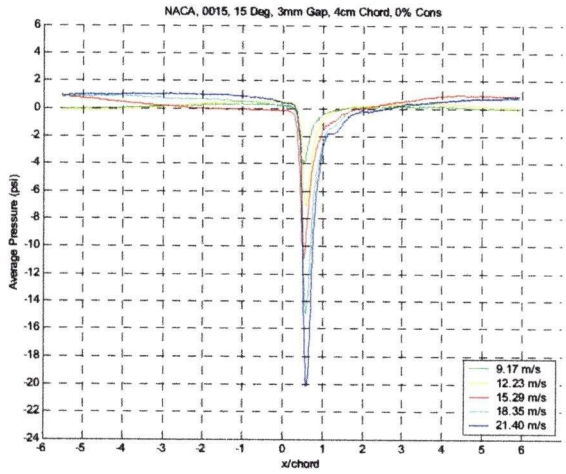
NACA, 0015, 15 Deg, 3mm Gap, 4cm Chord, 0% Cons
Average Pressure (psi)
x/chord
9.17 m/s
12.23 m/s
15.29 m/s
18.35 m/s
21.40 m/s

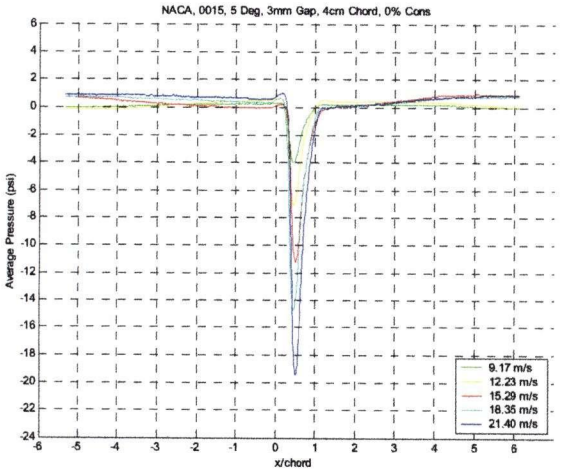
NACA, 0015, 5 Deg, 3mm Gap, 4cm Chord, 0% Cons
Average Pressure (psi)
x/chord
9.17 m/s
12.23 m/s
15.29 m/s
18.35 m/s
21.40 m/s

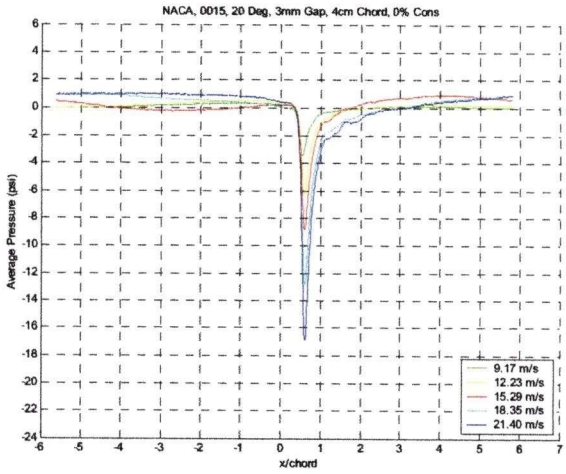
NACA, 0015, 20 Deg, 3mm Gap, 4cm Chord, 0% Cons
Average Pressure (psi)
x/chord
9.17 m/s
12.23 m/s
15.29 m/s
18.35 m/s
21.40 m/s

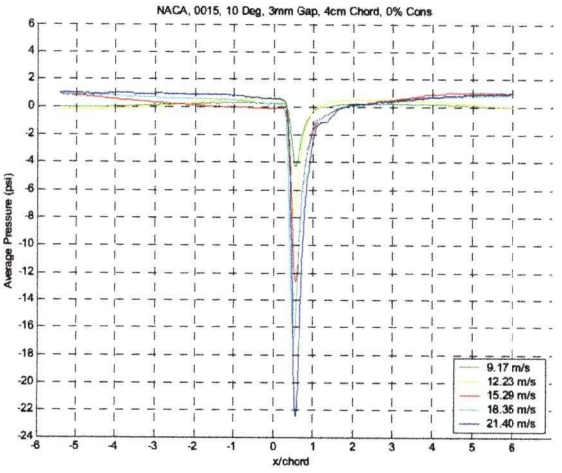
NACA, 0015, 10 Deg, 3mm Gap, 4cm Chord, 0% Cons
Average Pressure (psi)
x/chord
9.17 m/s
12.23 m/s
15.29 m/s
18.35 m/s
21.40 m/s

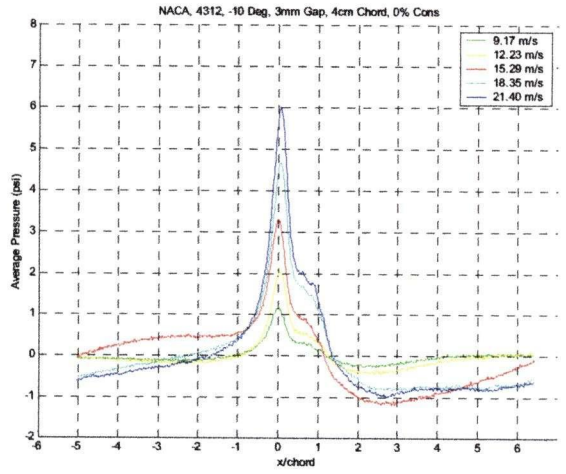
NACA, 4312, -10 Deg, 3mm Gap, 4cm Chord, 0% Cons
Average Pressure (psi)
x/chord
9.17 m/s
12.23 m/s
15.29 m/s
18.35 m/s
21.40 m/s

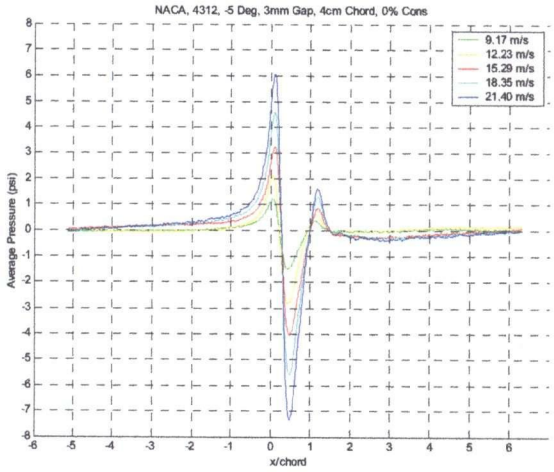
NACA, 4312, -5 Deg, 3mm Gap, 4cm Chord, 0% Cons
Average Pressure (psi)
x/chord
9.17 m/s
12.23 m/s
15.29 m/s
18.35 m/s
21.40 m/s

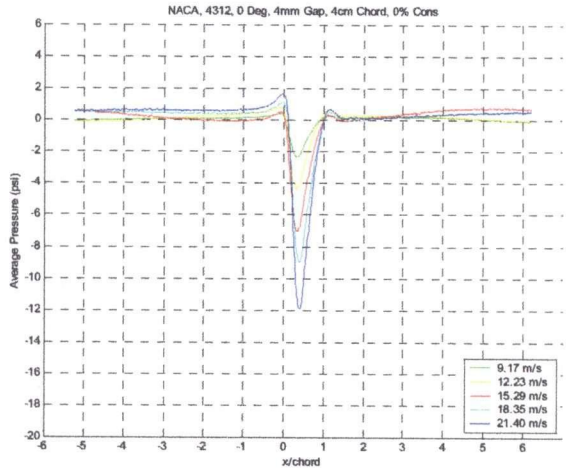
NACA, 4312, 0 Deg, 4mm Gap, 4cm Chord, 0% Cons
Average Pressure (psi)
x/chord
9.17 m/s
12.23 m/s
15.29 m/s
18.35 m/s
21.40 m/s

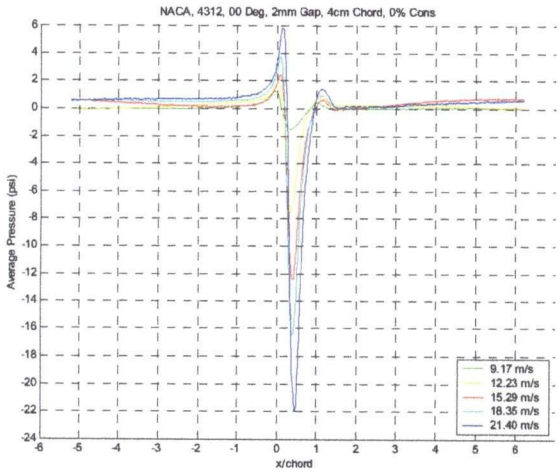
NACA, 4312, 00 Deg, 2mm Gap, 4cm Chord, 0% Cons
Average Pressure (psi)
x/chord
9.17 m/s
12.23 m/s
15.29 m/s
18.35 m/s
21.40 m/s

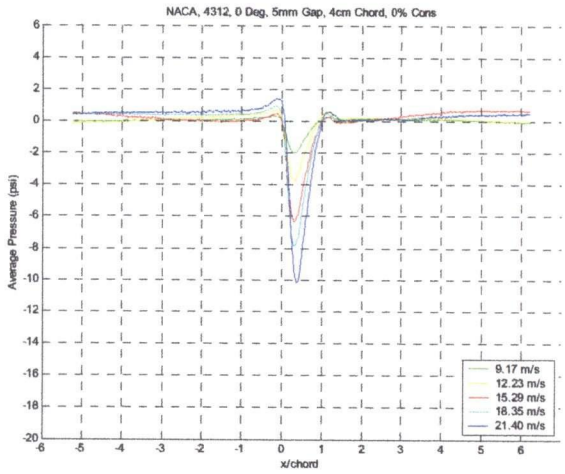
NACA, 4312, 0 Deg, 5mm Gap, 4cm Chord, 0% Cons
Average Pressure (psi)
x/chord
9.17 m/s
12.23 m/s
15.29 m/s
18.35 m/s
21.40 m/s

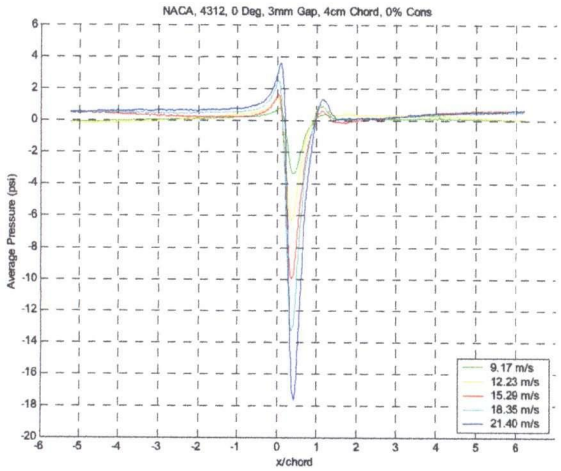
NACA, 4312, 0 Deg, 3mm Gap, 4cm Chord, 0% Cons
Average Pressure (psi)
x/chord
9.17 m/s
12.23 m/s
15.29 m/s
18.35 m/s
21.40 m/s

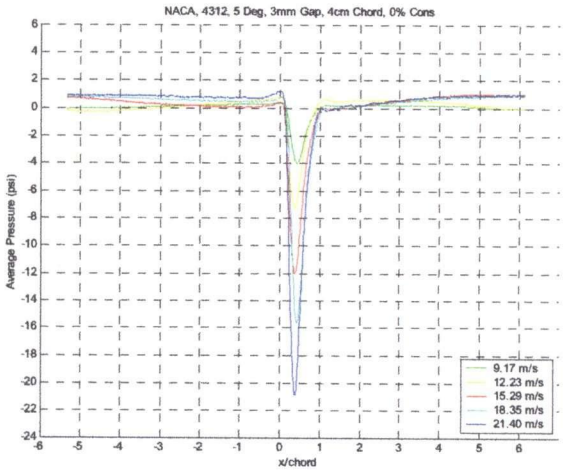
NACA, 4312, 5 Deg, 3mm Gap, 4cm Chord, 0% Cons
Average Pressure (psi)
x/chord
9.17 m/s
12.23 m/s
15.29 m/s
18.35 m/s
21.40 m/s

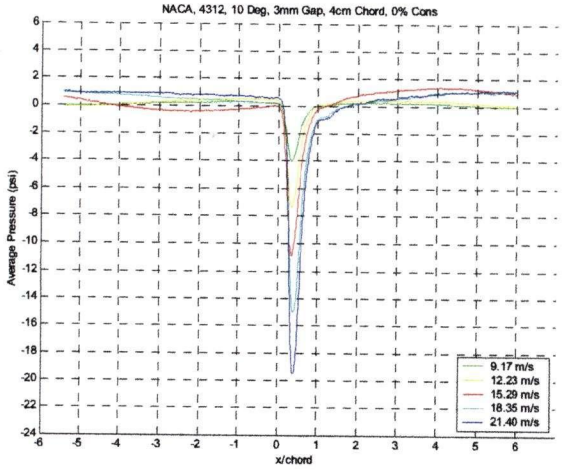
NACA, 4312, 10 Deg, 3mm Gap, 4cm Chord, 0% Cons
Average Pressure (psi)
x/chord
9.17 m/s
12.23 m/s
15.29 m/s
18.35 m/s
21.40 m/s

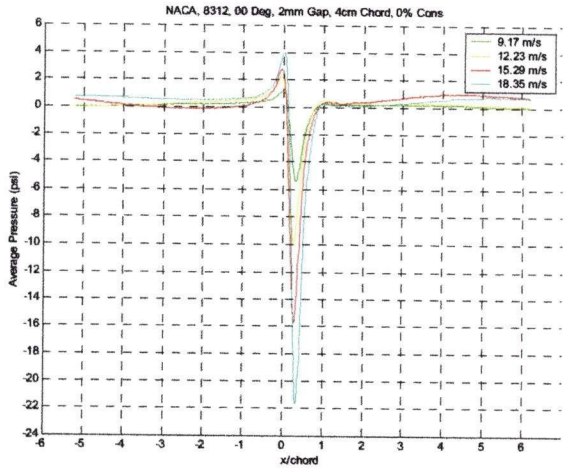
NACA, 8312, 00 Deg, 2mm Gap, 4cm Chord, 0% Cons
Average Pressure (psi)
x/chord
9.17 m/s
12.23 m/s
15.29 m/s
18.35 m/s

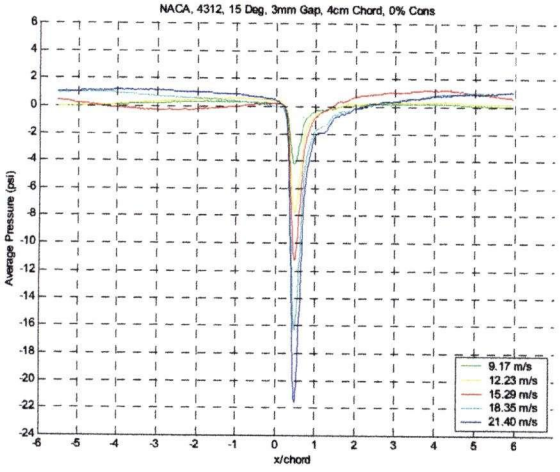
NACA, 4312, 15 Deg, 3mm Gap, 4cm Chord, 0% Cons
Average Pressure (psi)
x/chord
9.17 m/s
12.23 m/s
15.29 m/s
18.35 m/s
21.40 m/s

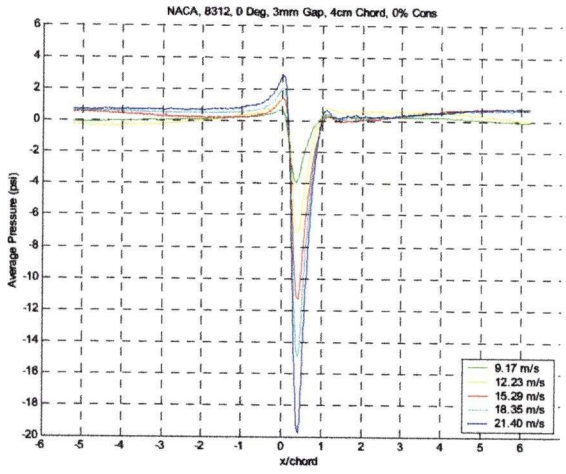
NACA, 8312, 0 Deg, 3mm Gap, 4cm Chord, 0% Cons
Average Pressure (psi)
x/chord
9.17 m/s
12.23 m/s
15.29 m/s
18.35 m/s
21.40 m/s

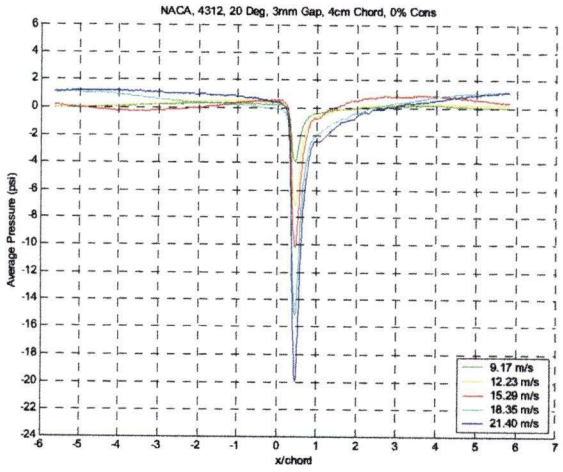
NACA, 4312, 20 Deg, 3mm Gap, 4cm Chord, 0% Cons
Average Pressure (psi)
x/chord
9.17 m/s
12.23 m/s
15.29 m/s
18.35 m/s
21.40 m/s

Appendix 2 – The Effect of Rotor Tip Speed on Suction Pulse Magnitude

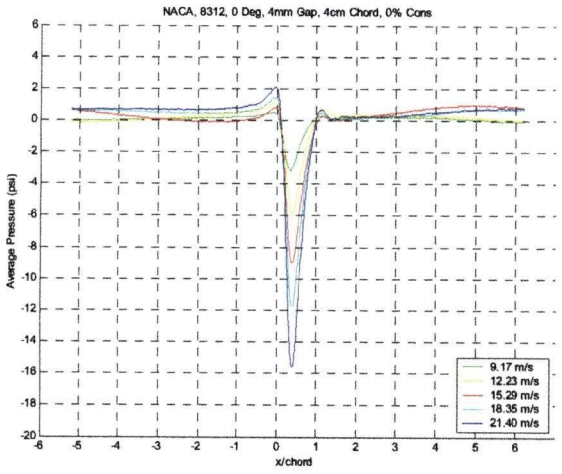

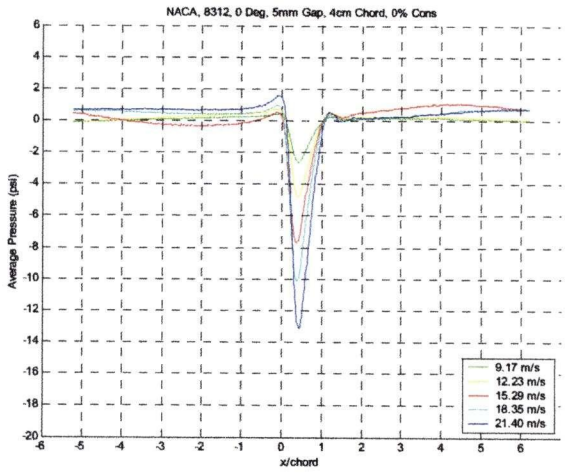

Appendix 3

Collapsed Pressure Pulse
c_p Curves

Appendix 3 – Collapsed Pressure Pulse c_p Curves

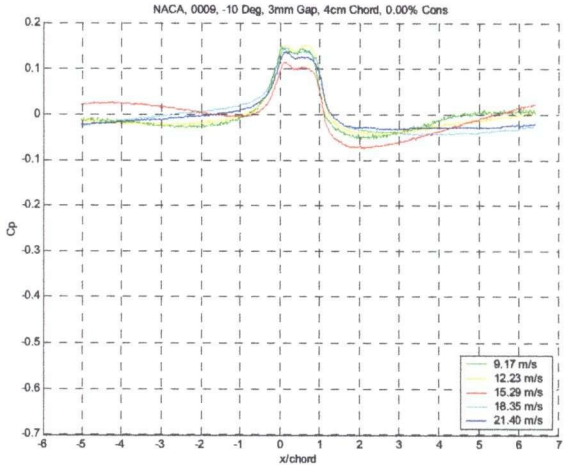

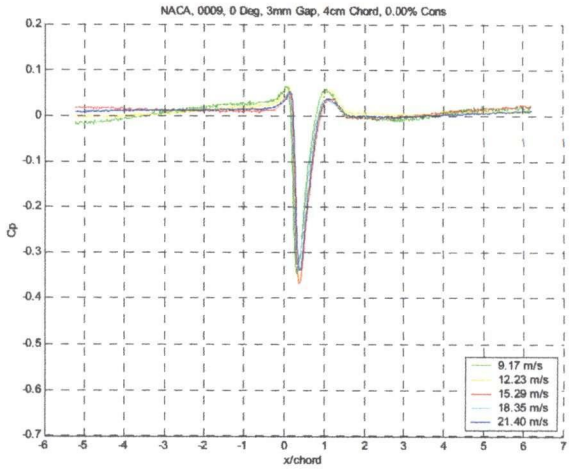

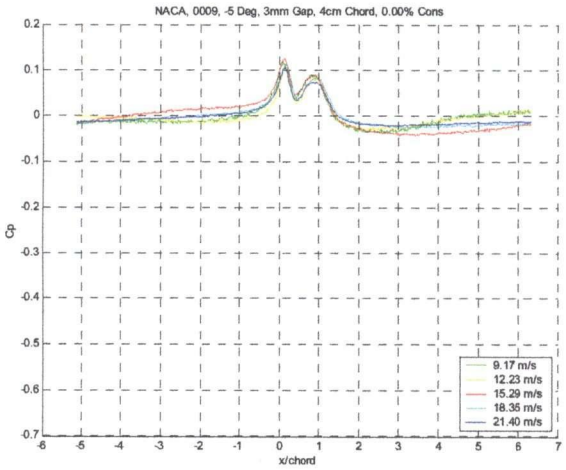

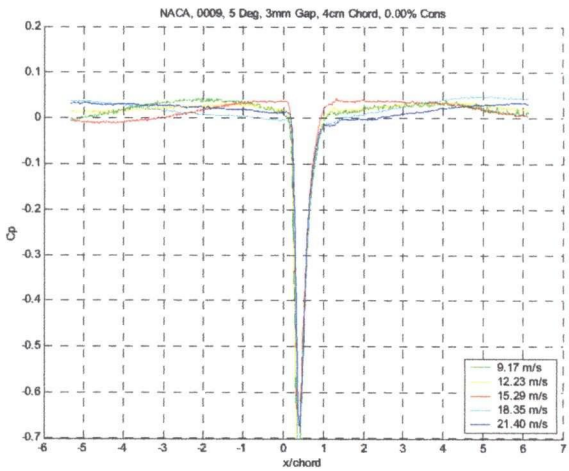

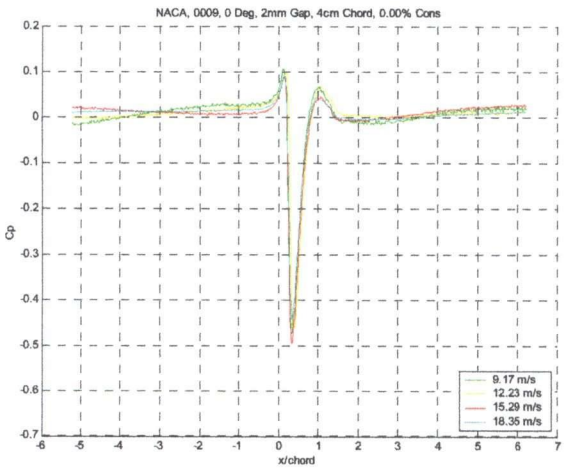

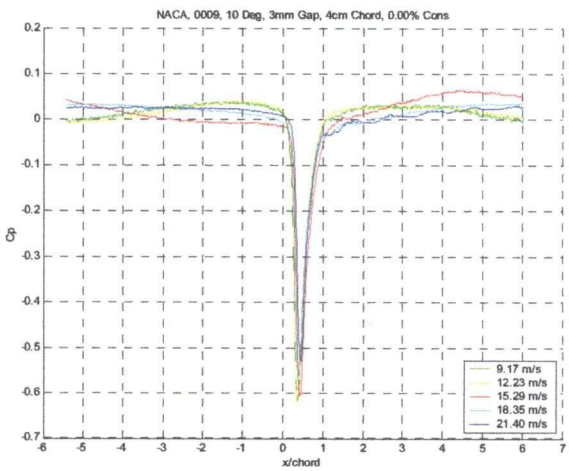

Appendix 3 – Collapsed Pressure Pulse c_p Curves

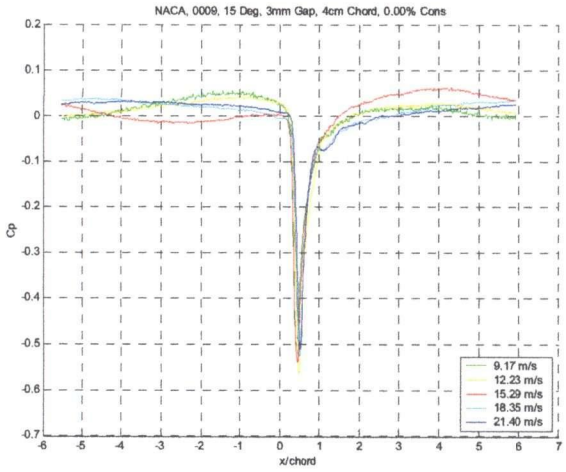

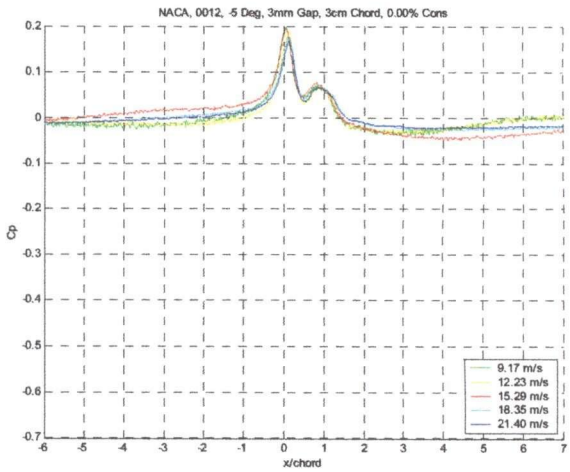

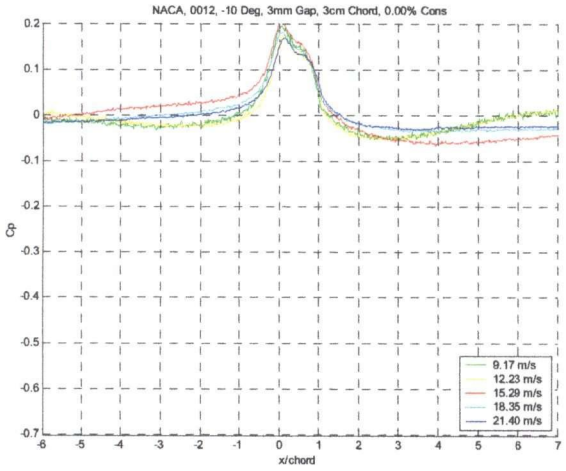

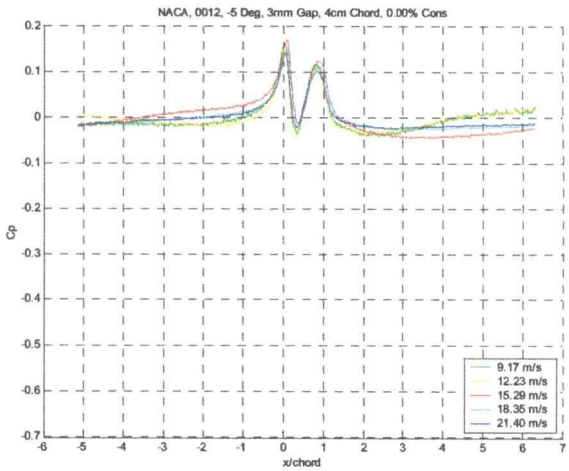

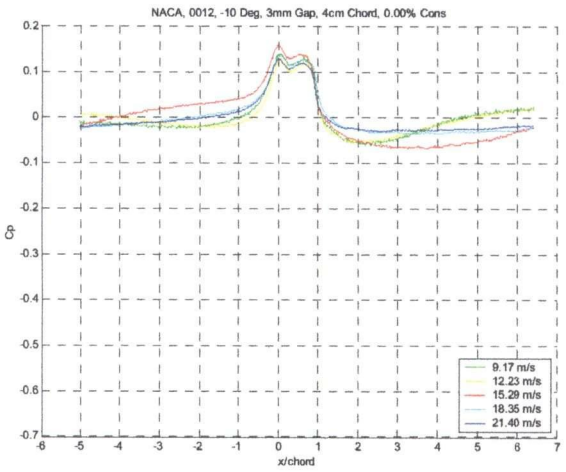

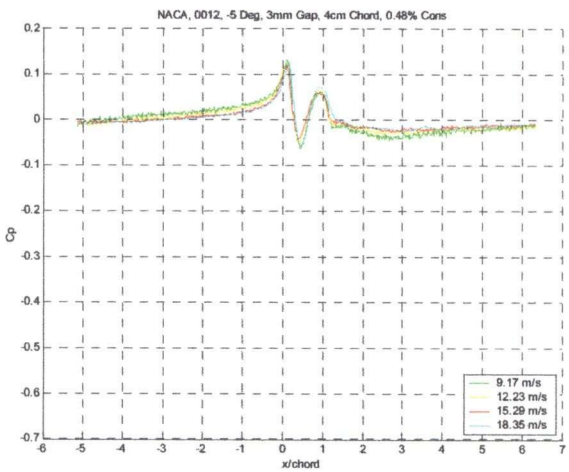

Appendix 3 – Collapsed Pressure Pulse c_p Curves

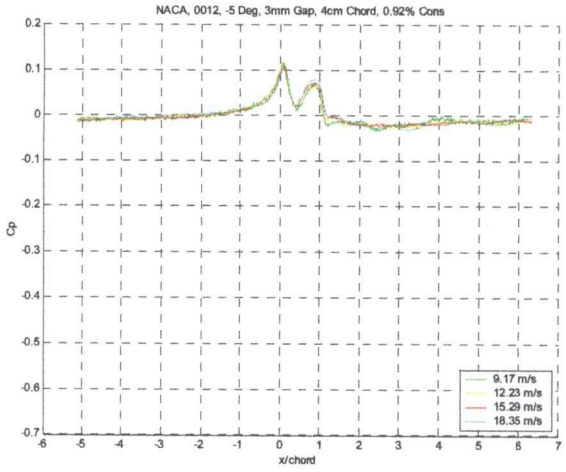

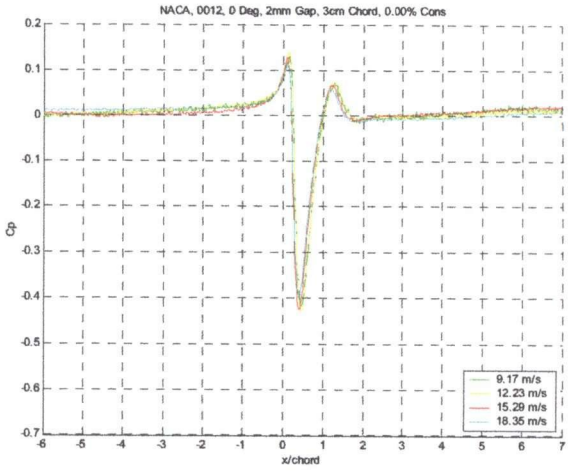

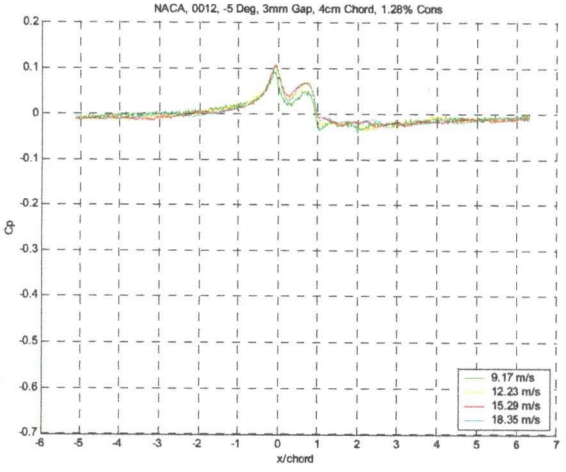

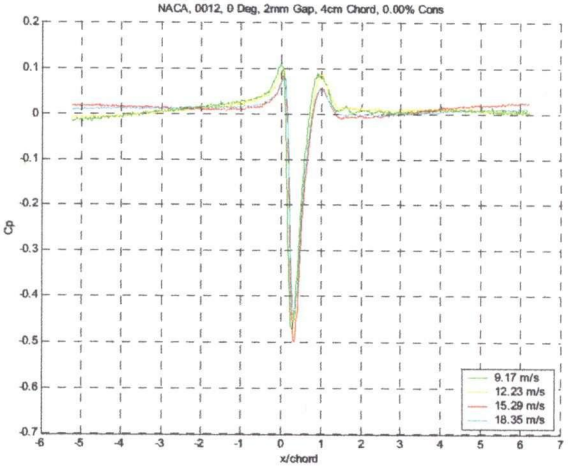

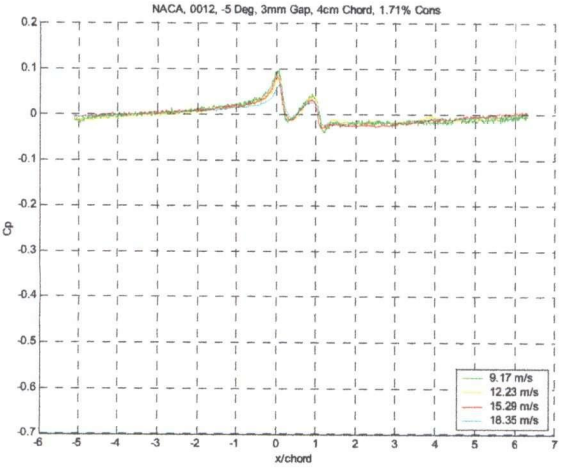

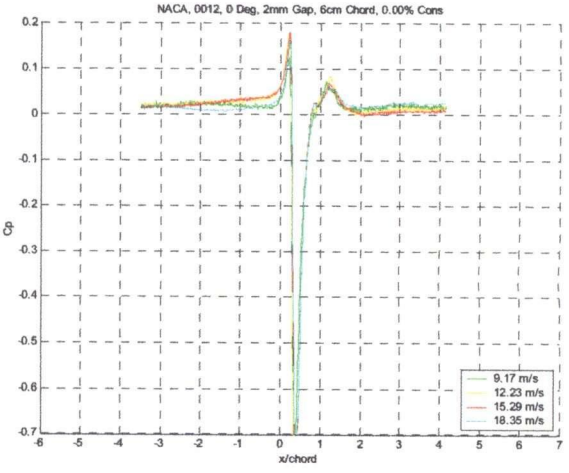

Appendix 3 – Collapsed Pressure Pulse c_p Curves

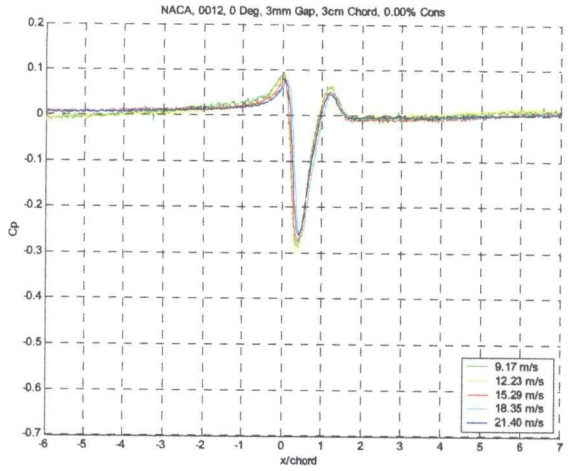

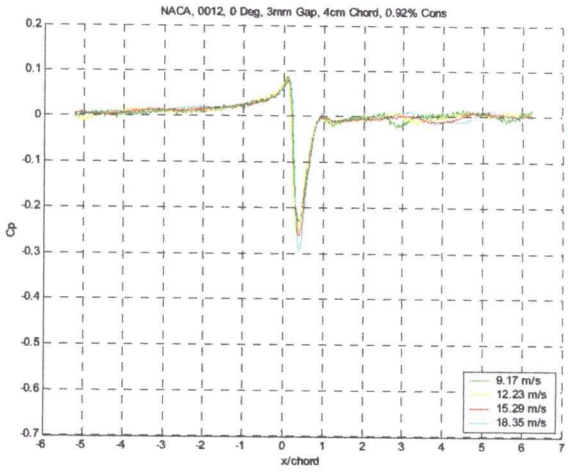

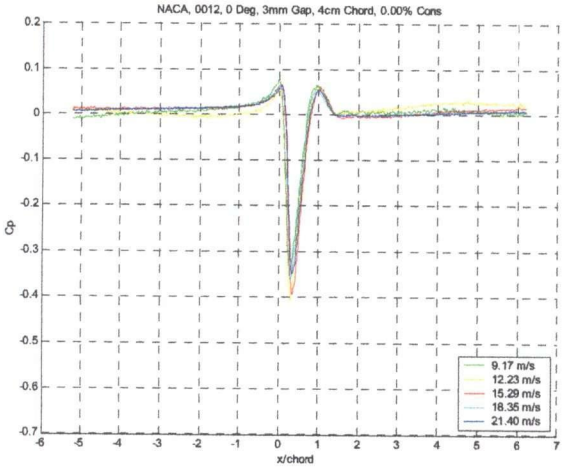

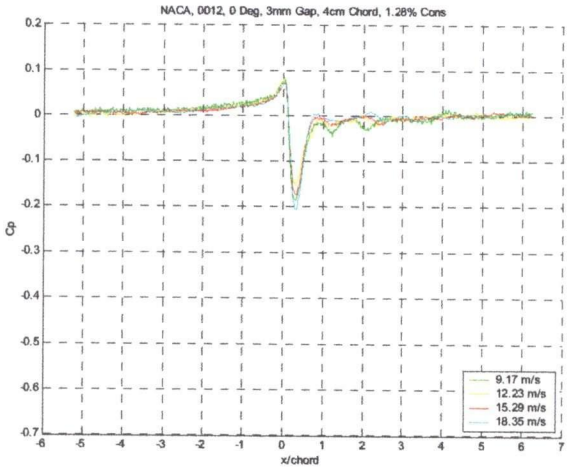

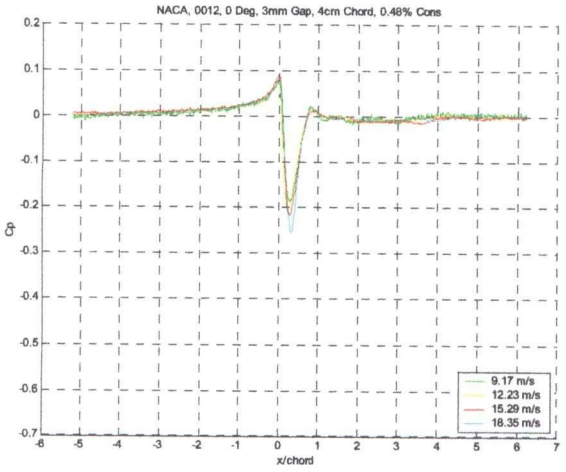

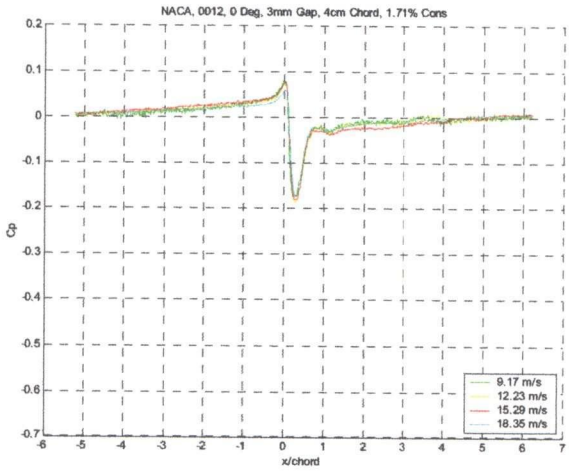

Appendix 3 – Collapsed Pressure Pulse c_p Curves

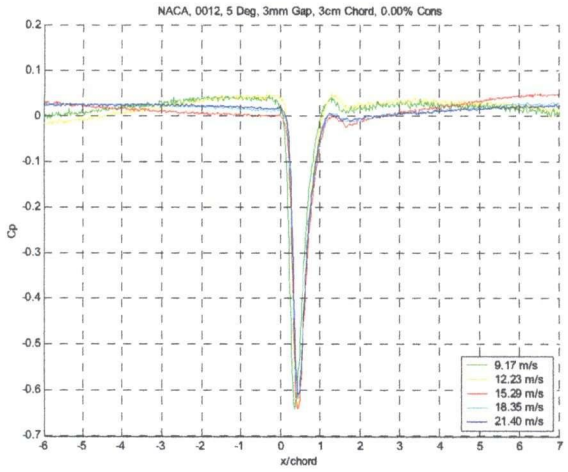

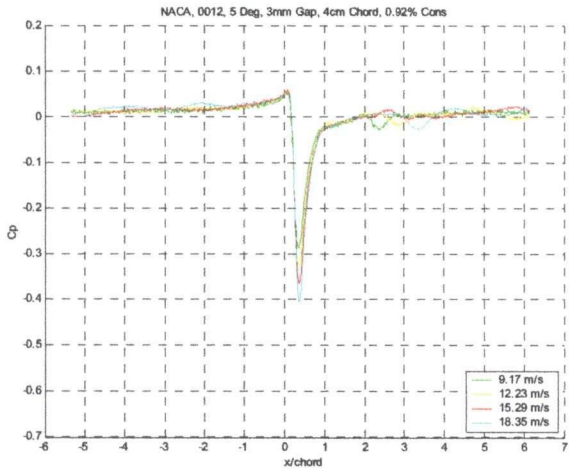

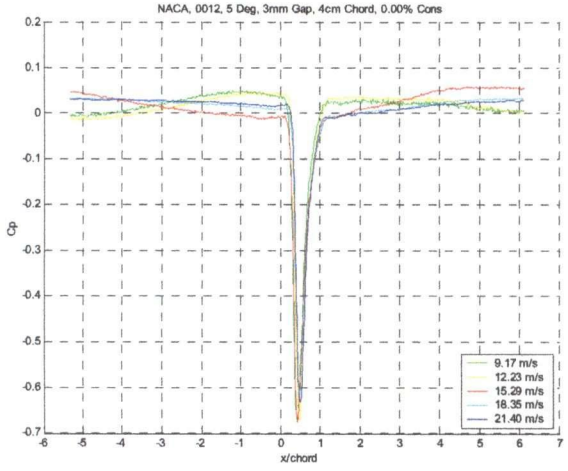

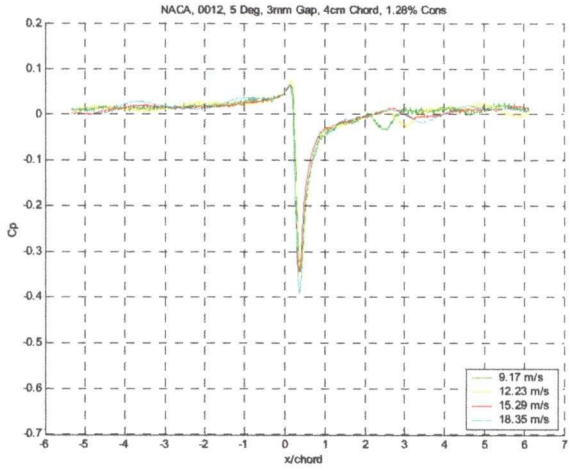

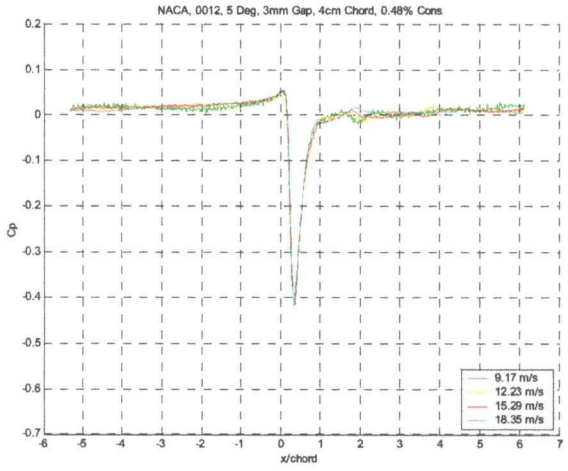

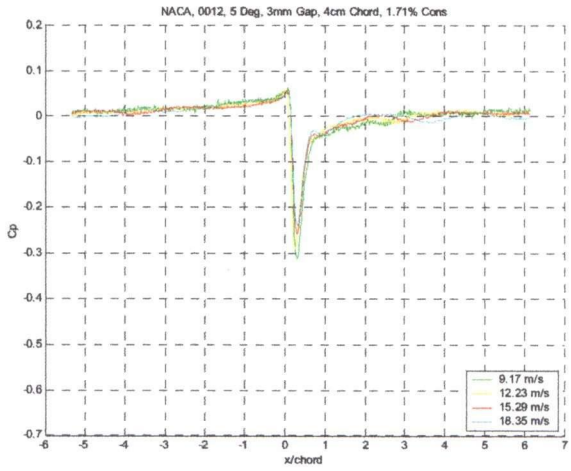

Appendix 3 – Collapsed Pressure Pulse c_p Curves

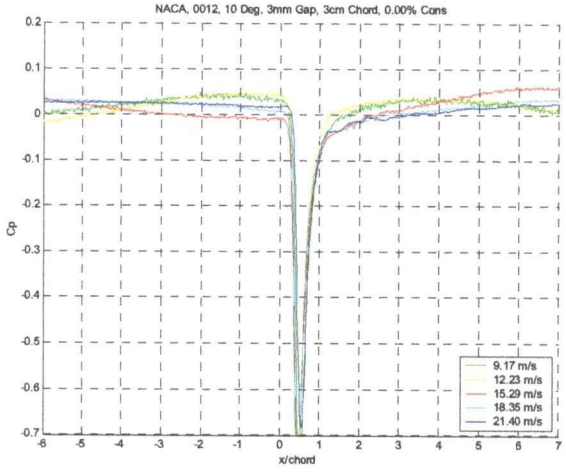

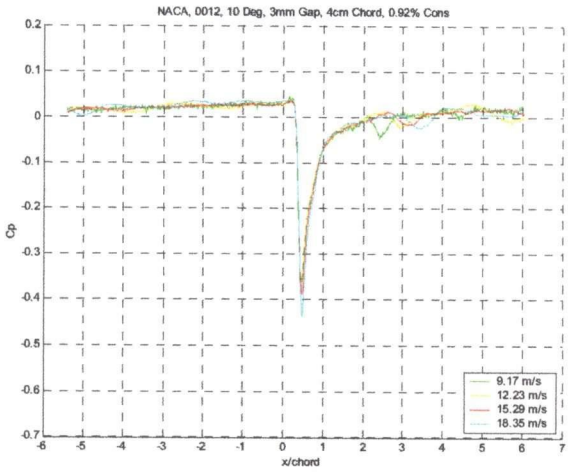

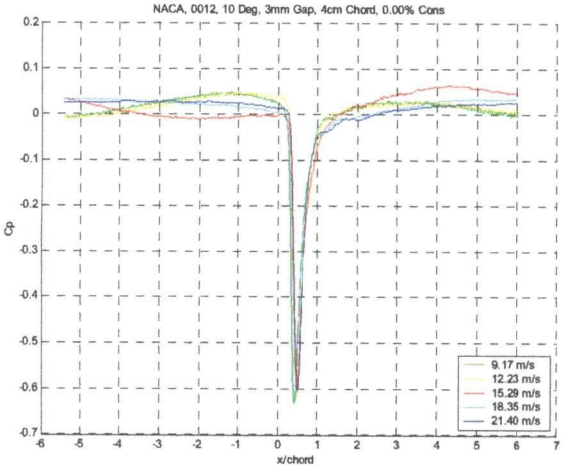

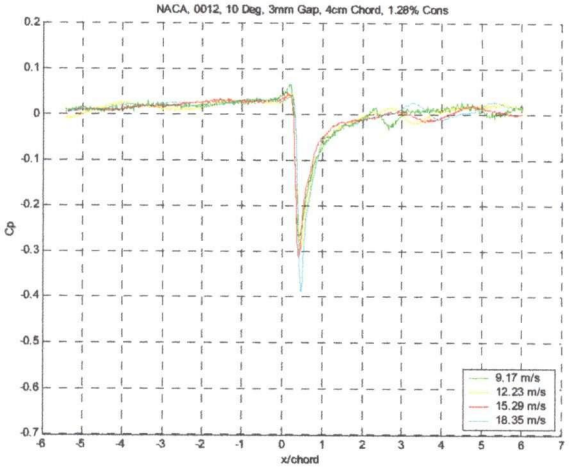

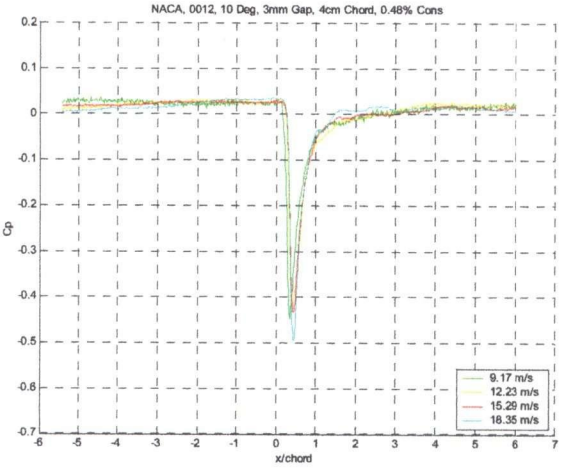

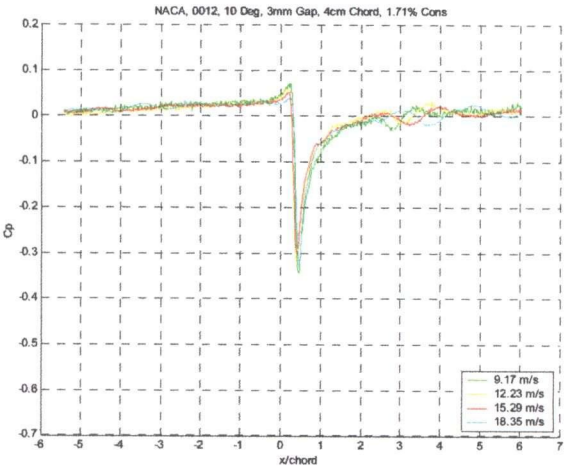

Appendix 3 – Collapsed Pressure Pulse c_p Curves

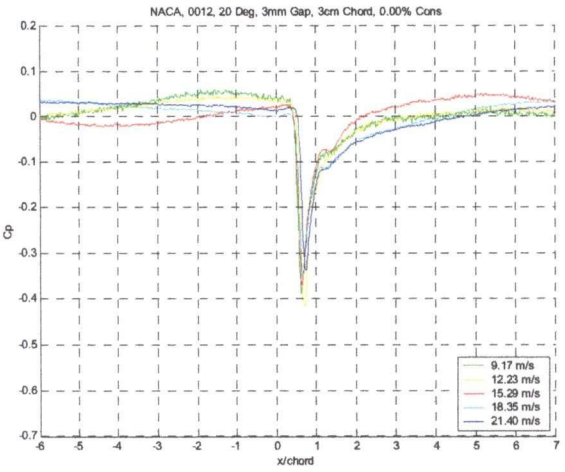

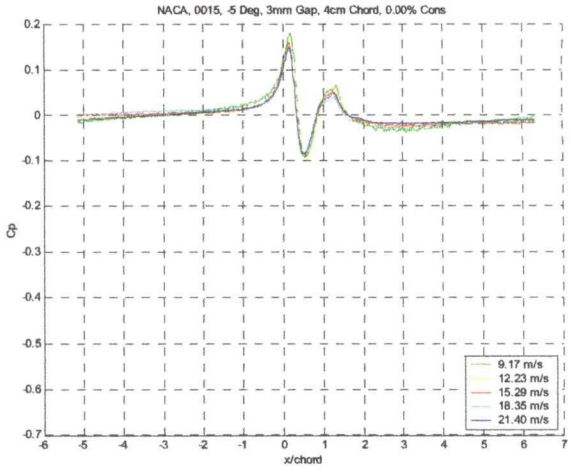

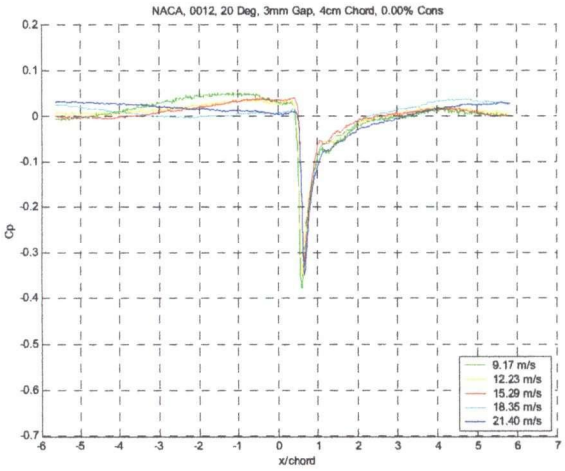

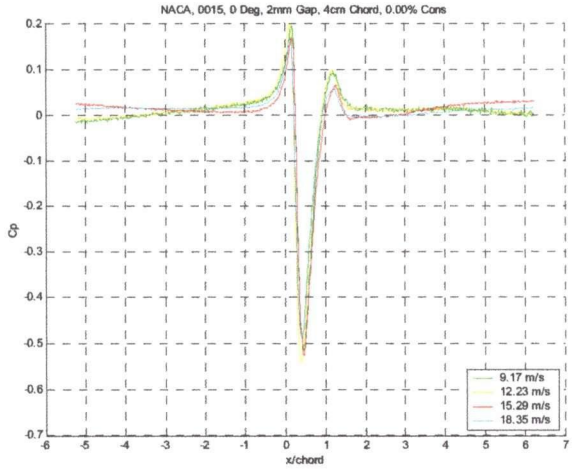

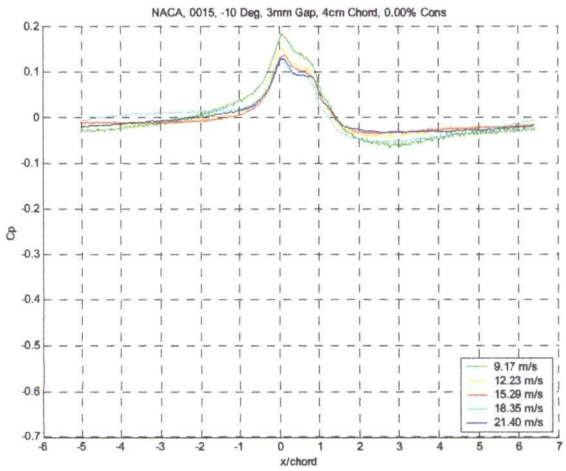

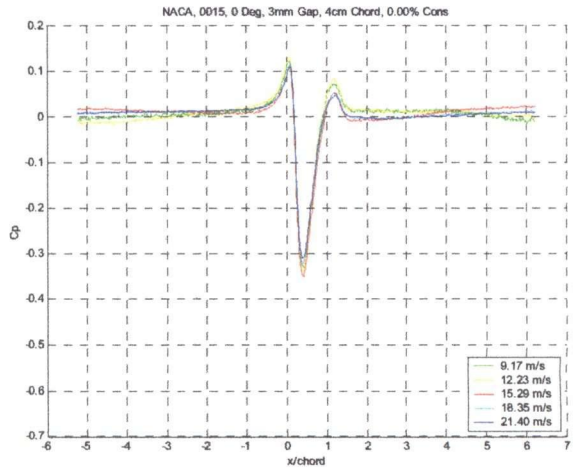

Appendix 3 – Collapsed Pressure Pulse c_p Curves

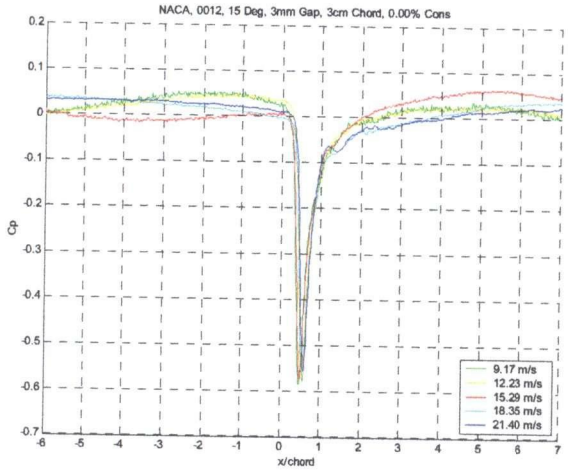

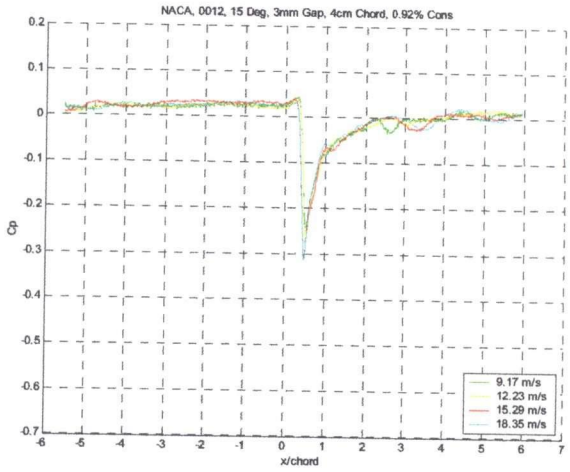

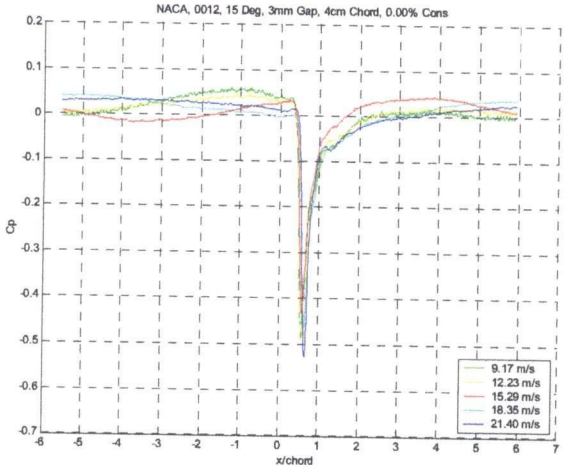

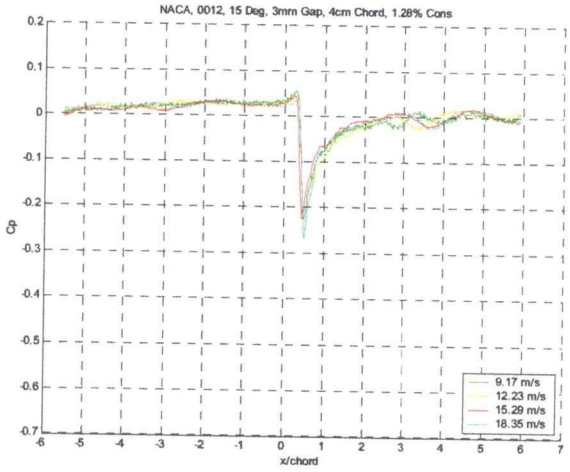

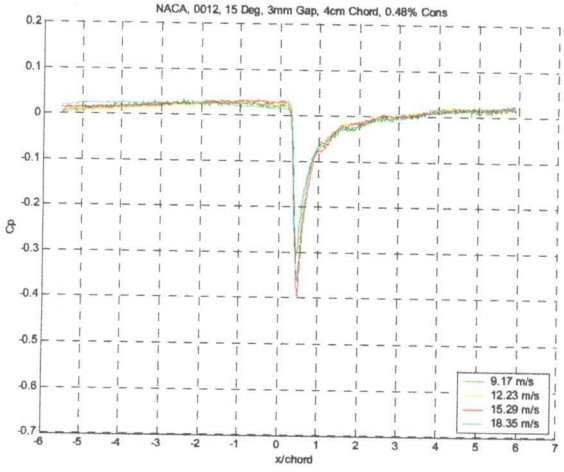

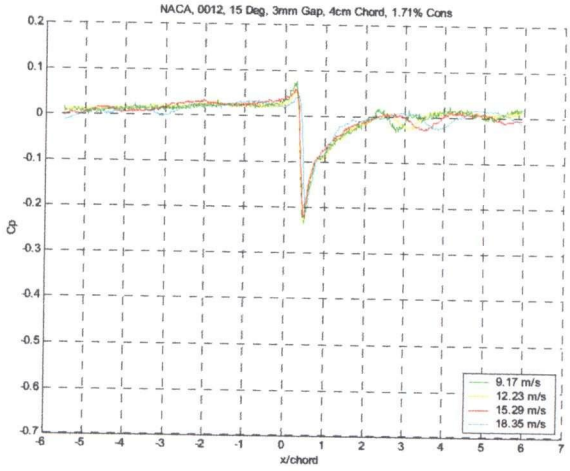

Appendix 3 – Collapsed Pressure Pulse c_p Curves

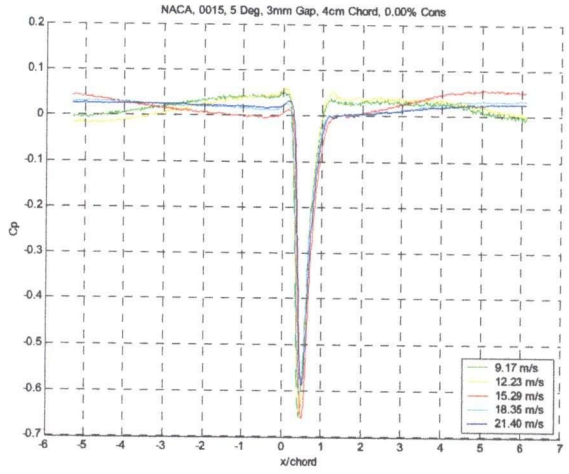

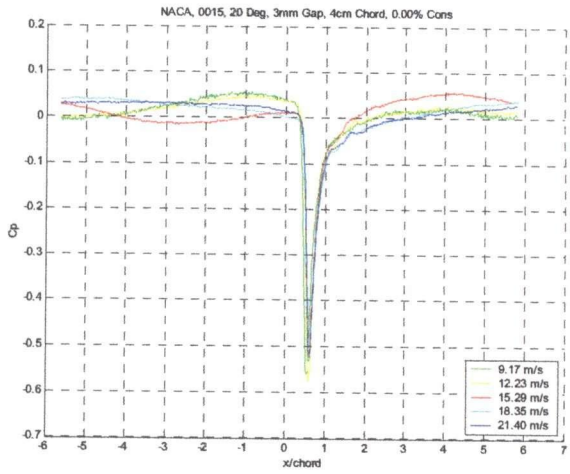

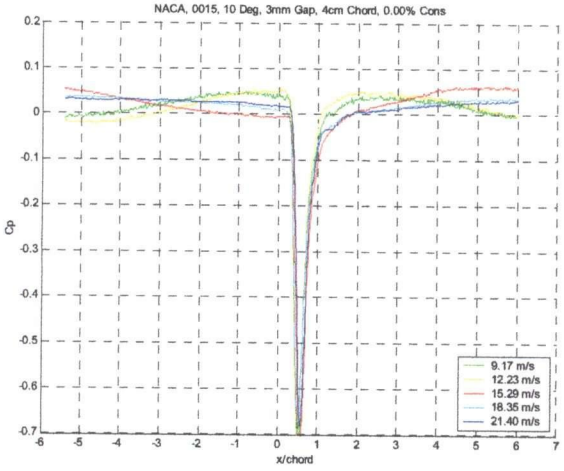

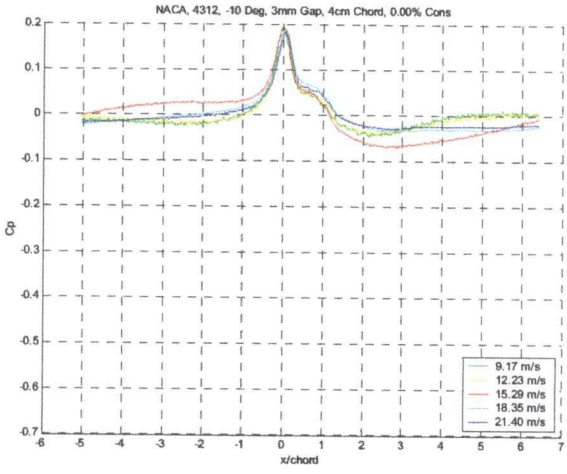

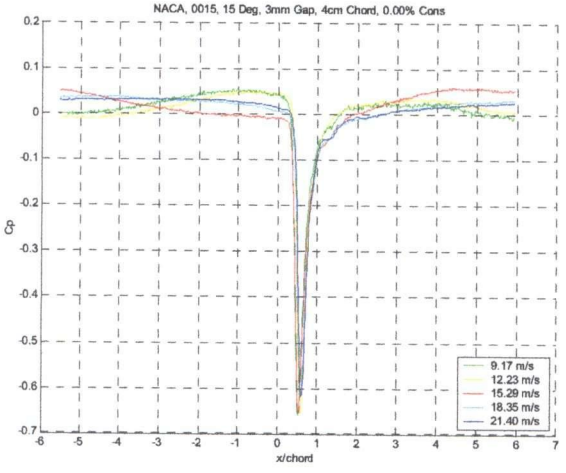

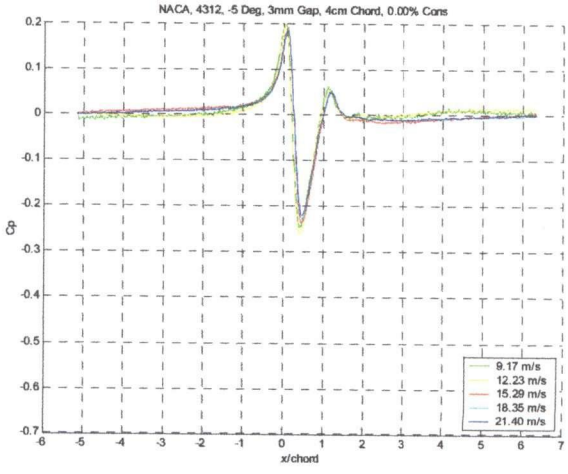

Appendix 3 – Collapsed Pressure Pulse c_p Curves

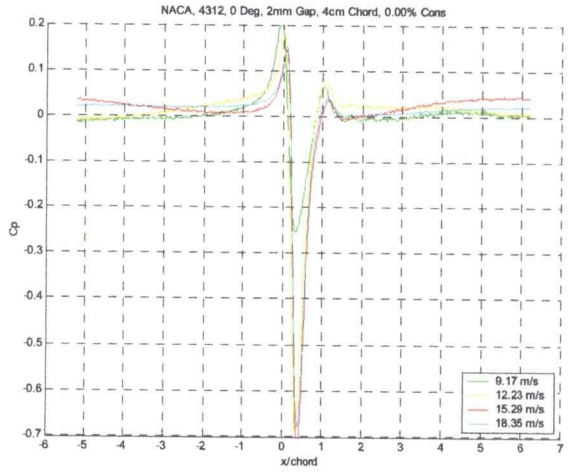

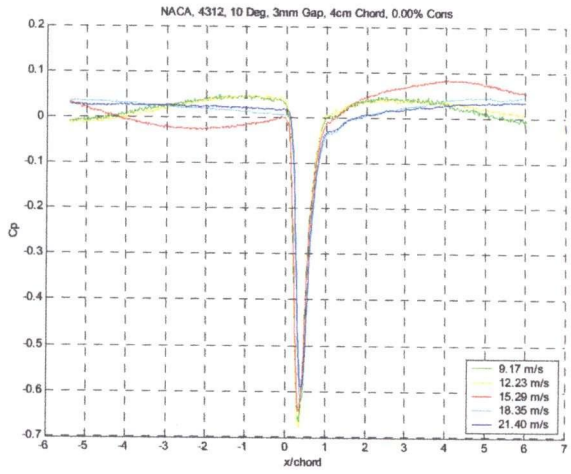

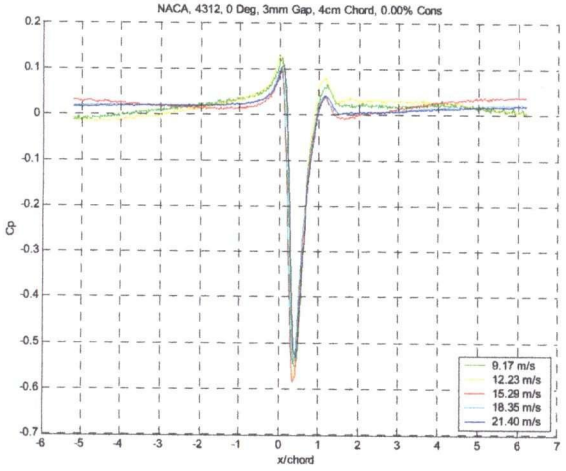

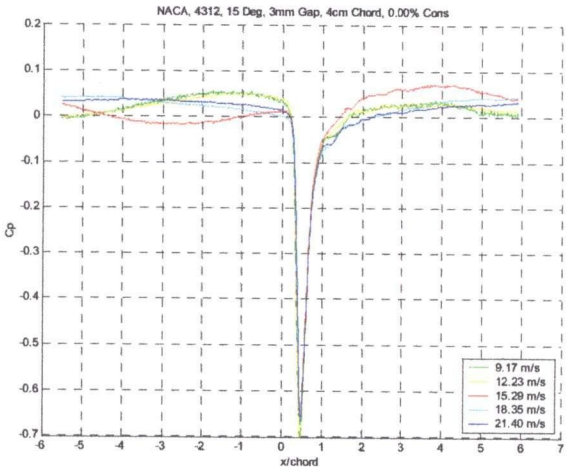

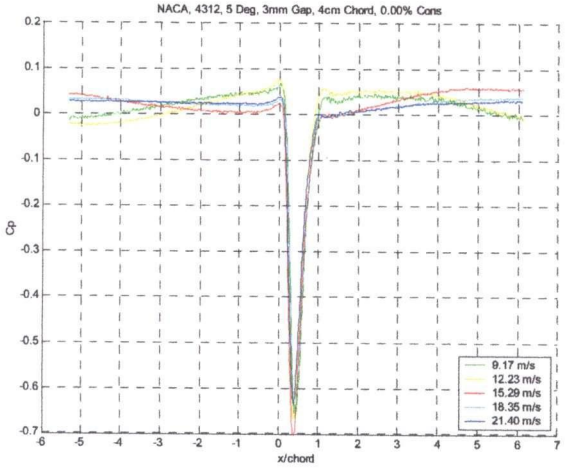

Appendix 3 – Collapsed Pressure Pulse c_p Curves

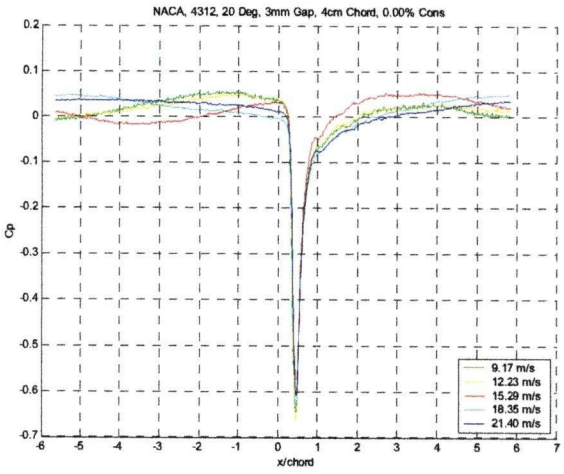

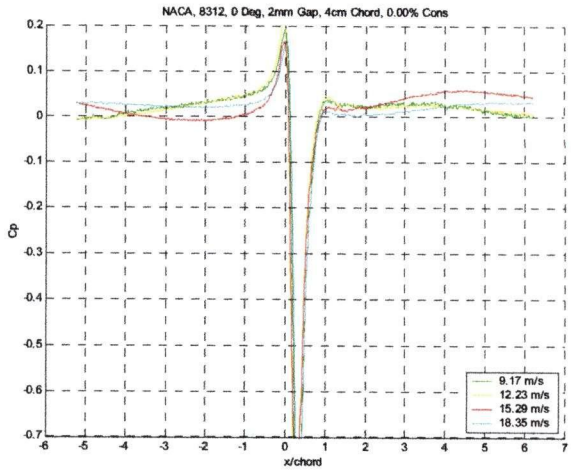

Appendix 4

The Effect of Rotor Tip Clearance on Pressure Pulse Magnitude

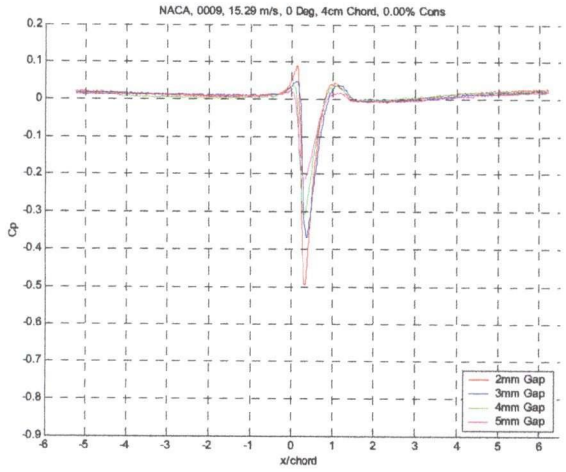
NACA, 0009, 15.29 m/s, 0 Deg, 4cm Chord, 0.00% Cons
Cp
x/chord
2mm Gap
3mm Gap
4mm Gap
5mm Gap

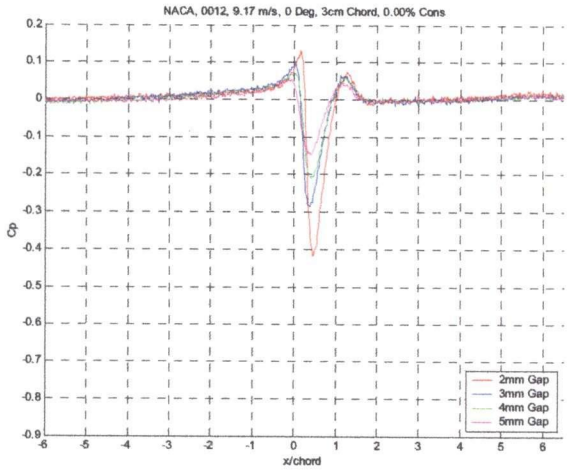
NACA, 0012, 9.17 m/s, 0 Deg, 3cm Chord, 0.00% Cons
Cp
x/chord
2mm Gap
3mm Gap
4mm Gap
5mm Gap

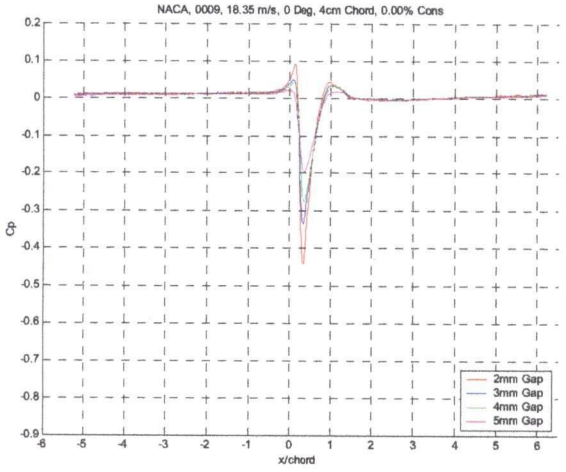
NACA, 0009, 18.35 m/s, 0 Deg, 4cm Chord, 0.00% Cons
Cp
x/chord
2mm Gap
3mm Gap
4mm Gap
5mm Gap

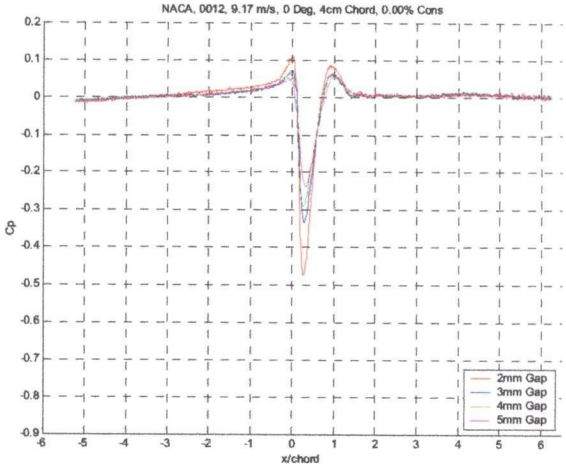
NACA, 0012, 9.17 m/s, 0 Deg, 4cm Chord, 0.00% Cons
Cp
x/chord
2mm Gap
3mm Gap
4mm Gap
5mm Gap

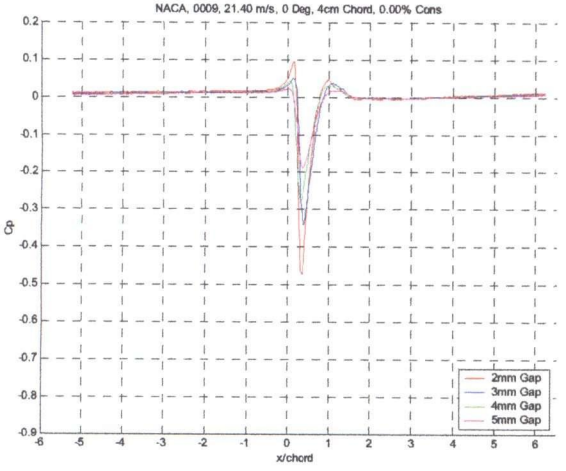
NACA, 0009, 21.40 m/s, 0 Deg, 4cm Chord, 0.00% Cons
Cp
x/chord
2mm Gap
3mm Gap
4mm Gap
5mm Gap

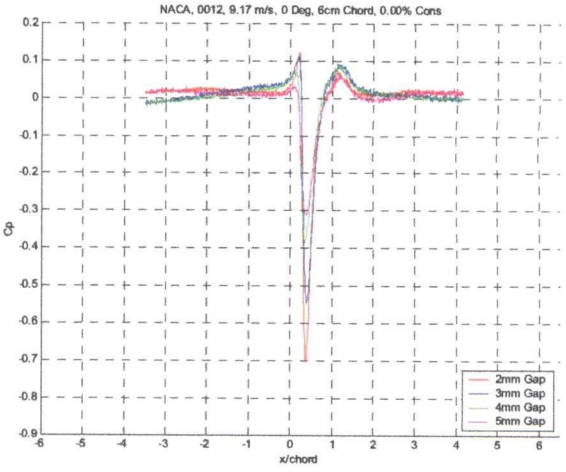
NACA, 0012, 9.17 m/s, 0 Deg, 6cm Chord, 0.00% Cons
Cp
x/chord
2mm Gap
3mm Gap
4mm Gap
5mm Gap

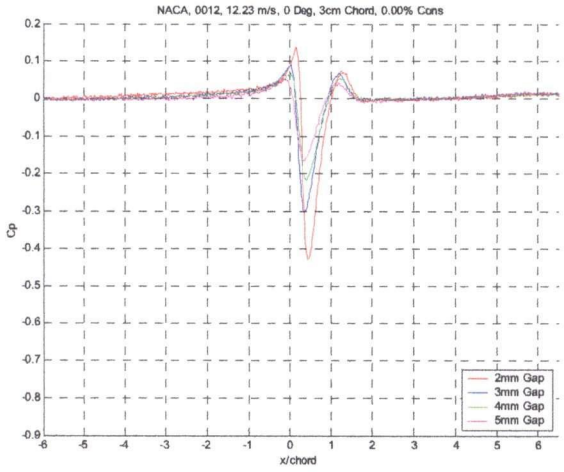
NACA, 0012, 12.23 m/s, 0 Deg, 3cm Chord, 0.00% Cons
Cp
x/chord
2mm Gap
3mm Gap
4mm Gap
5mm Gap

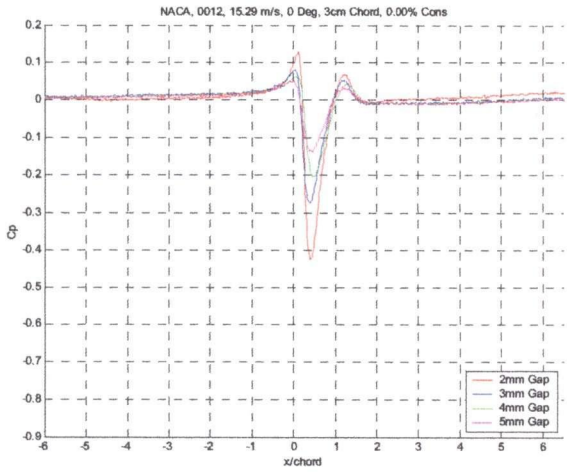
NACA, 0012, 15.29 m/s, 0 Deg, 3cm Chord, 0.00% Cons
Cp
x/chord
2mm Gap
3mm Gap
4mm Gap
5mm Gap

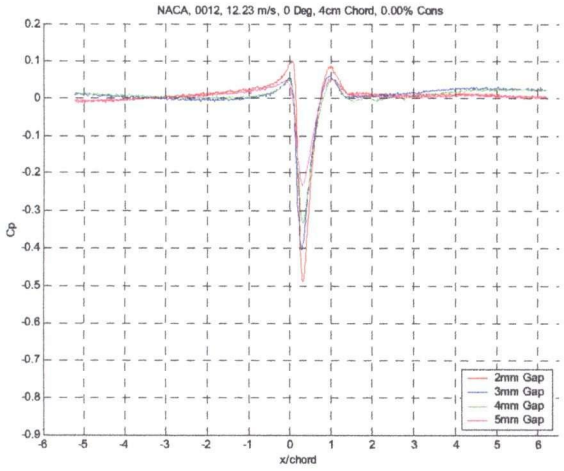
NACA, 0012, 12.23 m/s, 0 Deg, 4cm Chord, 0.00% Cons
Cp
x/chord
2mm Gap
3mm Gap
4mm Gap
5mm Gap

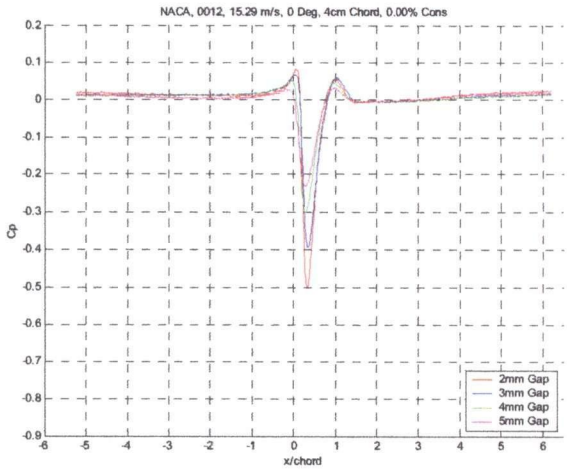
NACA, 0012, 15.29 m/s, 0 Deg, 4cm Chord, 0.00% Cons
Cp
x/chord
2mm Gap
3mm Gap
4mm Gap
5mm Gap

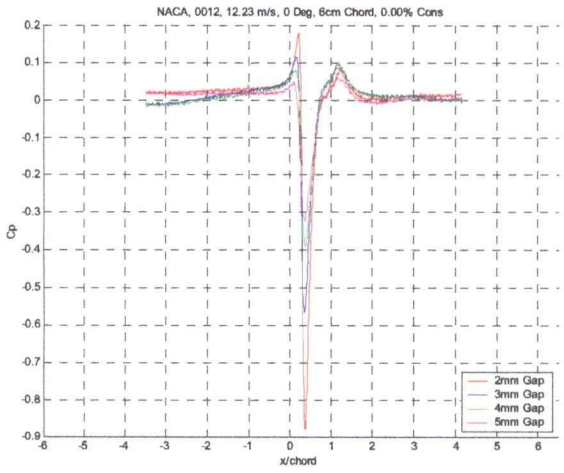
NACA, 0012, 12.23 m/s, 0 Deg, 6cm Chord, 0.00% Cons
Cp
x/chord
2mm Gap
3mm Gap
4mm Gap
5mm Gap

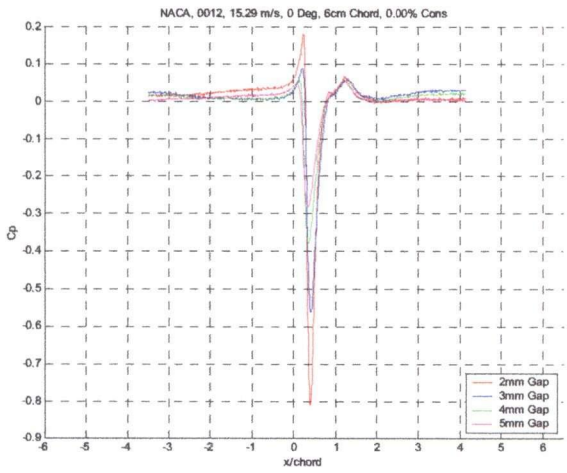
NACA, 0012, 15.29 m/s, 0 Deg, 6cm Chord, 0.00% Cons
Cp
x/chord
2mm Gap
3mm Gap
4mm Gap
5mm Gap

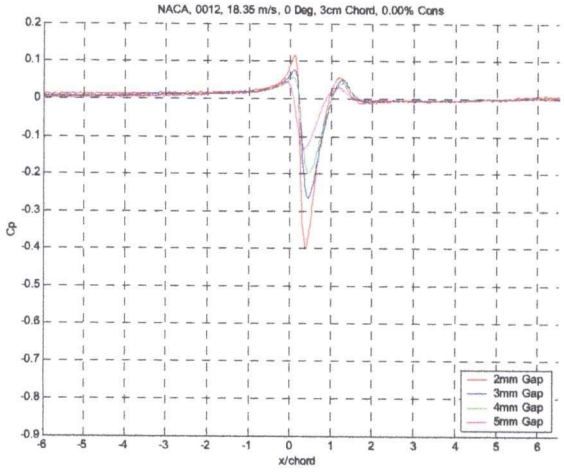
NACA, 0012, 18.35 m/s, 0 Deg, 3cm Chord, 0.00% Cons
Cp
x/chord
2mm Gap
3mm Gap
4mm Gap
5mm Gap

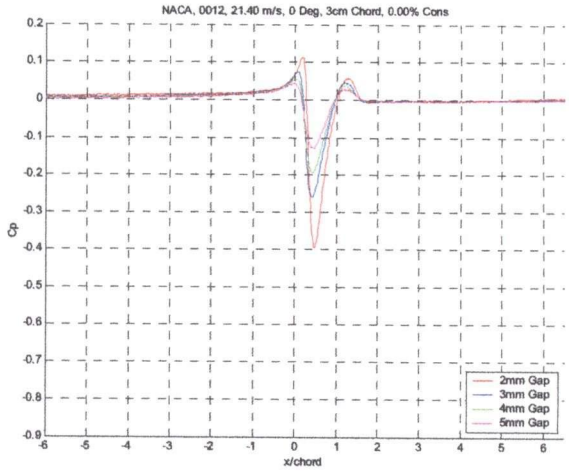
NACA, 0012, 21.40 m/s, 0 Deg, 3cm Chord, 0.00% Cons
Cp
x/chord
2mm Gap
3mm Gap
4mm Gap
5mm Gap

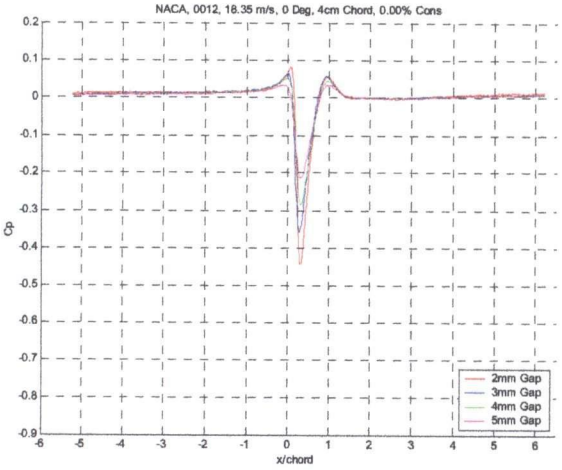
NACA, 0012, 18.35 m/s, 0 Deg, 4cm Chord, 0.00% Cons
Cp
x/chord
2mm Gap
3mm Gap
4mm Gap
5mm Gap

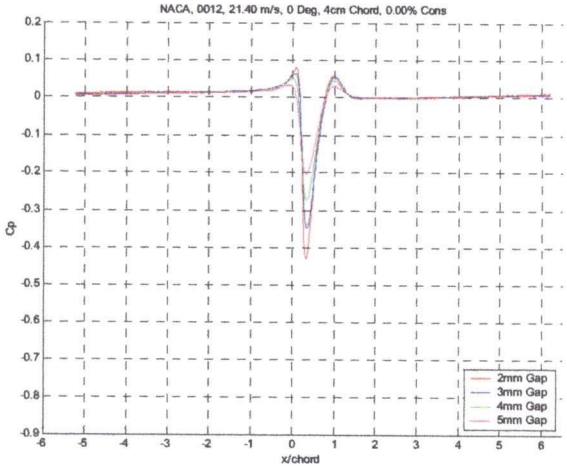
NACA, 0012, 21.40 m/s, 0 Deg, 4cm Chord, 0.00% Cons
Cp
x/chord
2mm Gap
3mm Gap
4mm Gap
5mm Gap

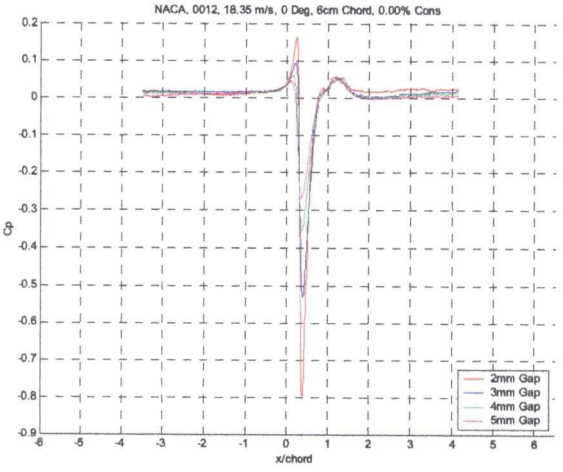
NACA, 0012, 18.35 m/s, 0 Deg, 6cm Chord, 0.00% Cons
Cp
x/chord
2mm Gap
3mm Gap
4mm Gap
5mm Gap

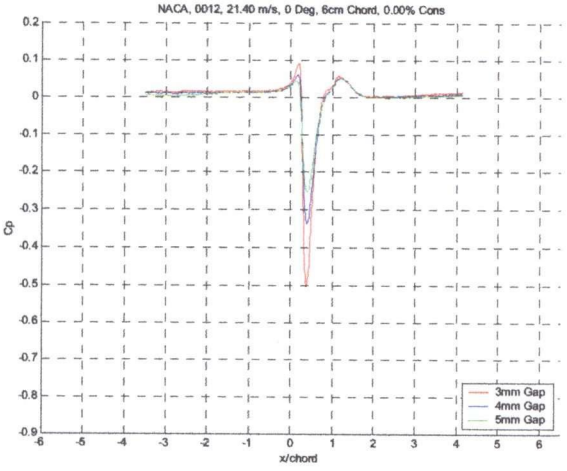
NACA, 0012, 21.40 m/s, 0 Deg, 6cm Chord, 0.00% Cons
Cp
x/chord
3mm Gap
4mm Gap
5mm Gap

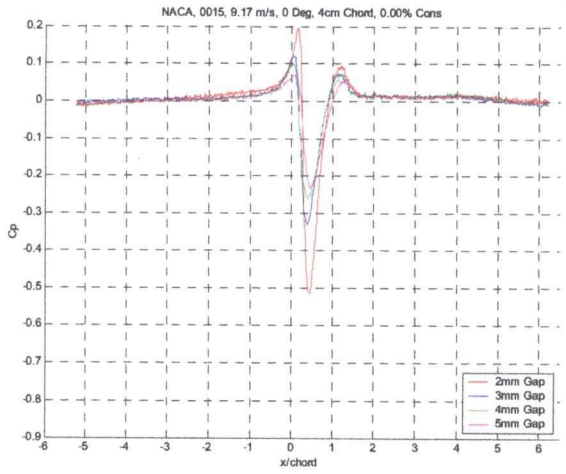
NACA, 0015, 9.17 m/s, 0 Deg, 4cm Chord, 0.00% Cons
Cp
x/chord
2mm Gap
3mm Gap
4mm Gap
5mm Gap

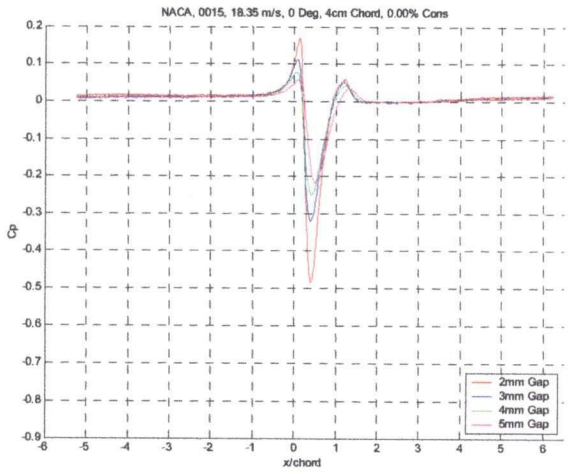
NACA, 0015, 18.35 m/s, 0 Deg, 4cm Chord, 0.00% Cons
Cp
x/chord
2mm Gap
3mm Gap
4mm Gap
5mm Gap

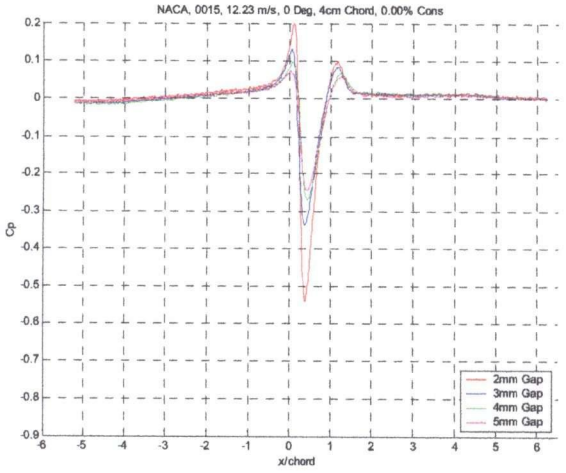
NACA, 0015, 12.23 m/s, 0 Deg, 4cm Chord, 0.00% Cons
Cp
x/chord
2mm Gap
3mm Gap
4mm Gap
5mm Gap

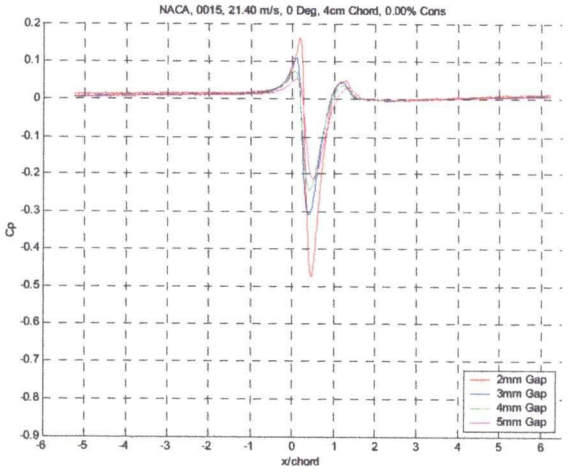
NACA, 0015, 21.40 m/s, 0 Deg, 4cm Chord, 0.00% Cons
Cp
x/chord
2mm Gap
3mm Gap
4mm Gap
5mm Gap

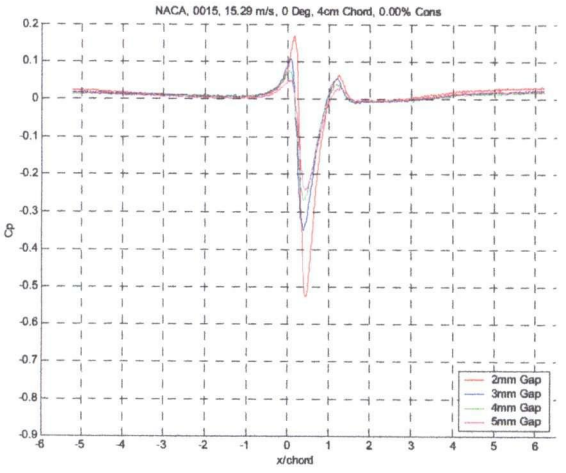
NACA, 0015, 15.29 m/s, 0 Deg, 4cm Chord, 0.00% Cons
Cp
x/chord
2mm Gap
3mm Gap
4mm Gap
5mm Gap

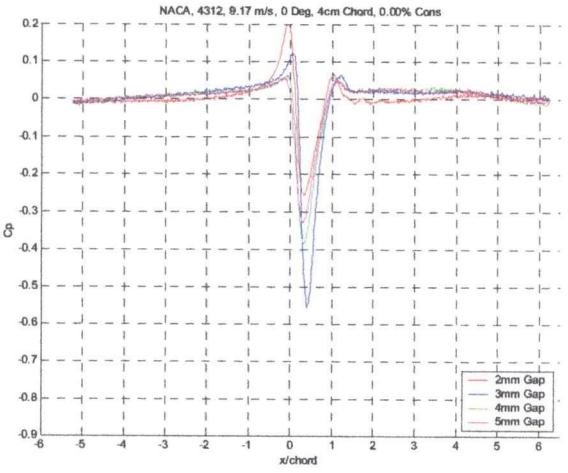
NACA, 4312, 9.17 m/s, 0 Deg, 4cm Chord, 0.00% Cons
Cp
x/chord
2mm Gap
3mm Gap
4mm Gap
5mm Gap

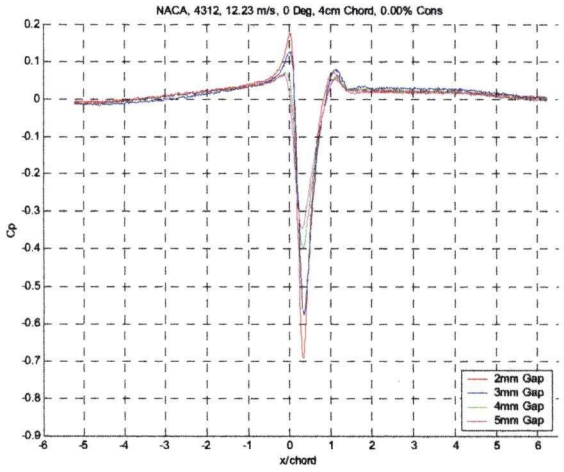
NACA, 4312, 12.23 m/s, 0 Deg, 4cm Chord, 0.00% Cons
Cp
x/chord
2mm Gap
3mm Gap
4mm Gap
5mm Gap

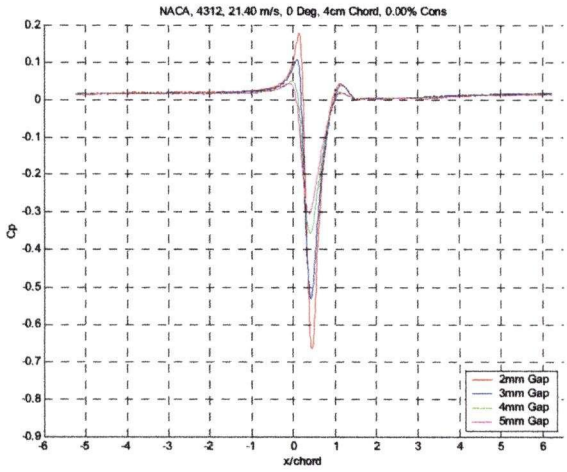
NACA, 4312, 21.40 m/s, 0 Deg, 4cm Chord, 0.00% Cons
Cp
x/chord
2mm Gap
3mm Gap
4mm Gap
5mm Gap

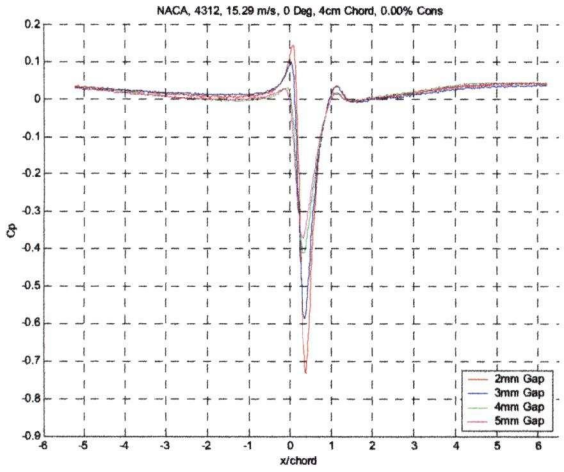
NACA, 4312, 15.29 m/s, 0 Deg, 4cm Chord, 0.00% Cons
Cp
x/chord
2mm Gap
3mm Gap
4mm Gap
5mm Gap

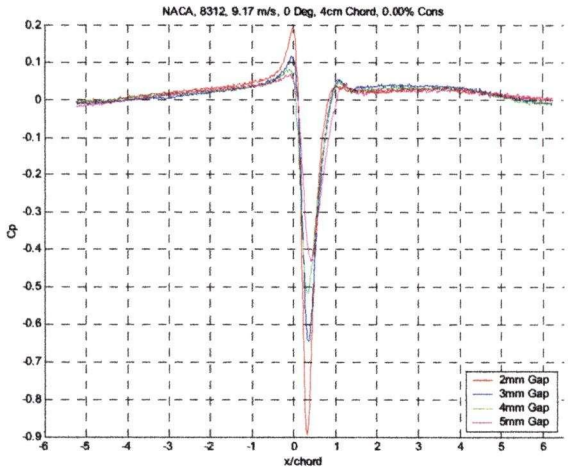
NACA, 8312, 9.17 m/s, 0 Deg, 4cm Chord, 0.00% Cons
Cp
x/chord
2mm Gap
3mm Gap
4mm Gap
5mm Gap

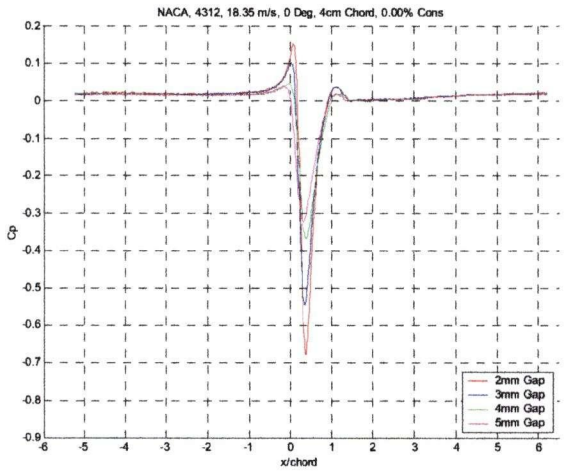
NACA, 4312, 18.35 m/s, 0 Deg, 4cm Chord, 0.00% Cons
Cp
x/chord
2mm Gap
3mm Gap
4mm Gap
5mm Gap

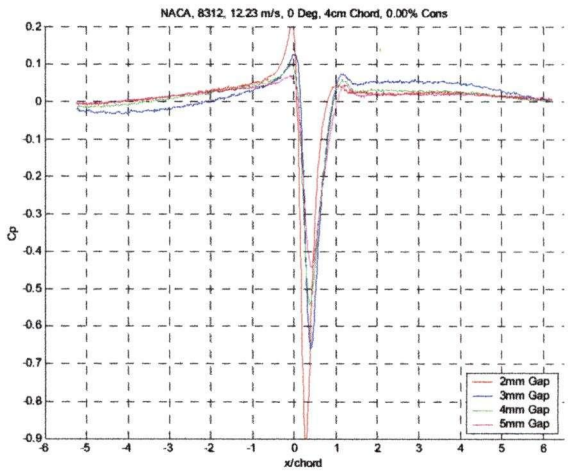
NACA, 8312, 12.23 m/s, 0 Deg, 4cm Chord, 0.00% Cons
Cp
x/chord
2mm Gap
3mm Gap
4mm Gap
5mm Gap

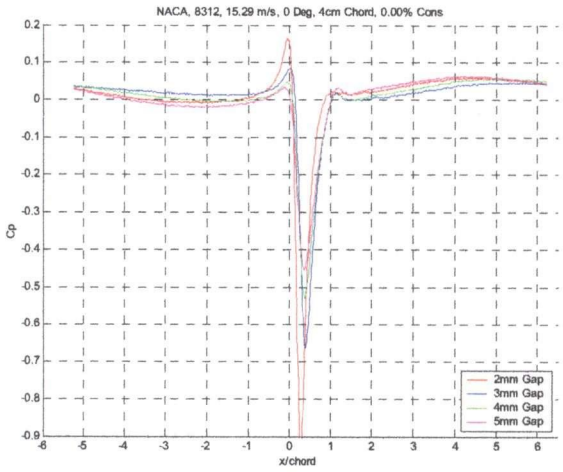
NACA, 8312, 15.29 m/s, 0 Deg, 4cm Chord, 0.00% Cons
Cp
x/chord
2mm Gap
3mm Gap
4mm Gap
5mm Gap

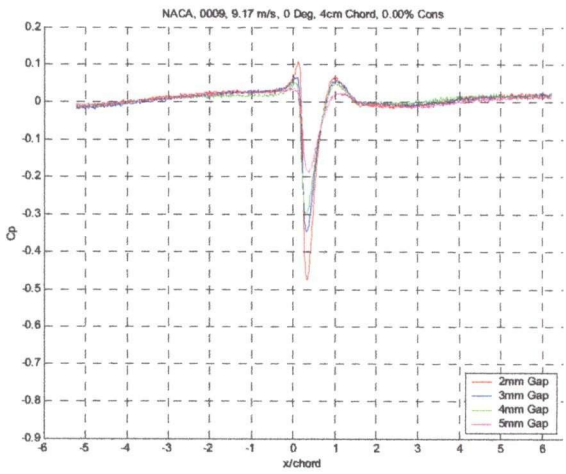
NACA, 0009, 9.17 m/s, 0 Deg, 4cm Chord, 0.00% Cons
Cp
x/chord
2mm Gap
3mm Gap
4mm Gap
5mm Gap

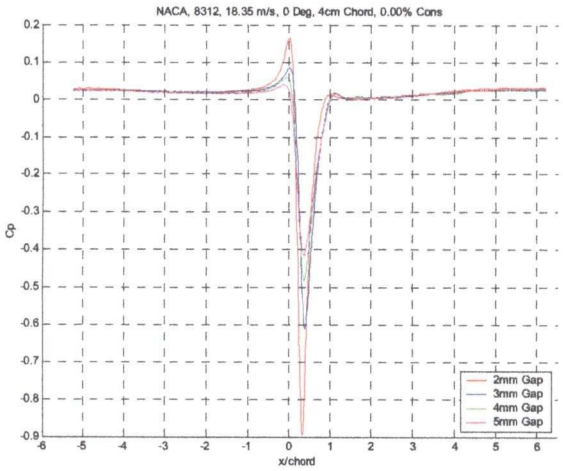
NACA, 8312, 18.35 m/s, 0 Deg, 4cm Chord, 0.00% Cons
Cp
x/chord
2mm Gap
3mm Gap
4mm Gap
5mm Gap

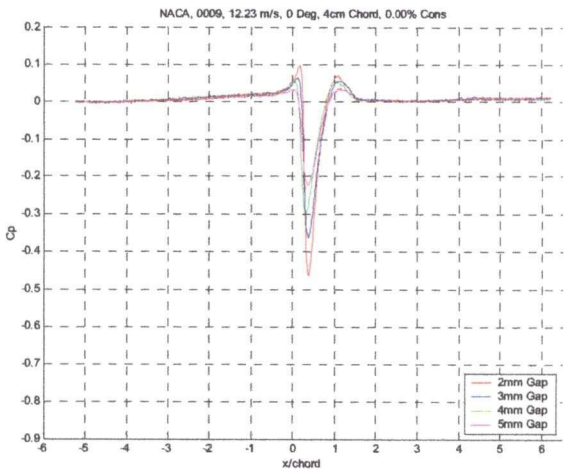
NACA, 0009, 12.23 m/s, 0 Deg, 4cm Chord, 0.00% Cons
Cp
x/chord
2mm Gap
3mm Gap
4mm Gap
5mm Gap

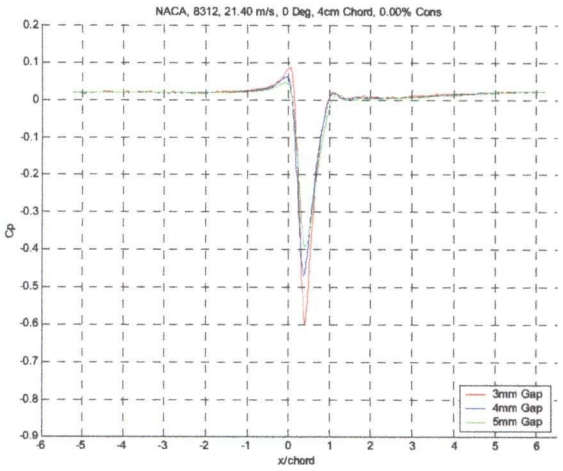
NACA, 8312, 21.40 m/s, 0 Deg, 4cm Chord, 0.00% Cons
Cp
x/chord
3mm Gap
4mm Gap
5mm Gap

Appendix 5

The Effect of Pulp Consistency on Pressure Pulse Magnitude

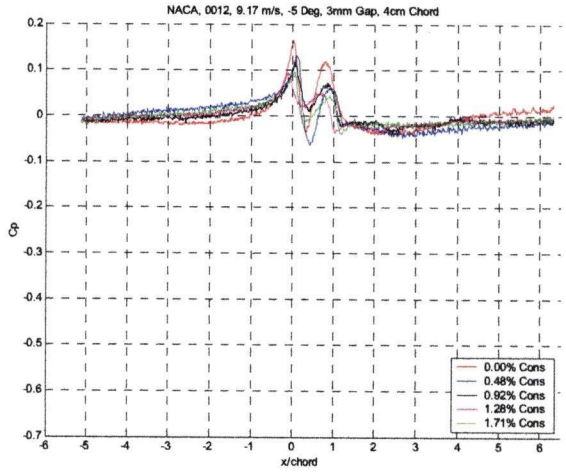
NACA, 0012, 9.17 m/s, -5 Deg, 3mm Gap, 4cm Chord
Cp
x/chord
0.00% Cons
0.48% Cons
0.92% Cons
1.28% Cons
1.71% Cons

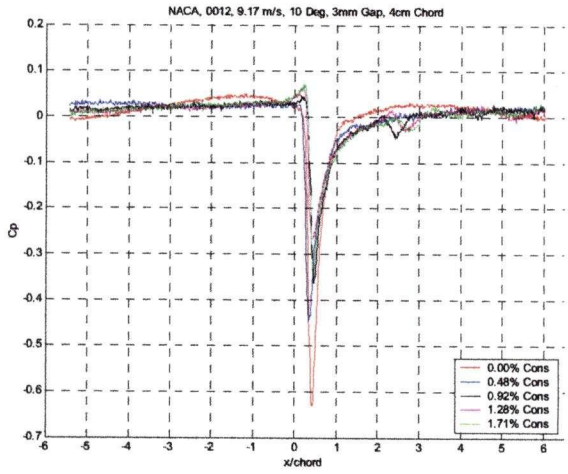
NACA, 0012, 9.17 m/s, 10 Deg, 3mm Gap, 4cm Chord
Cp
x/chord
0.00% Cons
0.48% Cons
0.92% Cons
1.28% Cons
1.71% Cons

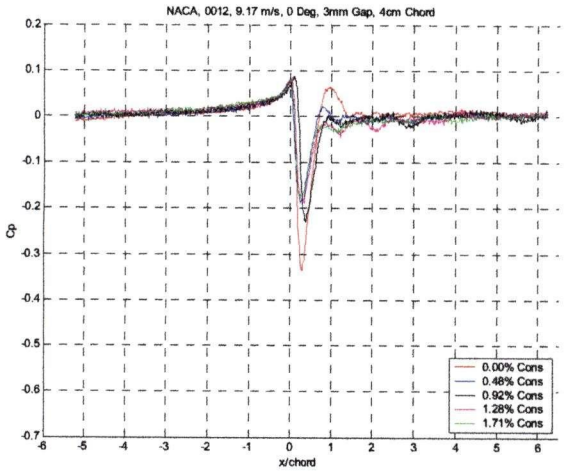
NACA, 0012, 9.17 m/s, 0 Deg, 3mm Gap, 4cm Chord
Cp
x/chord
0.00% Cons
0.48% Cons
0.92% Cons
1.28% Cons
1.71% Cons

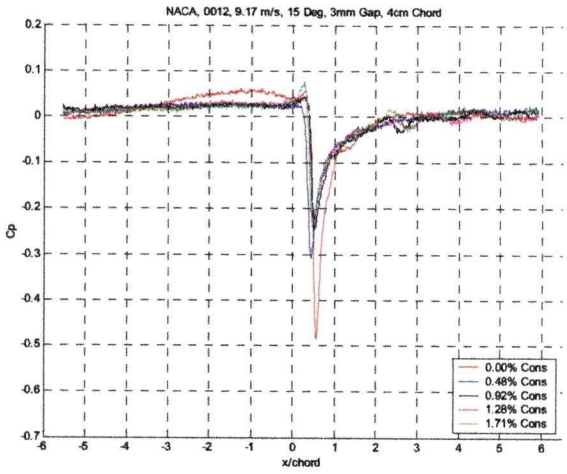
NACA, 0012, 9.17 m/s, 15 Deg, 3mm Gap, 4cm Chord
Cp
x/chord
0.00% Cons
0.48% Cons
0.92% Cons
1.28% Cons
1.71% Cons

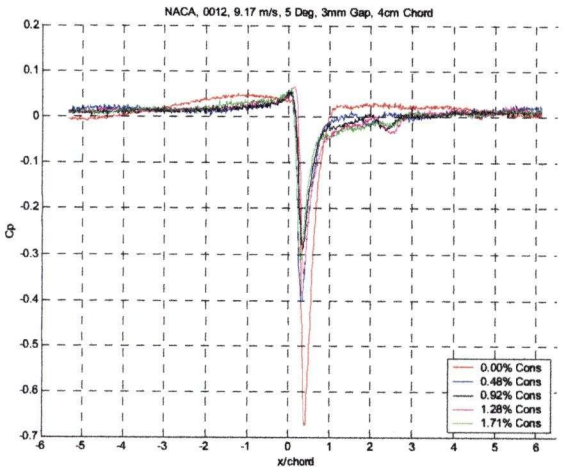
NACA, 0012, 9.17 m/s, 5 Deg, 3mm Gap, 4cm Chord
Cp
x/chord
0.00% Cons
0.48% Cons
0.92% Cons
1.28% Cons
1.71% Cons

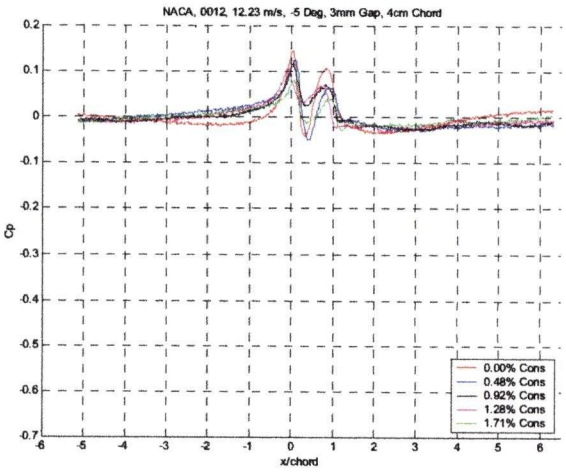
NACA, 0012, 12.23 m/s, -5 Deg, 3mm Gap, 4cm Chord
Cp
x/chord
0.00% Cons
0.48% Cons
0.92% Cons
1.28% Cons
1.71% Cons

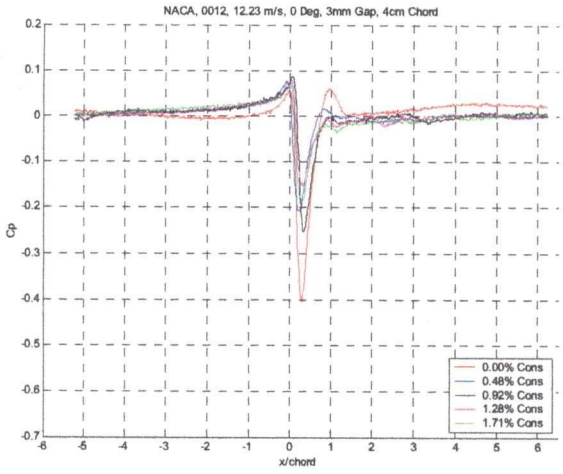
NACA, 0012, 12.23 m/s, 0 Deg, 3mm Gap, 4cm Chord
Cp
x/chord
0.00% Cons
0.48% Cons
0.92% Cons
1.28% Cons
1.71% Cons

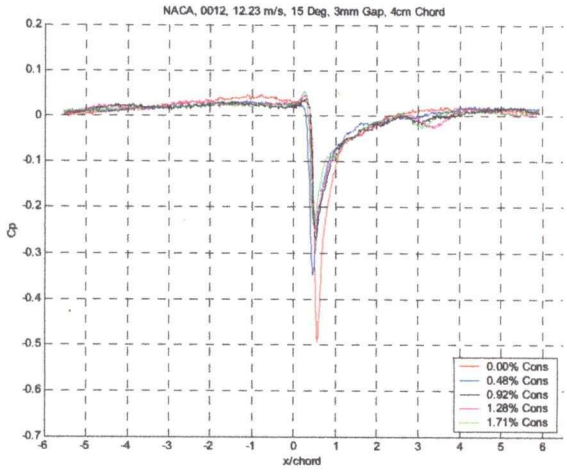
NACA, 0012, 12.23 m/s, 15 Deg, 3mm Gap, 4cm Chord
Cp
x/chord
0.00% Cons
0.48% Cons
0.92% Cons
1.28% Cons
1.71% Cons

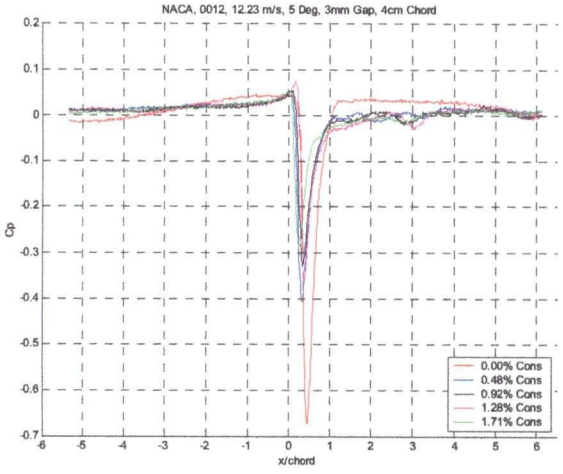
NACA, 0012, 12.23 m/s, 5 Deg, 3mm Gap, 4cm Chord
Cp
x/chord
0.00% Cons
0.48% Cons
0.92% Cons
1.28% Cons
1.71% Cons

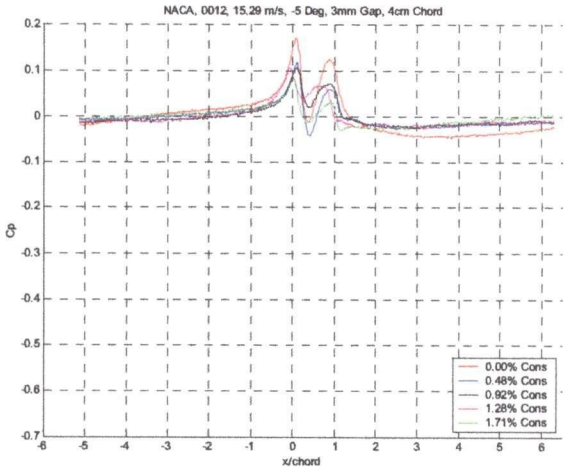
NACA, 0012, 15.29 m/s, -5 Deg, 3mm Gap, 4cm Chord
Cp
x/chord
0.00% Cons
0.48% Cons
0.92% Cons
1.28% Cons
1.71% Cons

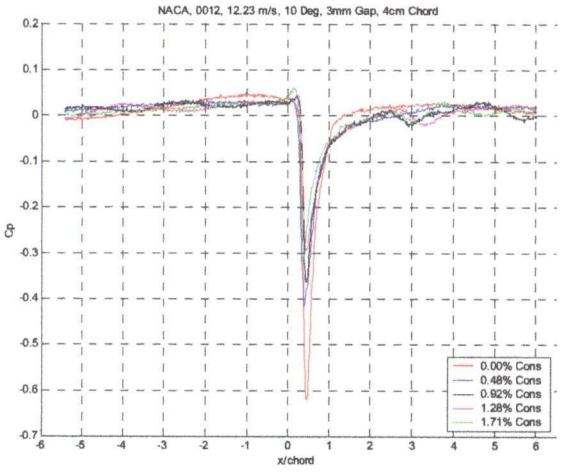
NACA, 0012, 12.23 m/s, 10 Deg, 3mm Gap, 4cm Chord
Cp
x/chord
0.00% Cons
0.48% Cons
0.92% Cons
1.28% Cons
1.71% Cons

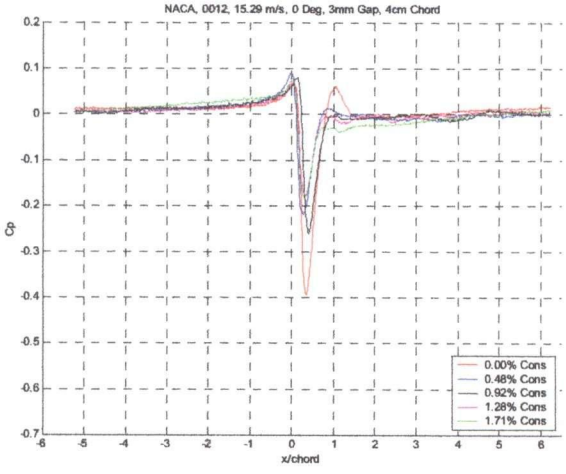
NACA, 0012, 15.29 m/s, 0 Deg, 3mm Gap, 4cm Chord
Cp
x/chord
0.00% Cons
0.48% Cons
0.92% Cons
1.28% Cons
1.71% Cons

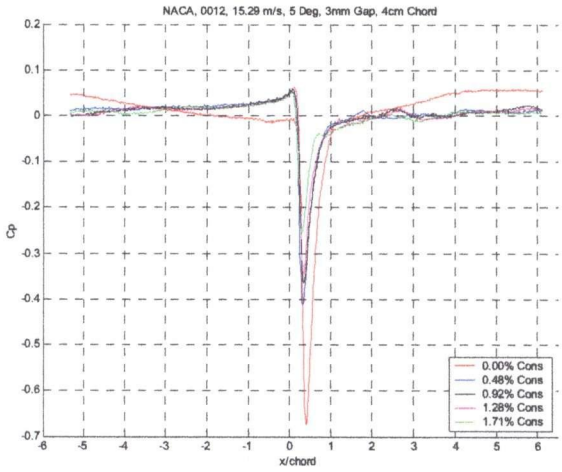
NACA, 0012, 15.29 m/s, 5 Deg, 3mm Gap, 4cm Chord
Cp
x/chord
0.00% Cons
0.48% Cons
0.92% Cons
1.28% Cons
1.71% Cons

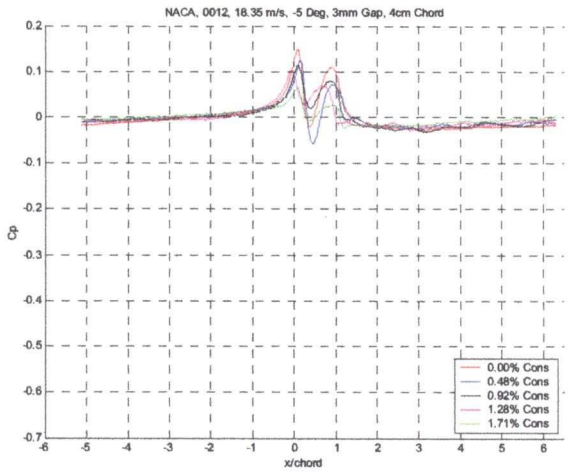
NACA, 0012, 18.35 m/s, -5 Deg, 3mm Gap, 4cm Chord
Cp
x/chord
0.00% Cons
0.48% Cons
0.92% Cons
1.28% Cons
1.71% Cons

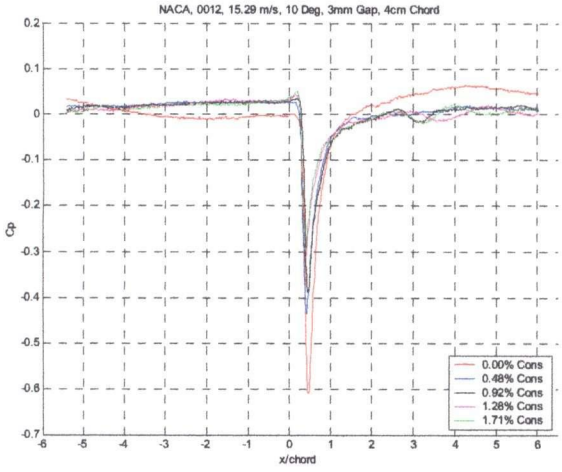
NACA, 0012, 15.29 m/s, 10 Deg, 3mm Gap, 4cm Chord
Cp
x/chord
0.00% Cons
0.48% Cons
0.92% Cons
1.28% Cons
1.71% Cons

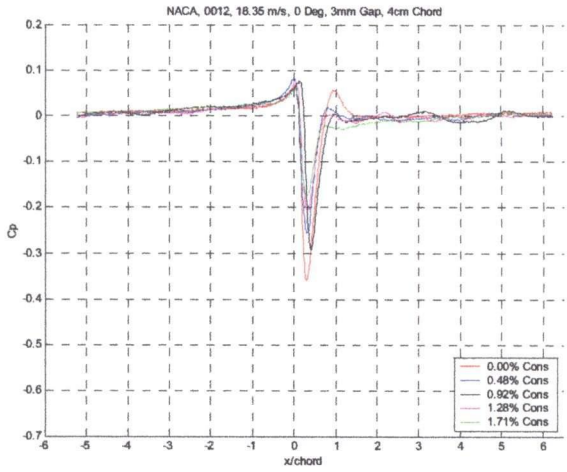
NACA, 0012, 18.35 m/s, 0 Deg, 3mm Gap, 4cm Chord
Cp
x/chord
0.00% Cons
0.48% Cons
0.92% Cons
1.28% Cons
1.71% Cons

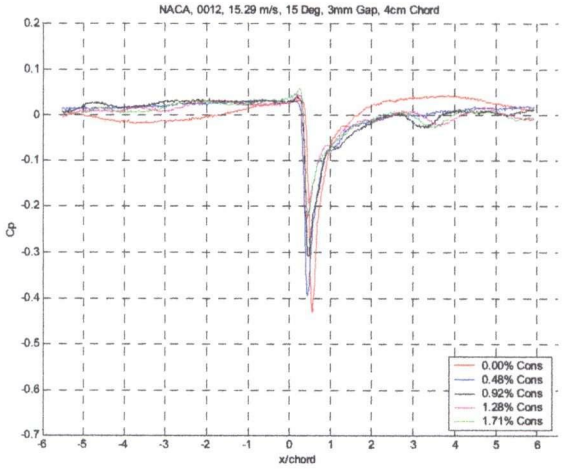
NACA, 0012, 15.29 m/s, 15 Deg, 3mm Gap, 4cm Chord
Cp
x/chord
0.00% Cons
0.48% Cons
0.92% Cons
1.28% Cons
1.71% Cons

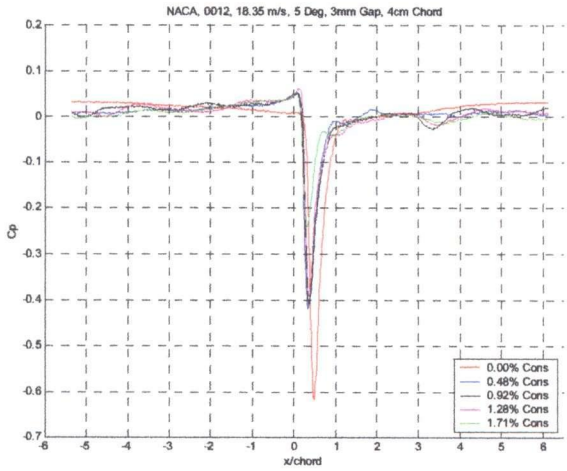
NACA, 0012, 18.35 m/s, 5 Deg, 3mm Gap, 4cm Chord
Cp
x/chord
0.00% Cons
0.48% Cons
0.92% Cons
1.28% Cons
1.71% Cons

Appendix 5 – The Effect of Pulp Consistency on Pressure Pulse Magnitude

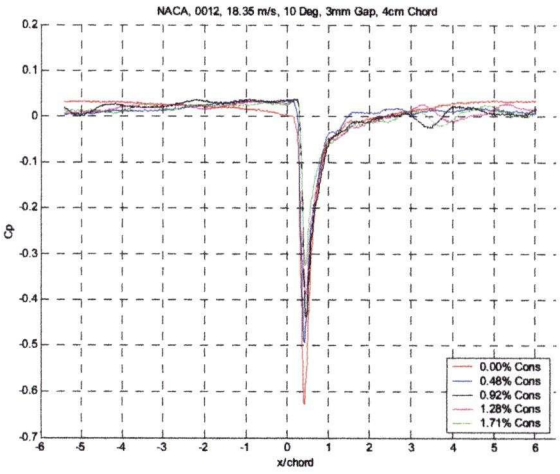

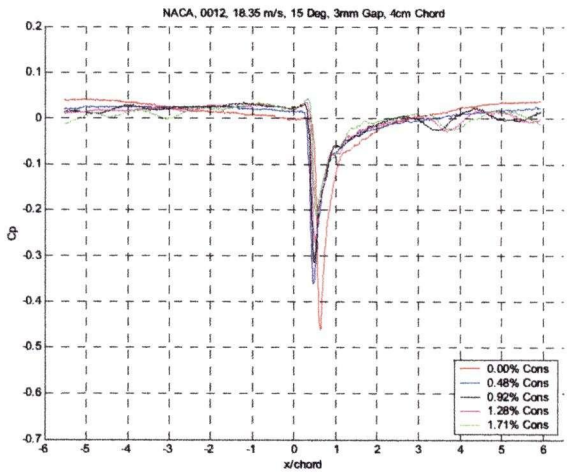

Appendix 6

The Effect of Foil Thickness on Pressure Pulse Magnitude

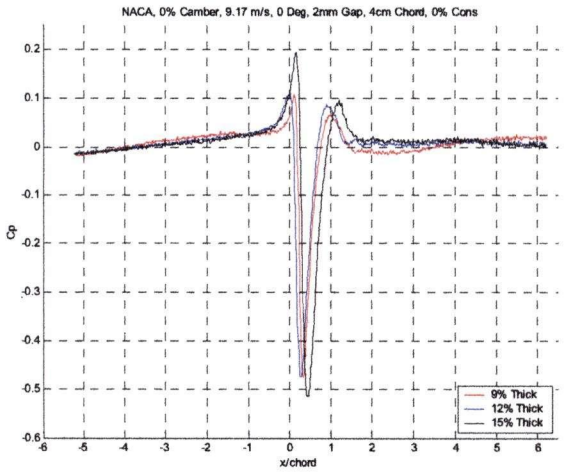
NACA, 0% Camber, 9.17 m/s, 0 Deg, 2mm Gap, 4cm Chord, 0% Cons
Cp
x/chord
9% Thick
12% Thick
15% Thick

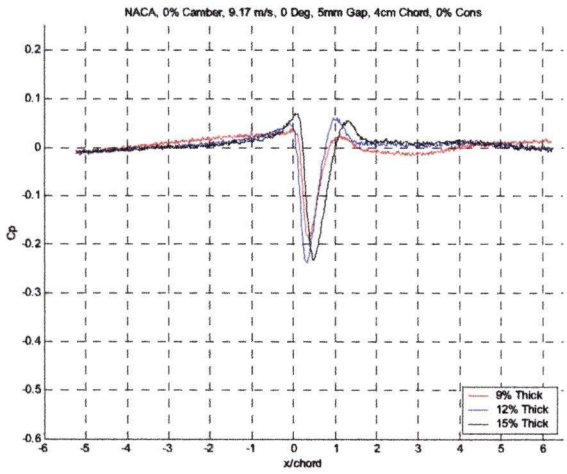
NACA, 0% Camber, 9.17 m/s, 0 Deg, 5mm Gap, 4cm Chord, 0% Cons
Cp
x/chord
9% Thick
12% Thick
15% Thick

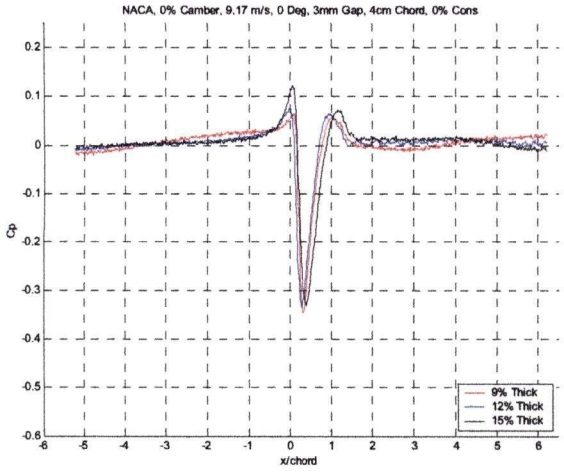
NACA, 0% Camber, 9.17 m/s, 0 Deg, 3mm Gap, 4cm Chord, 0% Cons
Cp
x/chord
9% Thick
12% Thick
15% Thick

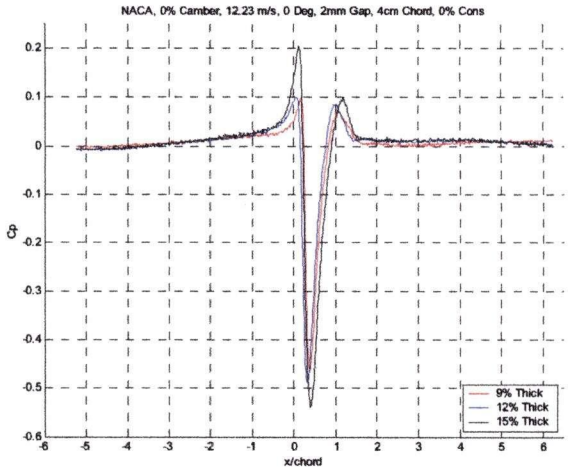
NACA, 0% Camber, 12.23 m/s, 0 Deg, 2mm Gap, 4cm Chord, 0% Cons
Cp
x/chord
9% Thick
12% Thick
15% Thick

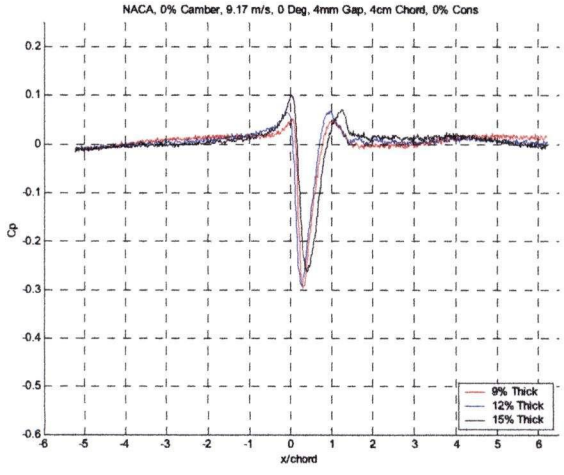
NACA, 0% Camber, 9.17 m/s, 0 Deg, 4mm Gap, 4cm Chord, 0% Cons
Cp
x/chord
9% Thick
12% Thick
15% Thick

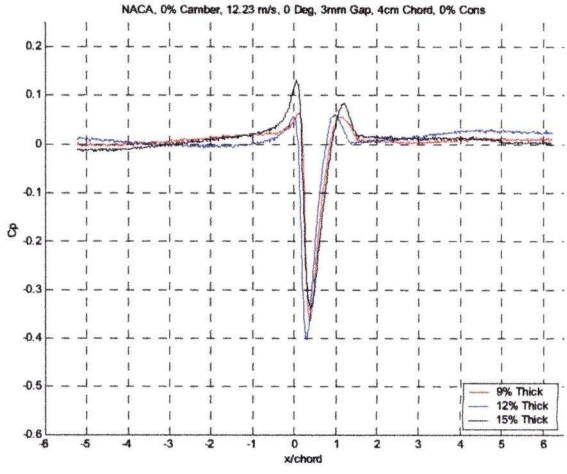
NACA, 0% Camber, 12.23 m/s, 0 Deg, 3mm Gap, 4cm Chord, 0% Cons
Cp
x/chord
9% Thick
12% Thick
15% Thick

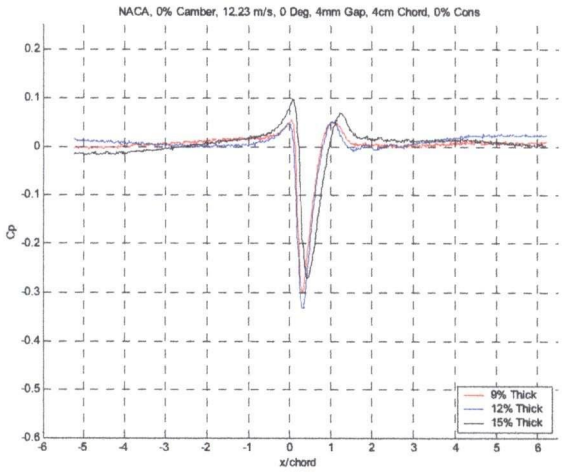
NACA, 0% Camber, 12.23 m/s, 0 Deg, 4mm Gap, 4cm Chord, 0% Cons
ΔP
x/chord
9% Thick
12% Thick
15% Thick

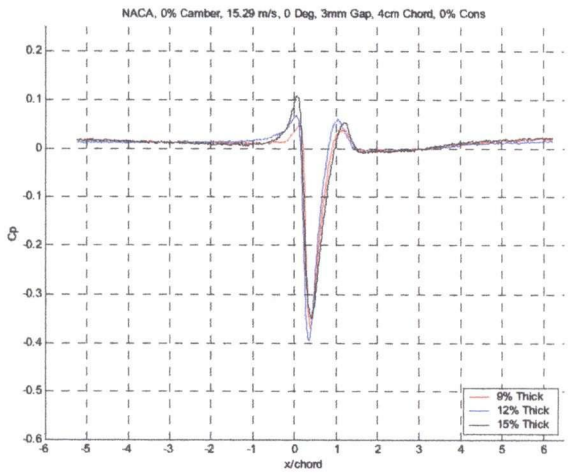
NACA, 0% Camber, 15.29 m/s, 0 Deg, 3mm Gap, 4cm Chord, 0% Cons
ΔP
x/chord
9% Thick
12% Thick
15% Thick

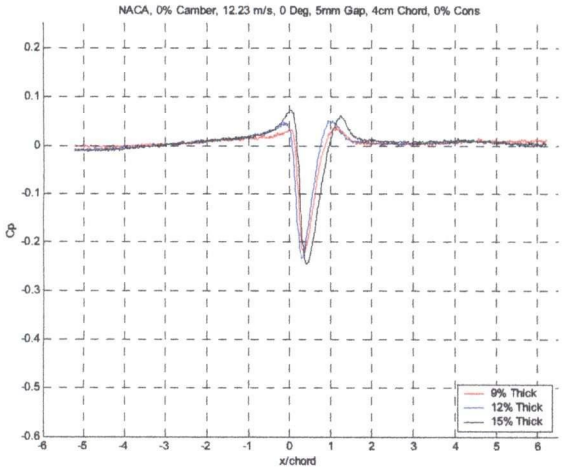
NACA, 0% Camber, 12.23 m/s, 0 Deg, 5mm Gap, 4cm Chord, 0% Cons
ΔP
x/chord
9% Thick
12% Thick
15% Thick

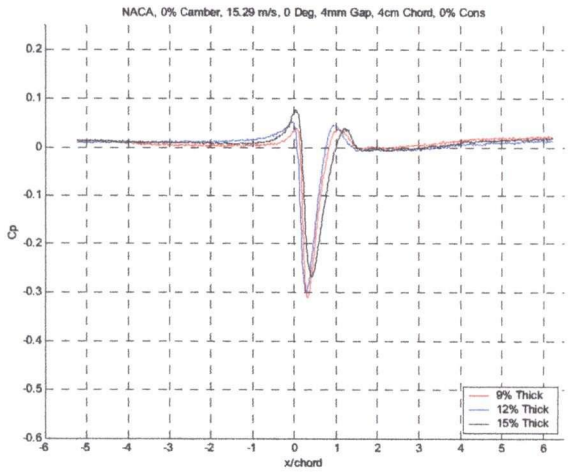
NACA, 0% Camber, 15.29 m/s, 0 Deg, 4mm Gap, 4cm Chord, 0% Cons
ΔP
x/chord
9% Thick
12% Thick
15% Thick

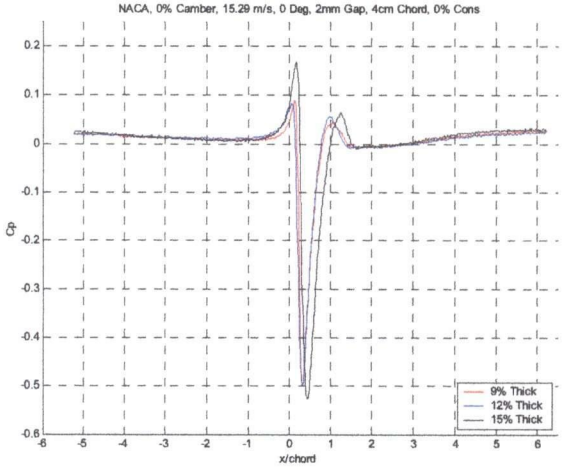
NACA, 0% Camber, 15.29 m/s, 0 Deg, 2mm Gap, 4cm Chord, 0% Cons
ΔP
x/chord
9% Thick
12% Thick
15% Thick

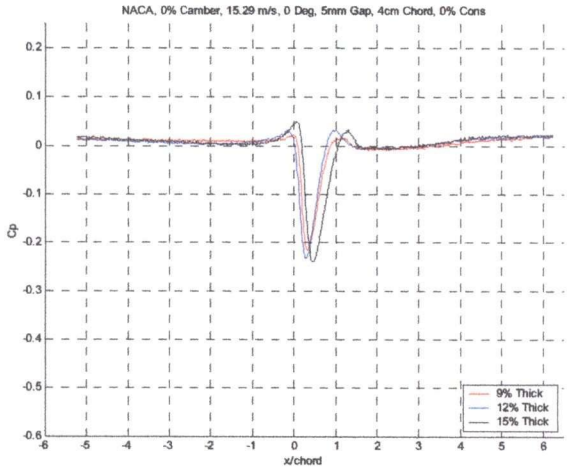
NACA, 0% Camber, 15.29 m/s, 0 Deg, 5mm Gap, 4cm Chord, 0% Cons
ΔP
x/chord
9% Thick
12% Thick
15% Thick

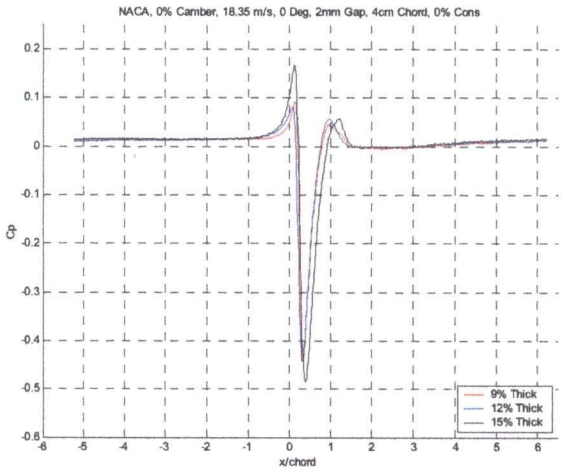
NACA, 0% Camber, 18.35 m/s, 0 Deg, 2mm Gap, 4cm Chord, 0% Cons
Cp
x/chord
9% Thick
12% Thick
15% Thick

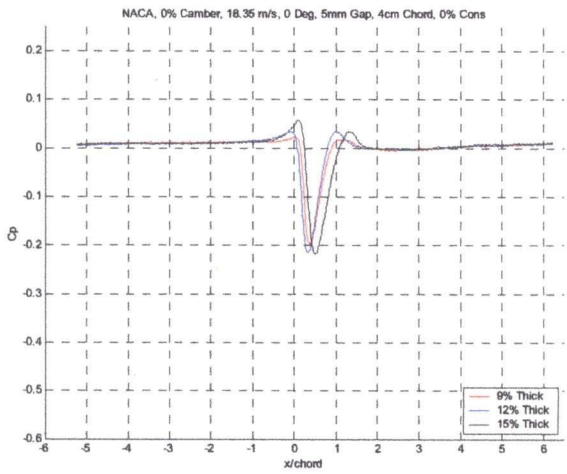
NACA, 0% Camber, 18.35 m/s, 0 Deg, 5mm Gap, 4cm Chord, 0% Cons
Cp
x/chord
9% Thick
12% Thick
15% Thick

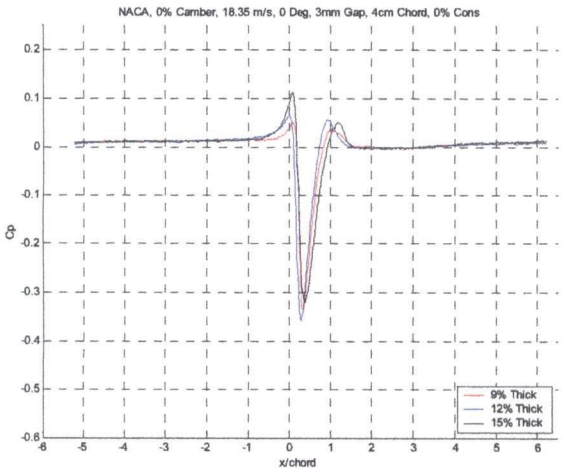
NACA, 0% Camber, 18.35 m/s, 0 Deg, 3mm Gap, 4cm Chord, 0% Cons
Cp
x/chord
9% Thick
12% Thick
15% Thick

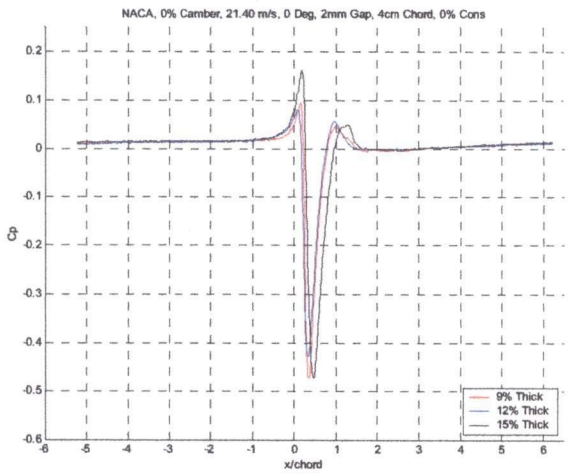
NACA, 0% Camber, 21.40 m/s, 0 Deg, 2mm Gap, 4cm Chord, 0% Cons
Cp
x/chord
9% Thick
12% Thick
15% Thick

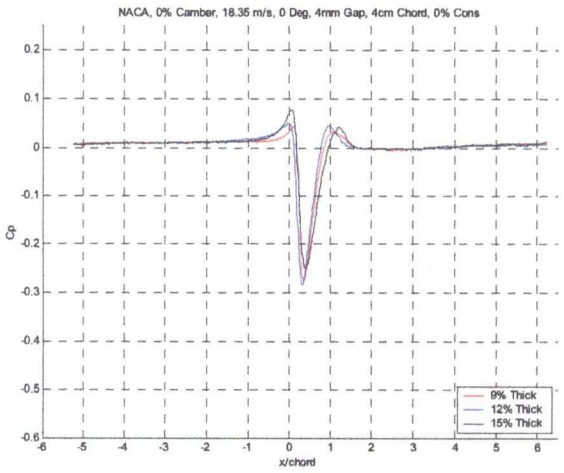
NACA, 0% Camber, 18.35 m/s, 0 Deg, 4mm Gap, 4cm Chord, 0% Cons
Cp
x/chord
9% Thick
12% Thick
15% Thick

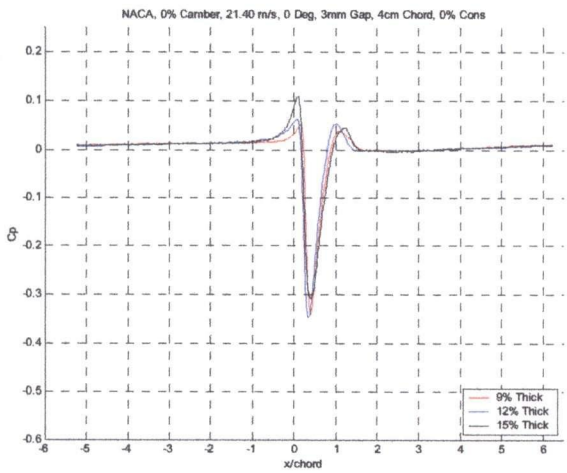
NACA, 0% Camber, 21.40 m/s, 0 Deg, 3mm Gap, 4cm Chord, 0% Cons
Cp
x/chord
9% Thick
12% Thick
15% Thick

Appendix 6 – The Effect of Foil Thickness on Pressure Pulse Magnitude

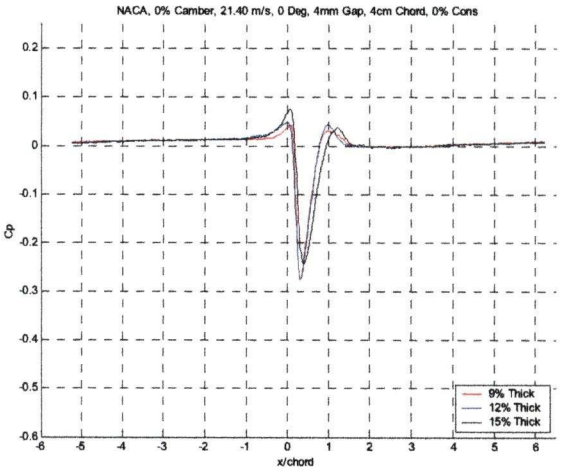

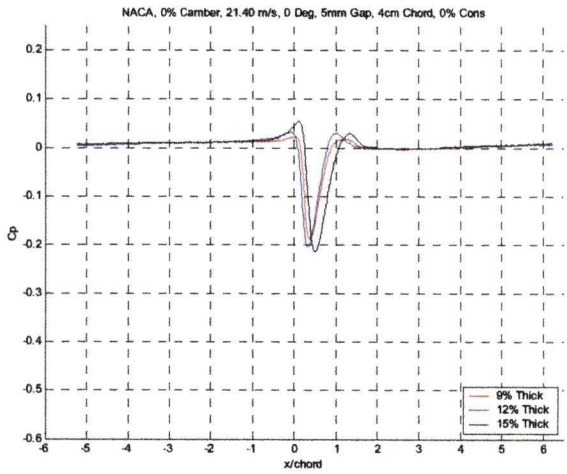

Appendix 7

The Effect of Camber on Pressure Pulse Magnitude

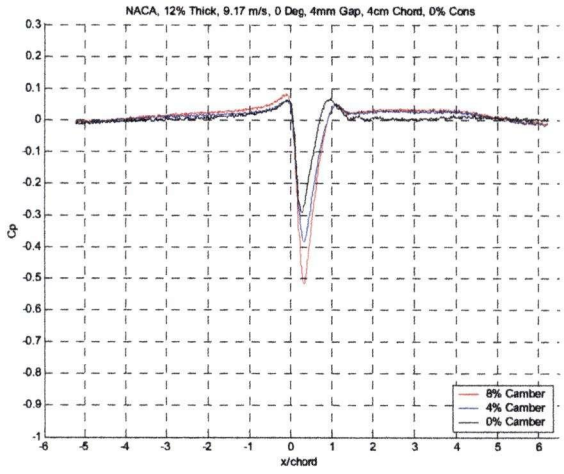
NACA, 12% Thick, 9.17 m/s, 0 Deg, 4mm Gap, 4cm Chord, 0% Cons
Cp
x/chord
8% Camber
4% Camber
0% Camber

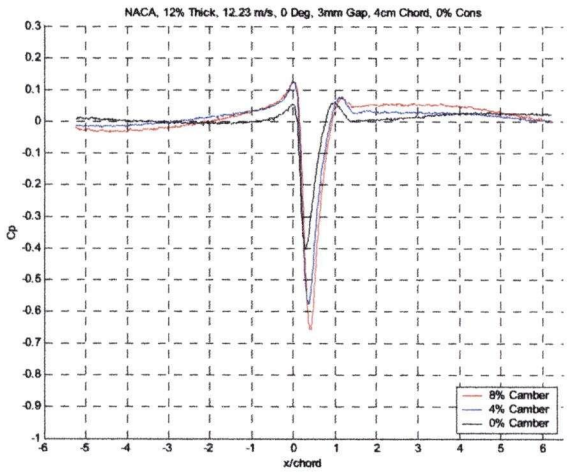
NACA, 12% Thick, 12.23 m/s, 0 Deg, 3mm Gap, 4cm Chord, 0% Cons
Cp
x/chord
8% Camber
4% Camber
0% Camber

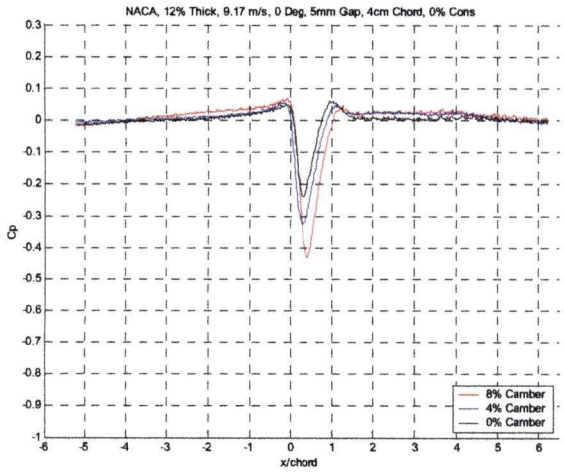
NACA, 12% Thick, 9.17 m/s, 0 Deg, 5mm Gap, 4cm Chord, 0% Cons
Cp
x/chord
8% Camber
4% Camber
0% Camber

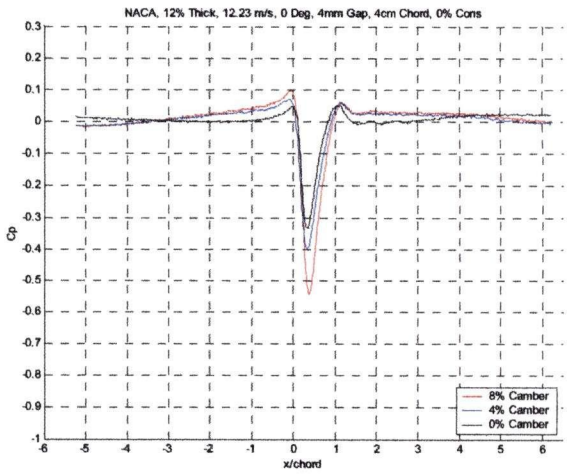
NACA, 12% Thick, 12.23 m/s, 0 Deg, 4mm Gap, 4cm Chord, 0% Cons
Cp
x/chord
8% Camber
4% Camber
0% Camber

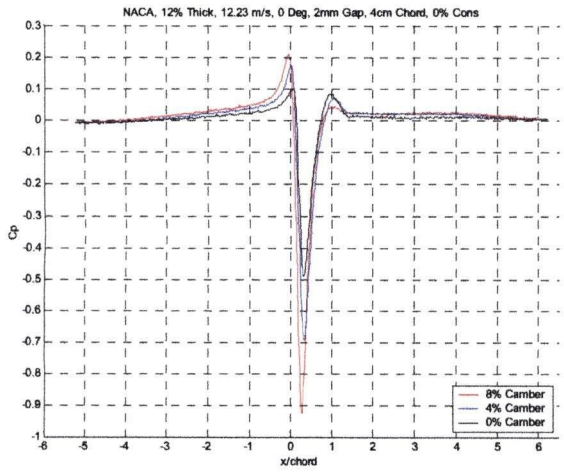
NACA, 12% Thick, 12.23 m/s, 0 Deg, 2mm Gap, 4cm Chord, 0% Cons
Cp
x/chord
8% Camber
4% Camber
0% Camber

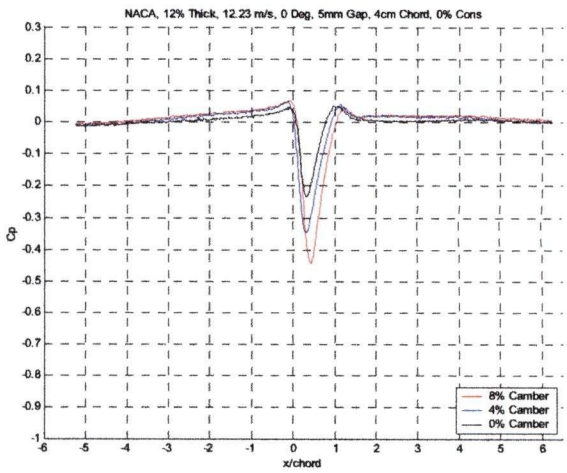
NACA, 12% Thick, 12.23 m/s, 0 Deg, 5mm Gap, 4cm Chord, 0% Cons
Cp
x/chord
8% Camber
4% Camber
0% Camber

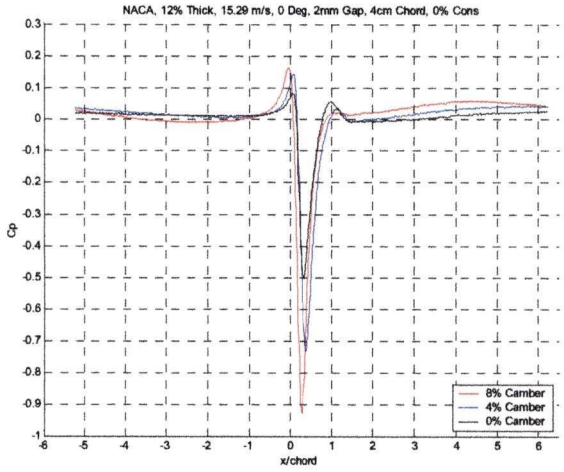
NACA, 12% Thick, 15.29 m/s, 0 Deg, 2mm Gap, 4cm Chord, 0% Cons
Cp
x/chord
8% Camber
4% Camber
0% Camber

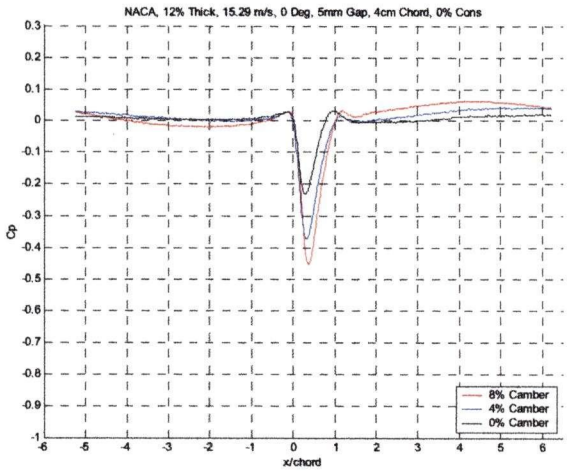
NACA, 12% Thick, 15.29 m/s, 0 Deg, 5mm Gap, 4cm Chord, 0% Cons
Cp
x/chord
8% Camber
4% Camber
0% Camber

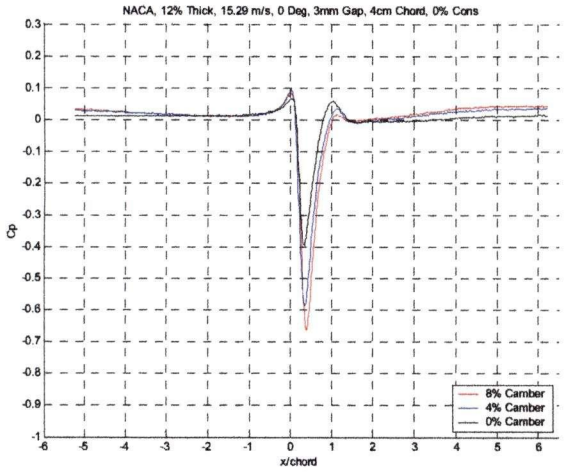
NACA, 12% Thick, 15.29 m/s, 0 Deg, 3mm Gap, 4cm Chord, 0% Cons
Cp
x/chord
8% Camber
4% Camber
0% Camber

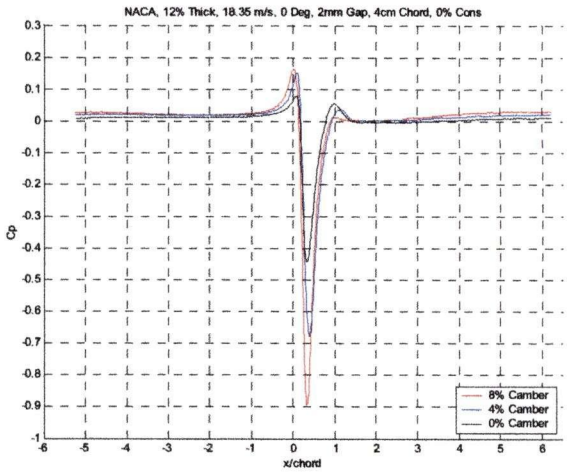
NACA, 12% Thick, 18.35 m/s, 0 Deg, 2mm Gap, 4cm Chord, 0% Cons
Cp
x/chord
8% Camber
4% Camber
0% Camber

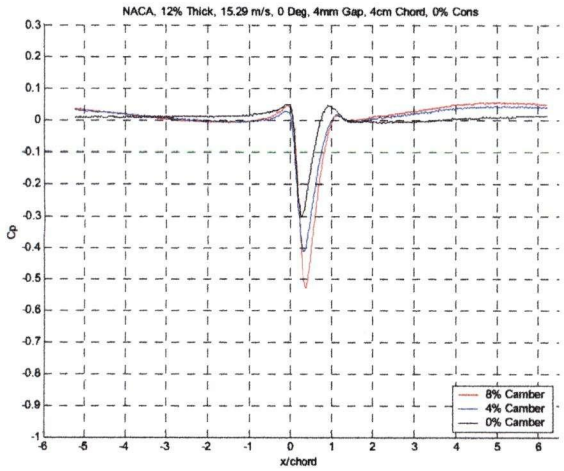
NACA, 12% Thick, 15.29 m/s, 0 Deg, 4mm Gap, 4cm Chord, 0% Cons
Cp
x/chord
8% Camber
4% Camber
0% Camber

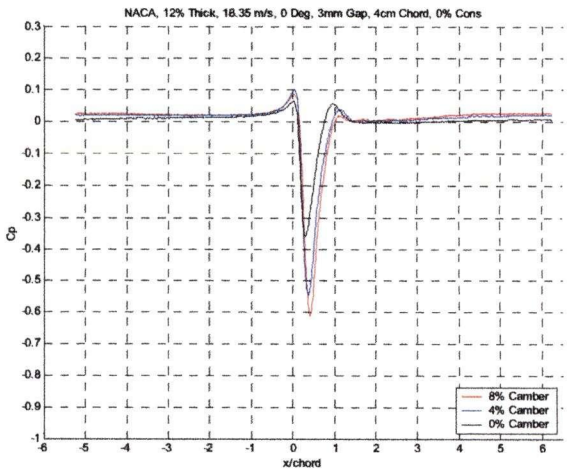
NACA, 12% Thick, 18.35 m/s, 0 Deg, 3mm Gap, 4cm Chord, 0% Cons
Cp
x/chord
8% Camber
4% Camber
0% Camber

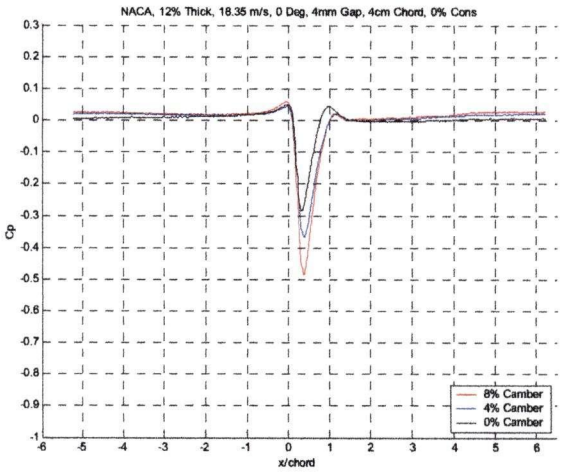
NACA, 12% Thick, 18.35 m/s, 0 Deg, 4mm Gap, 4cm Chord, 0% Cons
Cp
x/chord
8% Camber
4% Camber
0% Camber

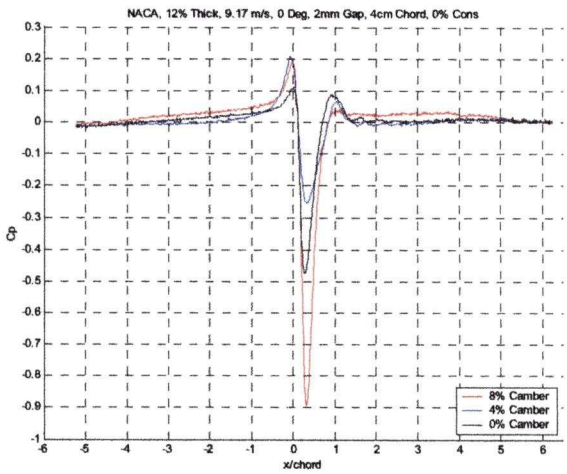
NACA, 12% Thick, 9.17 m/s, 0 Deg, 2mm Gap, 4cm Chord, 0% Cons
Cp
x/chord
8% Camber
4% Camber
0% Camber

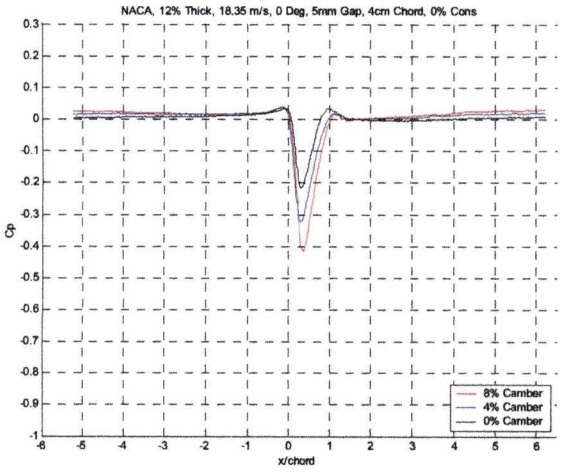
NACA, 12% Thick, 18.35 m/s, 0 Deg, 5mm Gap, 4cm Chord, 0% Cons
Cp
x/chord
8% Camber
4% Camber
0% Camber

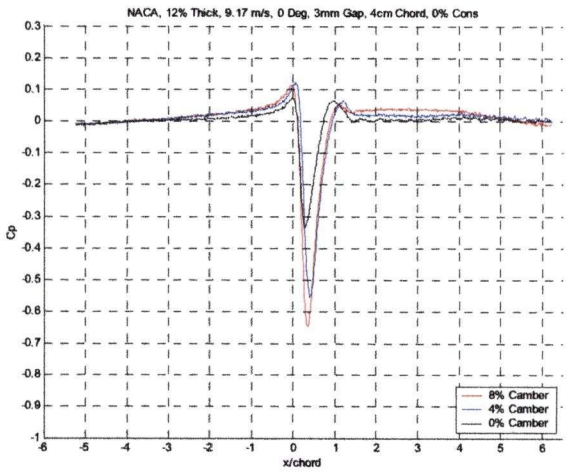
NACA, 12% Thick, 9.17 m/s, 0 Deg, 3mm Gap, 4cm Chord, 0% Cons
Cp
x/chord
8% Camber
4% Camber
0% Camber

Appendix 8

The Effect of Foil Chord Length on Pressure Pulse Magnitude

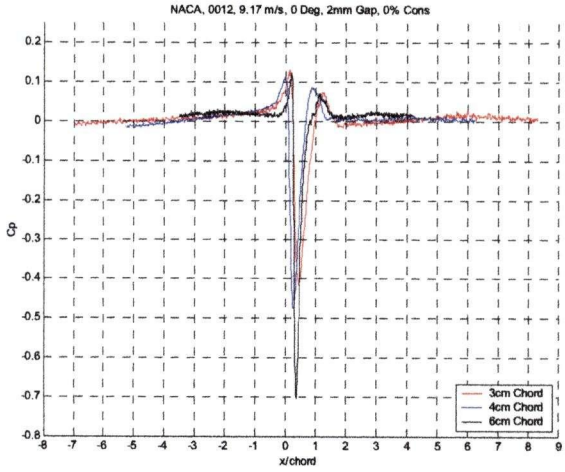
NACA, 0012, 9.17 m/s, 0 Deg, 2mm Gap, 0% Cons
Cp
x/chord
3cm Chord
4cm Chord
6cm Chord

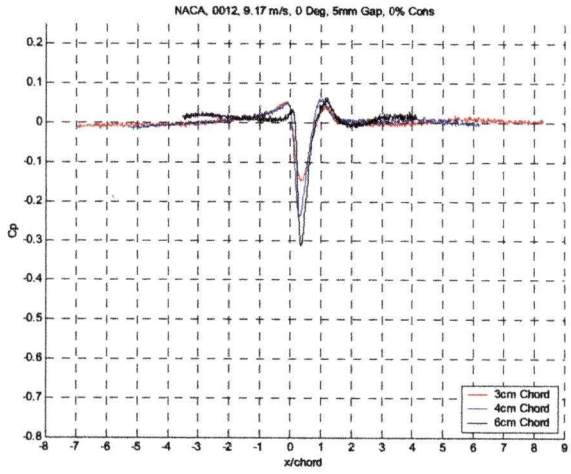
NACA, 0012, 9.17 m/s, 0 Deg, 5mm Gap, 0% Cons
Cp
x/chord
3cm Chord
4cm Chord
6cm Chord

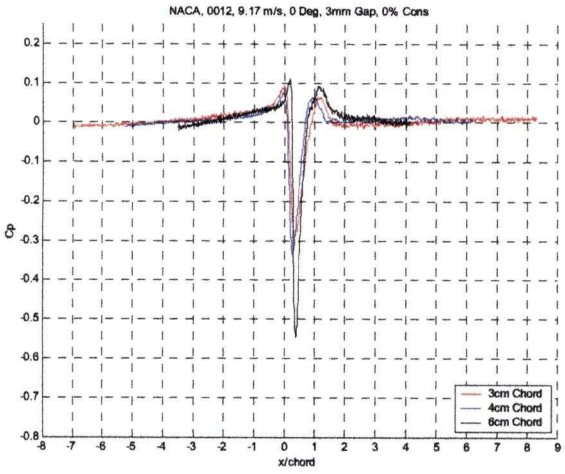
NACA, 0012, 9.17 m/s, 0 Deg, 3mm Gap, 0% Cons
Cp
x/chord
3cm Chord
4cm Chord
6cm Chord

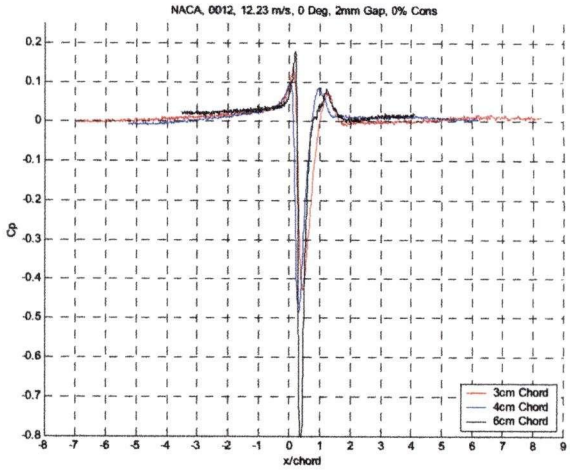
NACA, 0012, 12.23 m/s, 0 Deg, 2mm Gap, 0% Cons
Cp
x/chord
3cm Chord
4cm Chord
6cm Chord

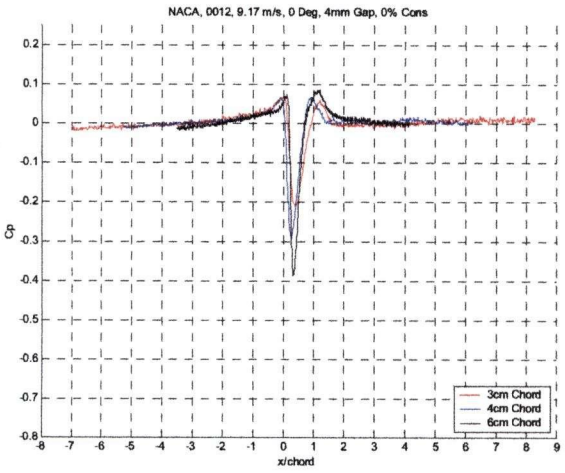
NACA, 0012, 9.17 m/s, 0 Deg, 4mm Gap, 0% Cons
Cp
x/chord
3cm Chord
4cm Chord
6cm Chord

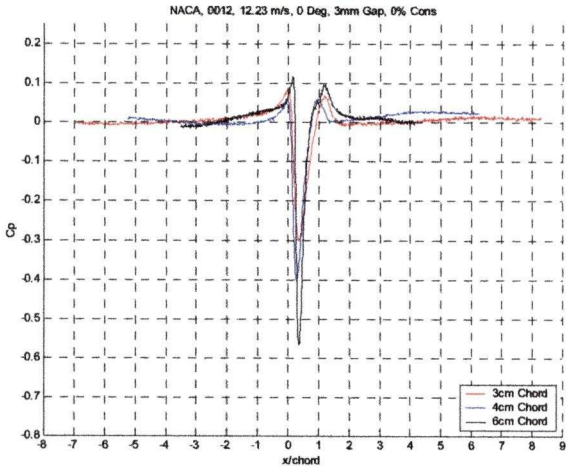
NACA, 0012, 12.23 m/s, 0 Deg, 3mm Gap, 0% Cons
Cp
x/chord
3cm Chord
4cm Chord
6cm Chord

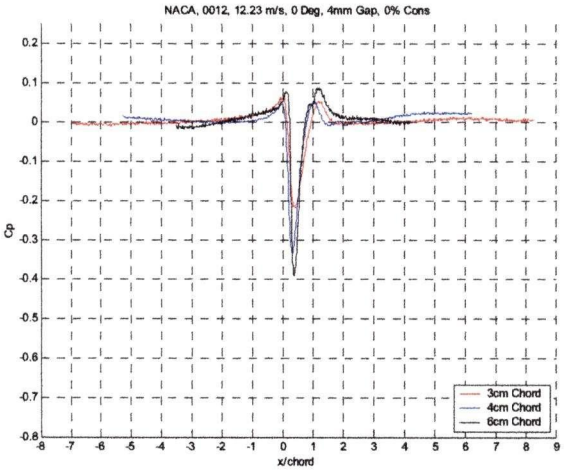
NACA, 0012, 12.23 m/s, 0 Deg, 4mm Gap, 0% Cons
Cp
x/chord
3cm Chord
4cm Chord
6cm Chord

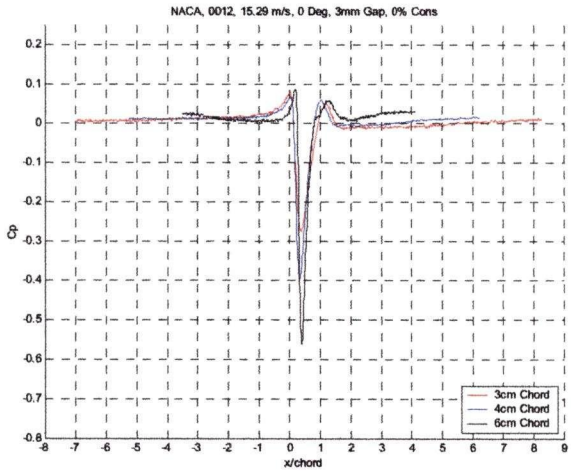
NACA, 0012, 15.29 m/s, 0 Deg, 3mm Gap, 0% Cons
Cp
x/chord
3cm Chord
4cm Chord
6cm Chord

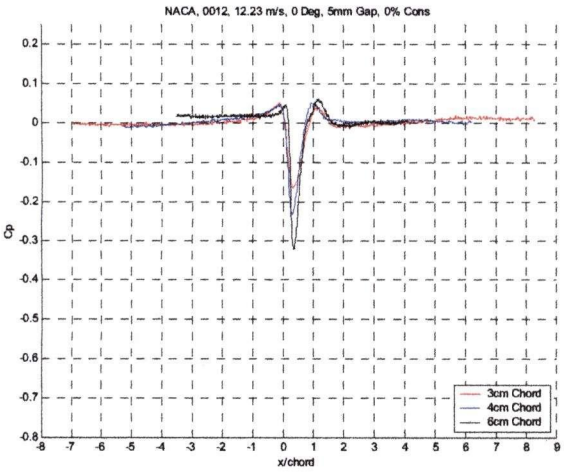
NACA, 0012, 12.23 m/s, 0 Deg, 5mm Gap, 0% Cons
Cp
x/chord
3cm Chord
4cm Chord
6cm Chord

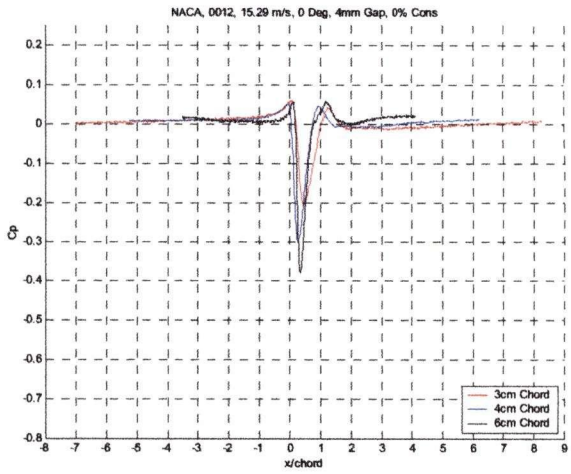
NACA, 0012, 15.29 m/s, 0 Deg, 4mm Gap, 0% Cons
Cp
x/chord
3cm Chord
4cm Chord
6cm Chord

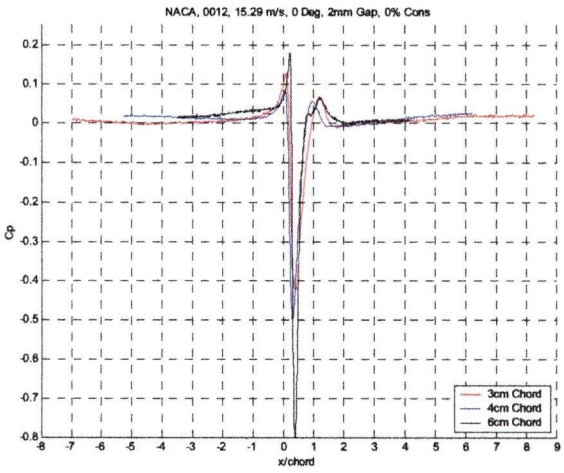
NACA, 0012, 15.29 m/s, 0 Deg, 2mm Gap, 0% Cons
Cp
x/chord
3cm Chord
4cm Chord
6cm Chord

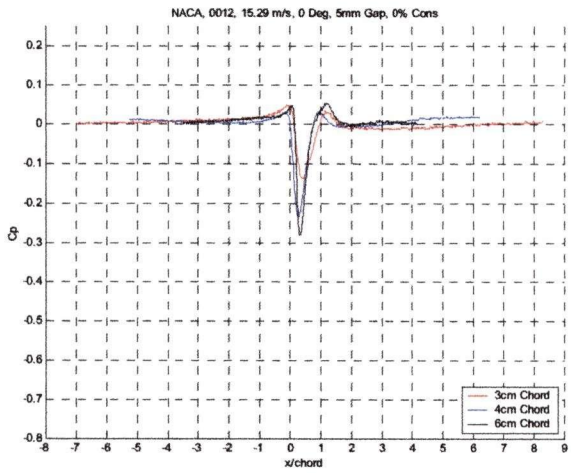
NACA, 0012, 15.29 m/s, 0 Deg, 5mm Gap, 0% Cons
Cp
x/chord
3cm Chord
4cm Chord
6cm Chord

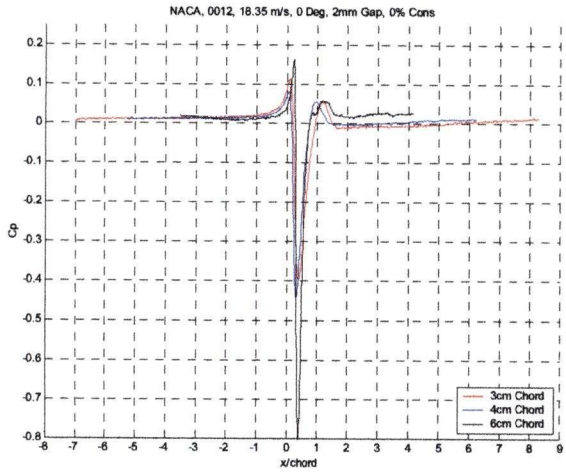
NACA, 0012, 18.35 m/s, 0 Deg, 2mm Gap, 0% Cons
Cp
x/chord
3cm Chord
4cm Chord
6cm Chord

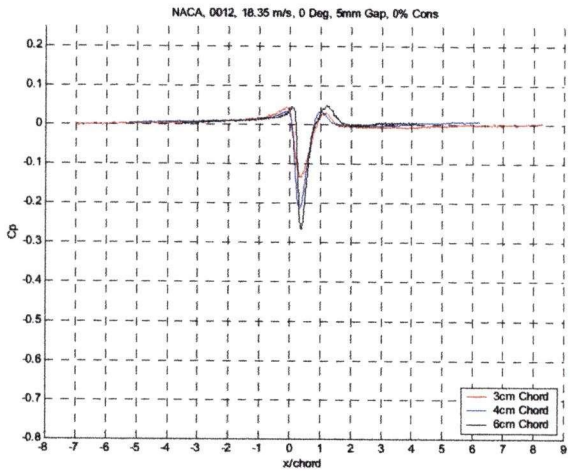
NACA, 0012, 18.35 m/s, 0 Deg, 5mm Gap, 0% Cons
Cp
x/chord
3cm Chord
4cm Chord
6cm Chord

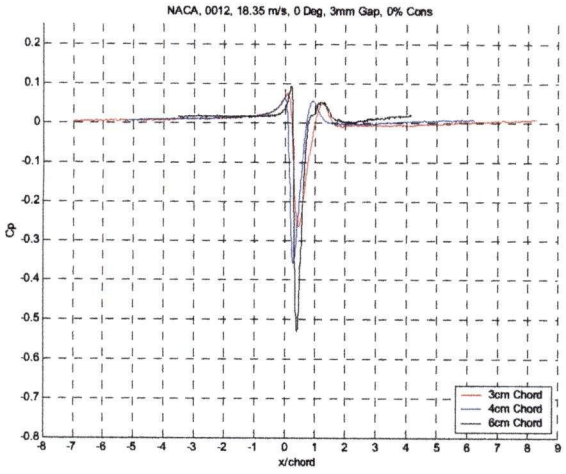
NACA, 0012, 18.35 m/s, 0 Deg, 3mm Gap, 0% Cons
Cp
x/chord
3cm Chord
4cm Chord
6cm Chord

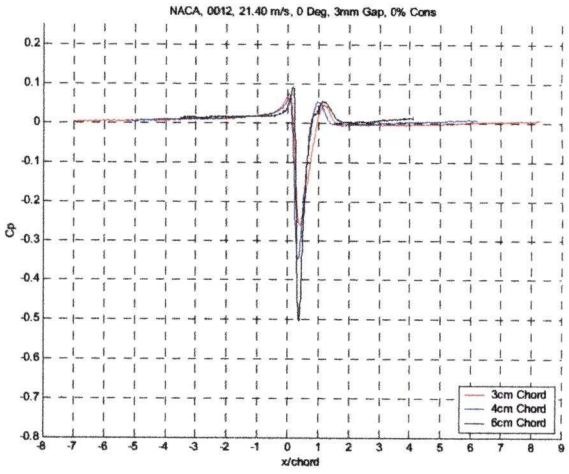
NACA, 0012, 21.40 m/s, 0 Deg, 3mm Gap, 0% Cons
Cp
x/chord
3cm Chord
4cm Chord
6cm Chord

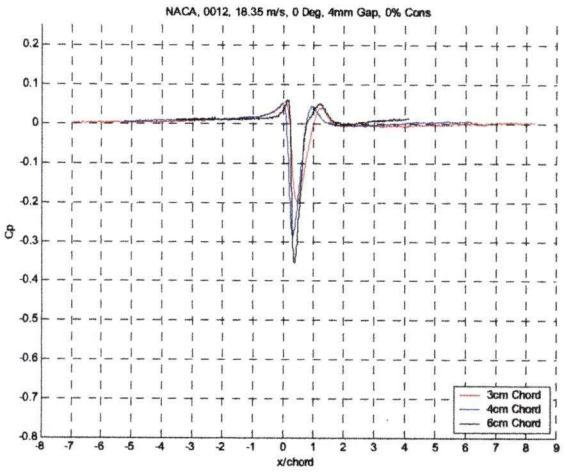
NACA, 0012, 18.35 m/s, 0 Deg, 4mm Gap, 0% Cons
Cp
x/chord
3cm Chord
4cm Chord
6cm Chord

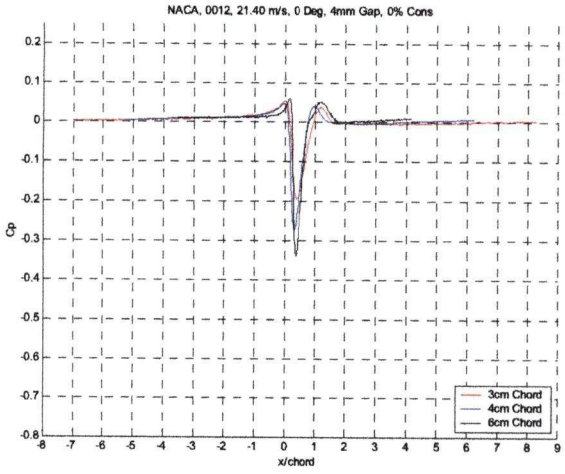
NACA, 0012, 21.40 m/s, 0 Deg, 4mm Gap, 0% Cons
Cp
x/chord
3cm Chord
4cm Chord
6cm Chord

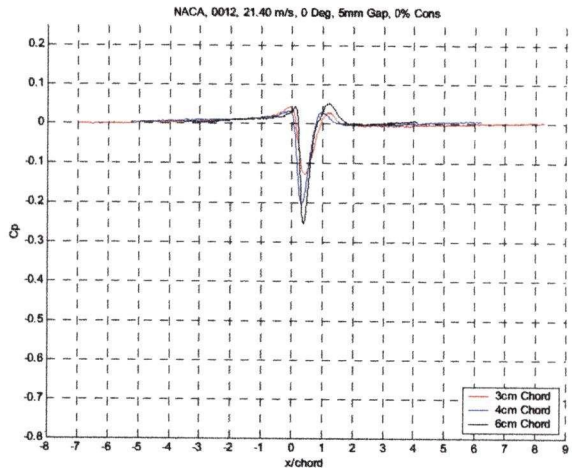
NACA, 0012, 21.40 m/s, 0 Deg, 5mm Gap, 0% Cons
Cp
x/chord
3cm Chord
4cm Chord
6cm Chord

Appendix 9

The Effect of Angle of Attack on Pressure Pulse Magnitude

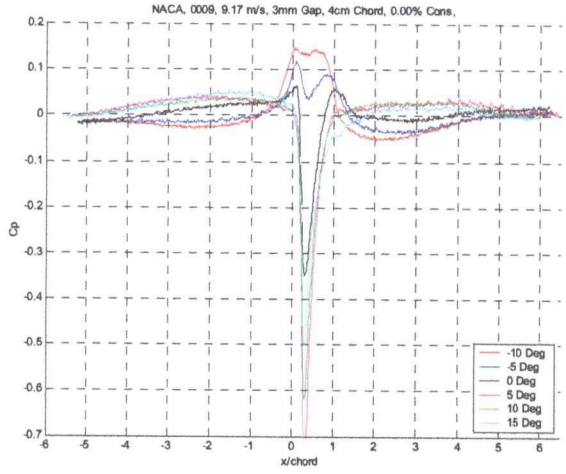
NACA, 0009, 9.17 m/s, 3mm Gap, 4cm Chord, 0.00% Cons,
Cp
x/chord
-10 Deg
-5 Deg
0 Deg
5 Deg
10 Deg
15 Deg

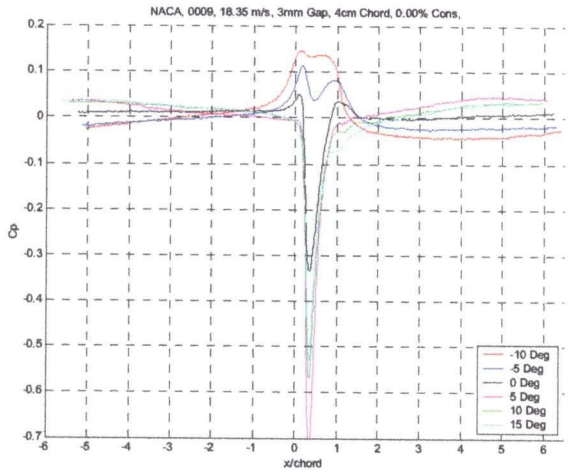
NACA, 0009, 18.35 m/s, 3mm Gap, 4cm Chord, 0.00% Cons,
Cp
x/chord
-10 Deg
-5 Deg
0 Deg
5 Deg
10 Deg
15 Deg

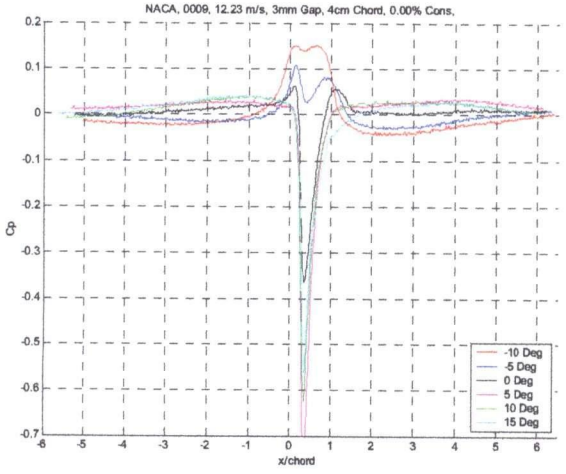
NACA, 0009, 12.23 m/s, 3mm Gap, 4cm Chord, 0.00% Cons,
Cp
x/chord
-10 Deg
-5 Deg
0 Deg
5 Deg
10 Deg
15 Deg

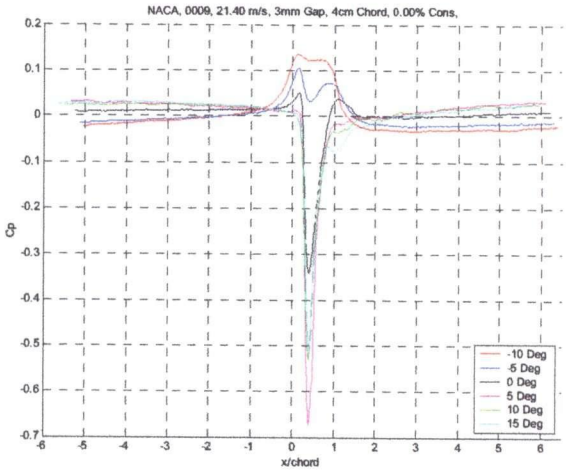
NACA, 0009, 21.40 m/s, 3mm Gap, 4cm Chord, 0.00% Cons,
Cp
x/chord
-10 Deg
-5 Deg
0 Deg
5 Deg
10 Deg
15 Deg

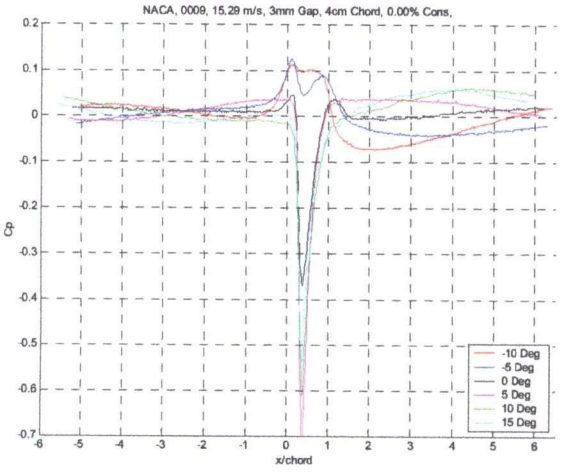
NACA, 0009, 15.29 m/s, 3mm Gap, 4cm Chord, 0.00% Cons,
Cp
x/chord
-10 Deg
-5 Deg
0 Deg
5 Deg
10 Deg
15 Deg

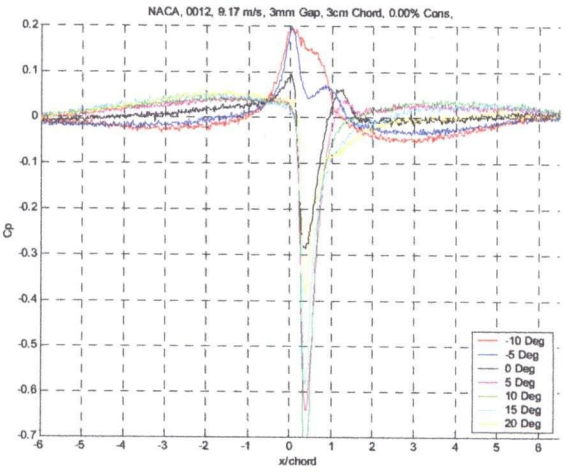
NACA, 0012, 9.17 m/s, 3mm Gap, 3cm Chord, 0.00% Cons,
Cp
x/chord
-10 Deg
-5 Deg
0 Deg
5 Deg
10 Deg
15 Deg
20 Deg

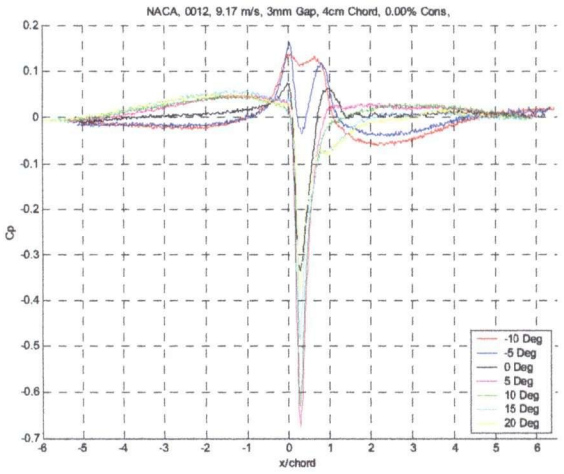
NACA, 0012, 9.17 m/s, 3mm Gap, 4cm Chord, 0.00% Cons,
Cp
x/chord
-10 Deg
-5 Deg
0 Deg
5 Deg
10 Deg
15 Deg
20 Deg

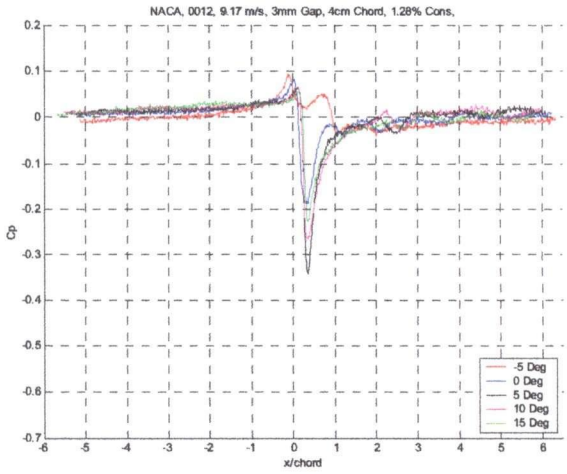
NACA, 0012, 9.17 m/s, 3mm Gap, 4cm Chord, 1.28% Cons,
Cp
x/chord
-5 Deg
0 Deg
5 Deg
10 Deg
15 Deg

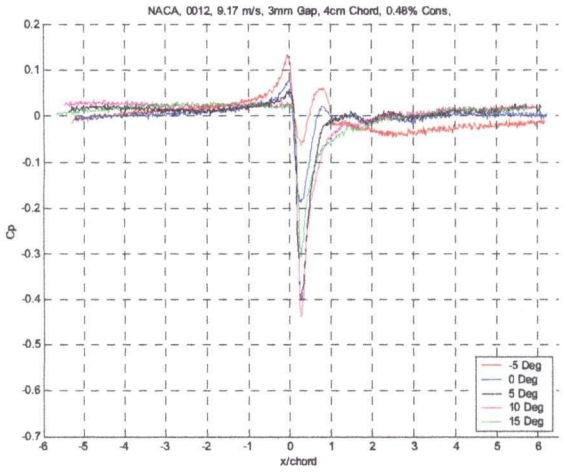
NACA, 0012, 9.17 m/s, 3mm Gap, 4cm Chord, 0.48% Cons,
Cp
x/chord
-5 Deg
0 Deg
5 Deg
10 Deg
15 Deg

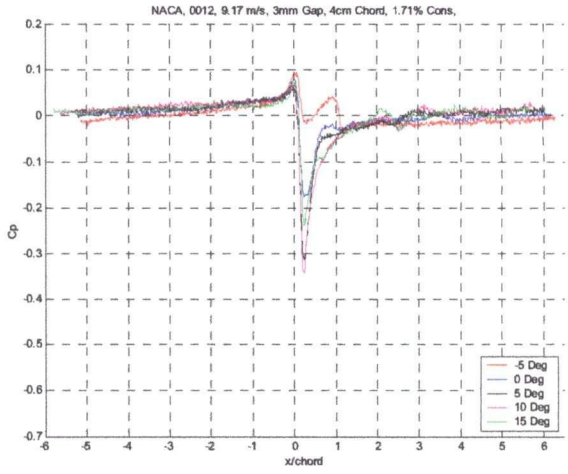
NACA, 0012, 9.17 m/s, 3mm Gap, 4cm Chord, 1.71% Cons,
Cp
x/chord
-5 Deg
0 Deg
5 Deg
10 Deg
15 Deg

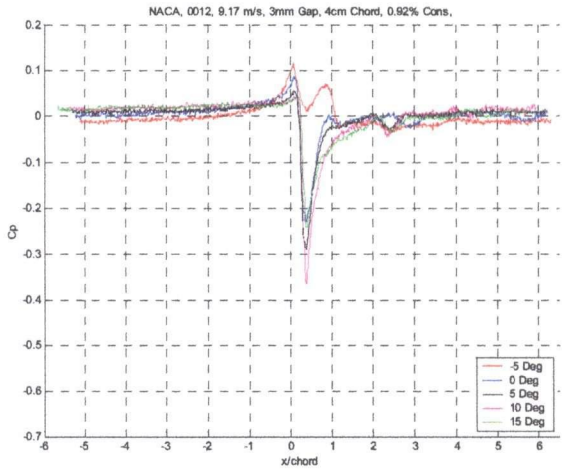
NACA, 0012, 9.17 m/s, 3mm Gap, 4cm Chord, 0.92% Cons,
Cp
x/chord
-5 Deg
0 Deg
5 Deg
10 Deg
15 Deg

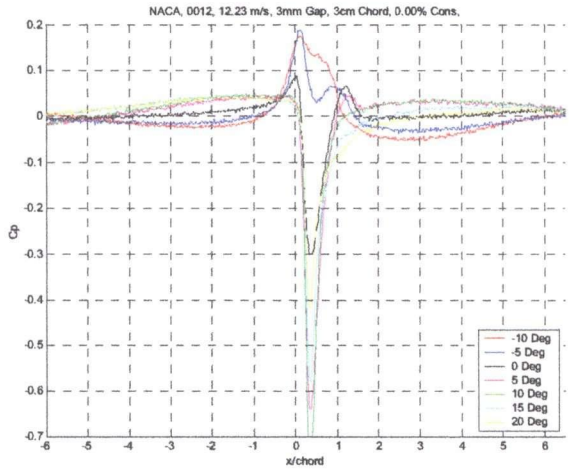
NACA, 0012, 12.23 m/s, 3mm Gap, 3cm Chord, 0.00% Cons,
Cp
x/chord
-10 Deg
-5 Deg
0 Deg
5 Deg
10 Deg
15 Deg
20 Deg

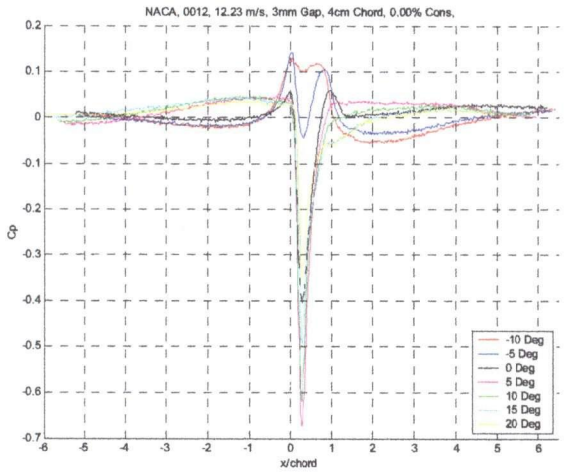
NACA, 0012, 12.23 m/s, 3mm Gap, 4cm Chord, 0.00% Cons,
Cp
x/chord
-10 Deg
-5 Deg
0 Deg
5 Deg
10 Deg
15 Deg
20 Deg

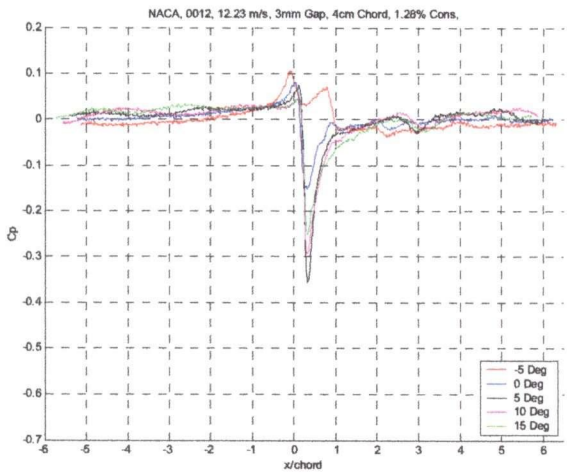
NACA, 0012, 12.23 m/s, 3mm Gap, 4cm Chord, 1.28% Cons,
Cp
x/chord
-5 Deg
0 Deg
5 Deg
10 Deg
15 Deg

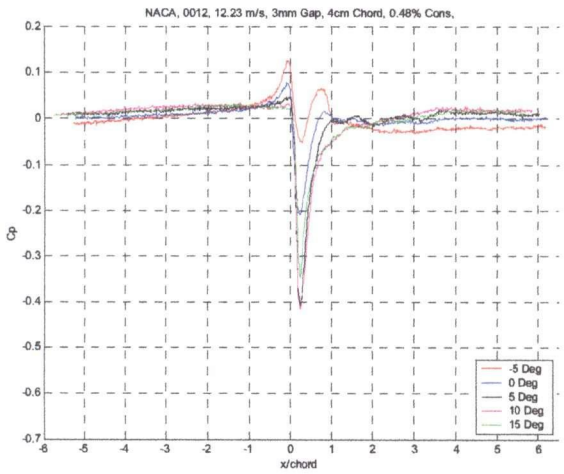
NACA, 0012, 12.23 m/s, 3mm Gap, 4cm Chord, 0.48% Cons,
Cp
x/chord
-5 Deg
0 Deg
5 Deg
10 Deg
15 Deg

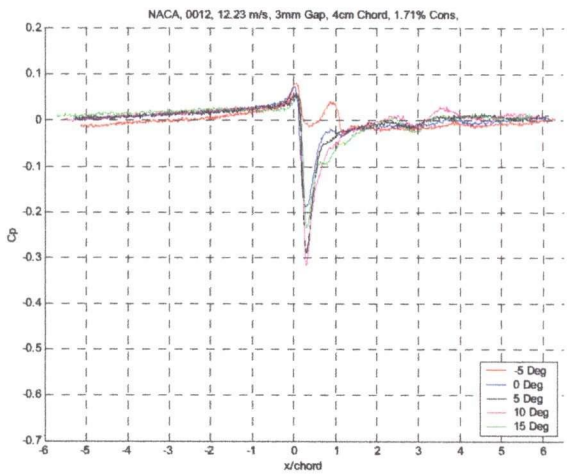
NACA, 0012, 12.23 m/s, 3mm Gap, 4cm Chord, 1.71% Cons,
Cp
x/chord
-5 Deg
0 Deg
5 Deg
10 Deg
15 Deg

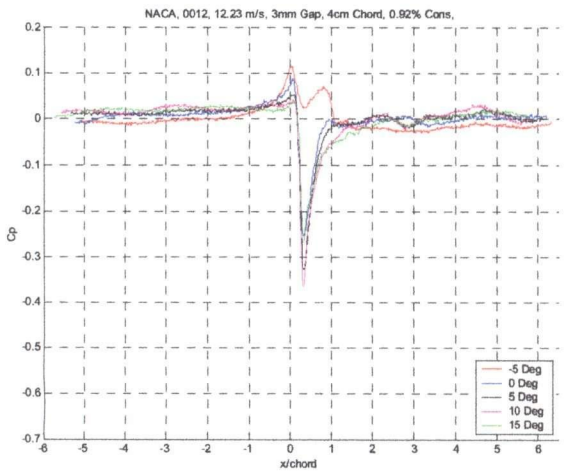
NACA, 0012, 12.23 m/s, 3mm Gap, 4cm Chord, 0.92% Cons,
Cp
x/chord
-5 Deg
0 Deg
5 Deg
10 Deg
15 Deg

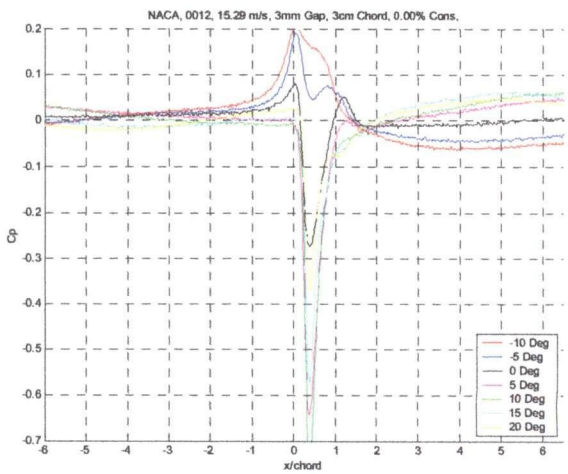
NACA, 0012, 15.29 m/s, 3mm Gap, 3cm Chord, 0.00% Cons,
Cp
x/chord
-10 Deg
-5 Deg
0 Deg
5 Deg
10 Deg
15 Deg
20 Deg

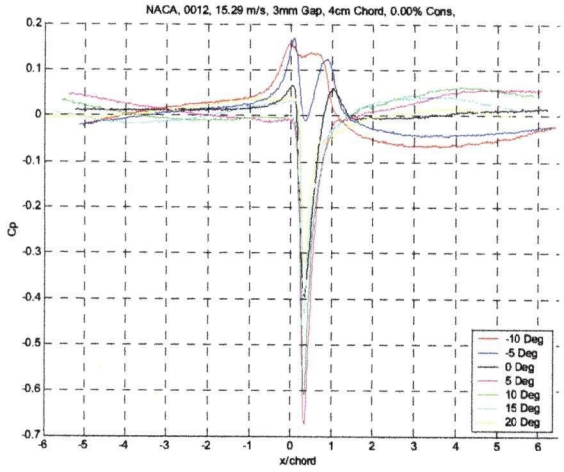
NACA, 0012, 15.29 m/s, 3mm Gap, 4cm Chord, 0.00% Cons,
Cp
x/chord
-10 Deg
-5 Deg
0 Deg
5 Deg
10 Deg
15 Deg
20 Deg

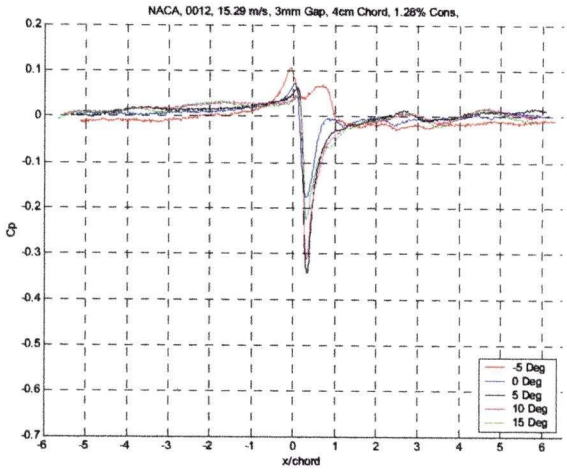
NACA, 0012, 15.29 m/s, 3mm Gap, 4cm Chord, 1.28% Cons,
Cp
x/chord
-5 Deg
0 Deg
5 Deg
10 Deg
15 Deg

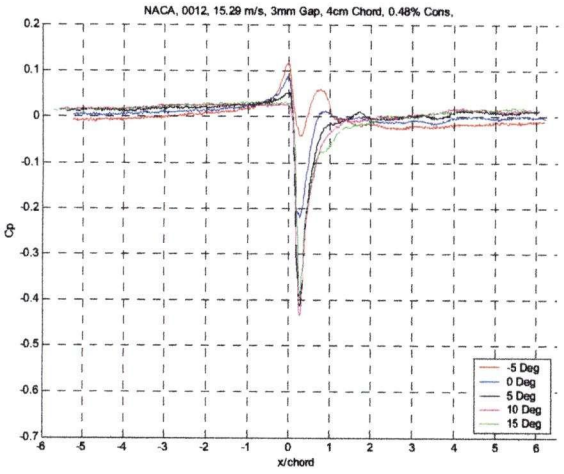
NACA, 0012, 15.29 m/s, 3mm Gap, 4cm Chord, 0.48% Cons,
Cp
x/chord
-5 Deg
0 Deg
5 Deg
10 Deg
15 Deg

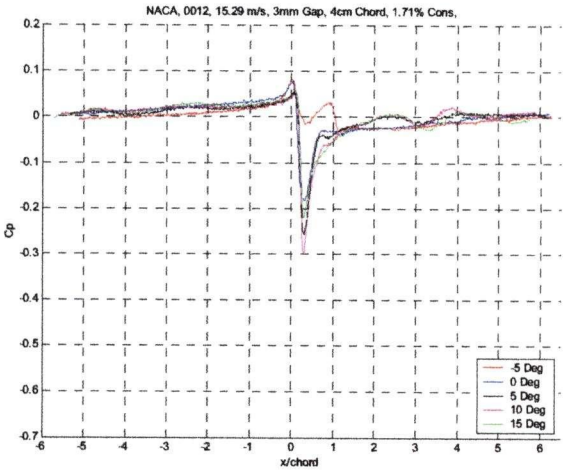
NACA, 0012, 15.29 m/s, 3mm Gap, 4cm Chord, 1.71% Cons,
Cp
x/chord
-5 Deg
0 Deg
5 Deg
10 Deg
15 Deg

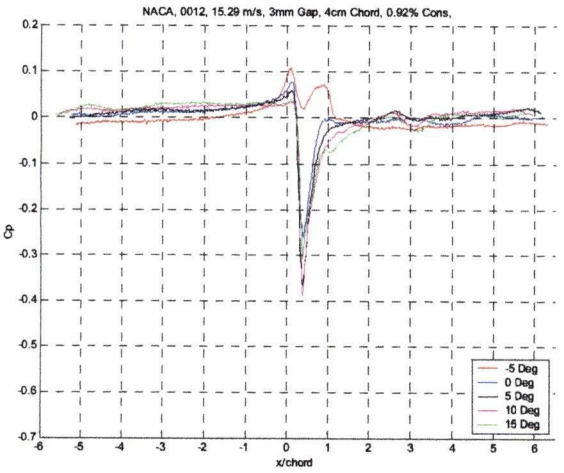
NACA, 0012, 15.29 m/s, 3mm Gap, 4cm Chord, 0.92% Cons,
Cp
x/chord
-5 Deg
0 Deg
5 Deg
10 Deg
15 Deg

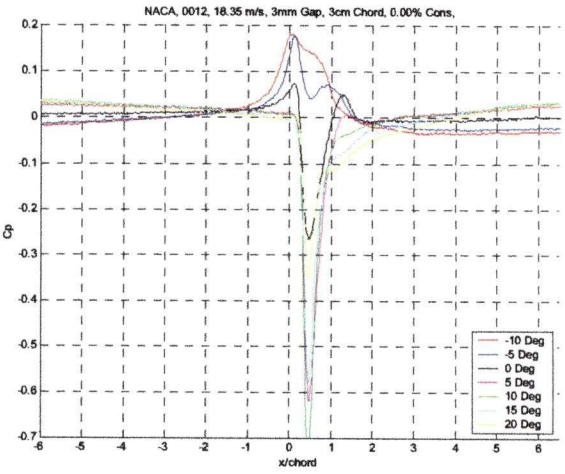
NACA, 0012, 18.35 m/s, 3mm Gap, 3cm Chord, 0.00% Cons,
Cp
x/chord
-10 Deg
-5 Deg
0 Deg
5 Deg
10 Deg
15 Deg
20 Deg

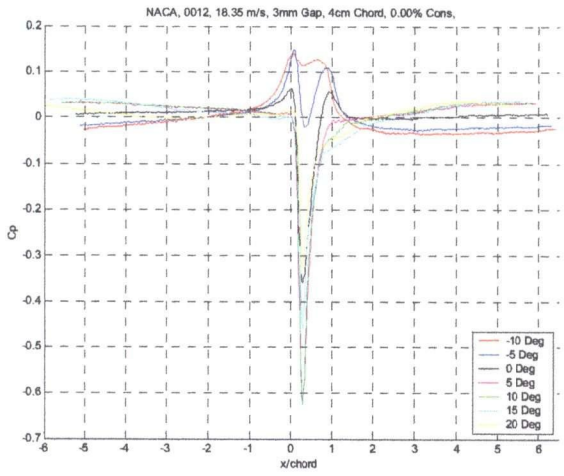
NACA, 0012, 18.35 m/s, 3mm Gap, 4cm Chord, 0.00% Cons,
Cp
x/chord
-10 Deg
-5 Deg
0 Deg
5 Deg
10 Deg
15 Deg
20 Deg

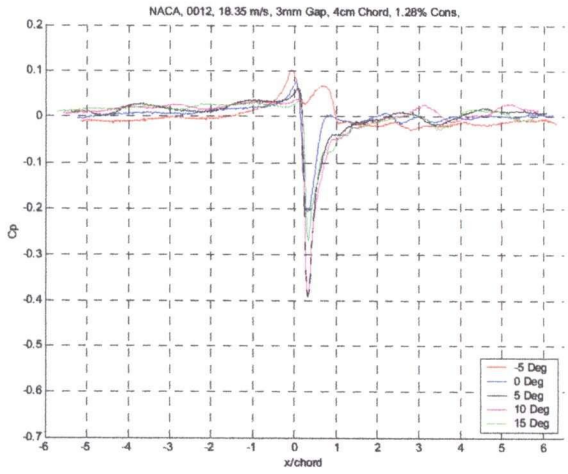
NACA, 0012, 18.35 m/s, 3mm Gap, 4cm Chord, 1.28% Cons,
Cp
x/chord
-5 Deg
0 Deg
5 Deg
10 Deg
15 Deg

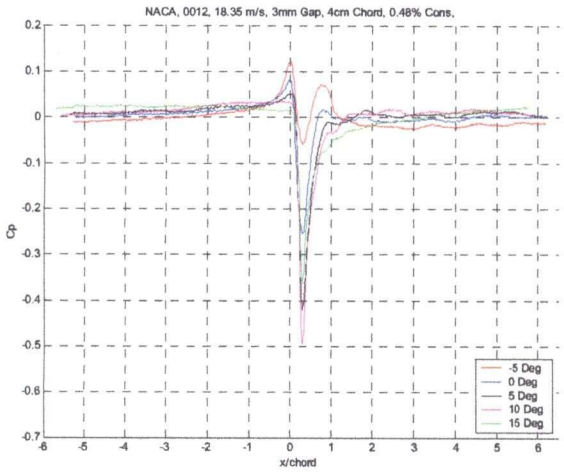
NACA, 0012, 18.35 m/s, 3mm Gap, 4cm Chord, 0.48% Cons,
Cp
x/chord
-5 Deg
0 Deg
5 Deg
10 Deg
15 Deg

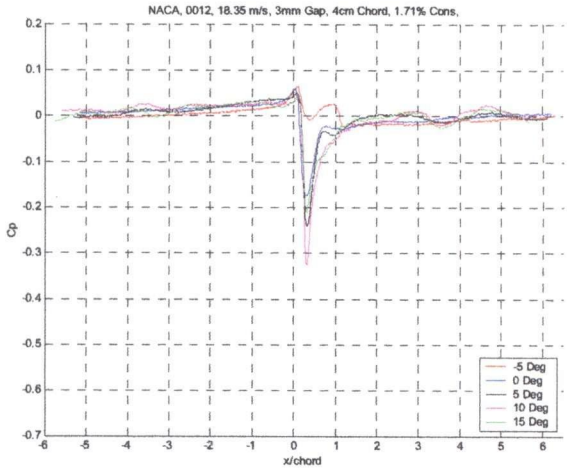
NACA, 0012, 18.35 m/s, 3mm Gap, 4cm Chord, 1.71% Cons,
Cp
x/chord
-5 Deg
0 Deg
5 Deg
10 Deg
15 Deg

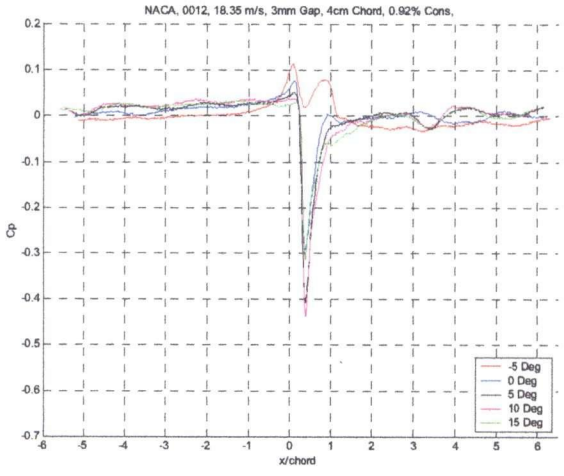
NACA, 0012, 18.35 m/s, 3mm Gap, 4cm Chord, 0.92% Cons,
Cp
x/chord
-5 Deg
0 Deg
5 Deg
10 Deg
15 Deg

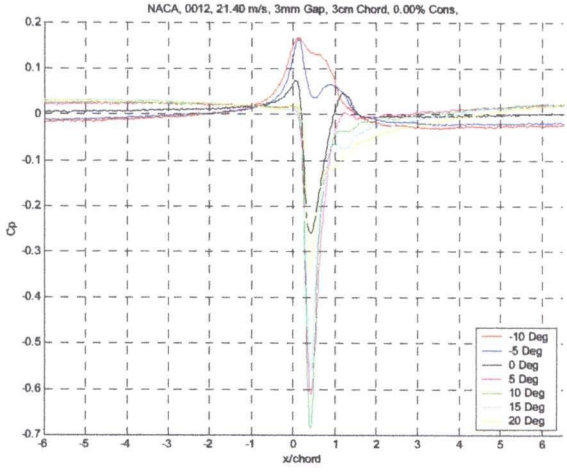
NACA, 0012, 21.40 m/s, 3mm Gap, 3cm Chord, 0.00% Cons,
Cp
x/chord
-10 Deg
-5 Deg
0 Deg
5 Deg
10 Deg
15 Deg
20 Deg

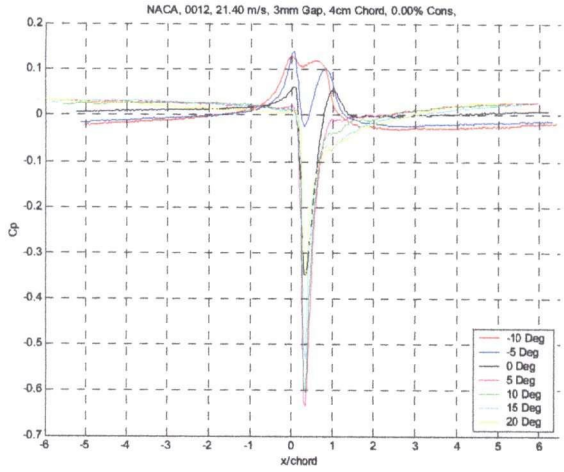
NACA, 0012, 21.40 m/s, 3mm Gap, 4cm Chord, 0.00% Cons,
Cp
x/chord
-10 Deg
-5 Deg
0 Deg
5 Deg
10 Deg
15 Deg
20 Deg

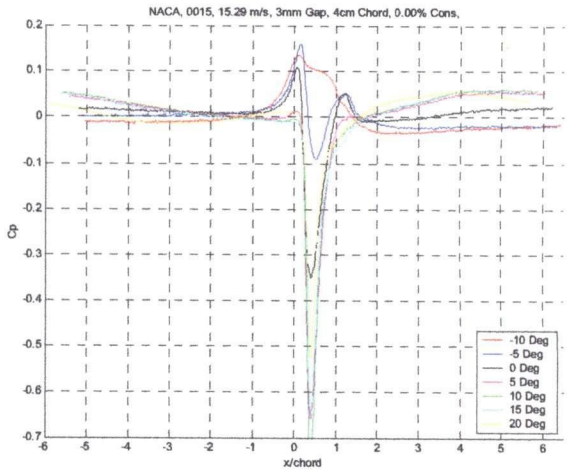
NACA, 0015, 15.29 m/s, 3mm Gap, 4cm Chord, 0.00% Cons,
Cp
x/chord
-10 Deg
-5 Deg
0 Deg
5 Deg
10 Deg
15 Deg
20 Deg

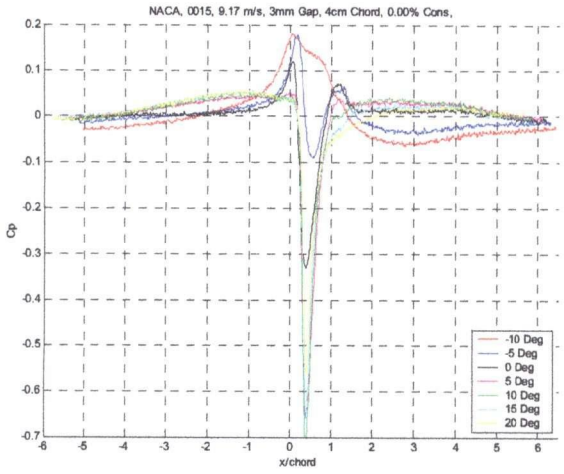
NACA, 0015, 9.17 m/s, 3mm Gap, 4cm Chord, 0.00% Cons,
Cp
x/chord
-10 Deg
-5 Deg
0 Deg
5 Deg
10 Deg
15 Deg
20 Deg

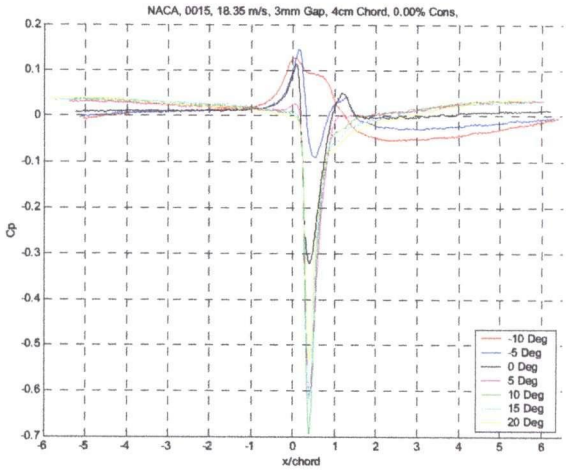
NACA, 0015, 18.35 m/s, 3mm Gap, 4cm Chord, 0.00% Cons,
Cp
x/chord
-10 Deg
-5 Deg
0 Deg
5 Deg
10 Deg
15 Deg
20 Deg

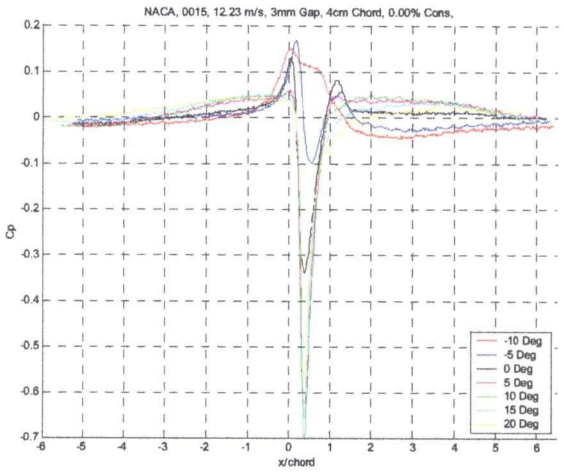
NACA, 0015, 12.23 m/s, 3mm Gap, 4cm Chord, 0.00% Cons,
Cp
x/chord
-10 Deg
-5 Deg
0 Deg
5 Deg
10 Deg
15 Deg
20 Deg

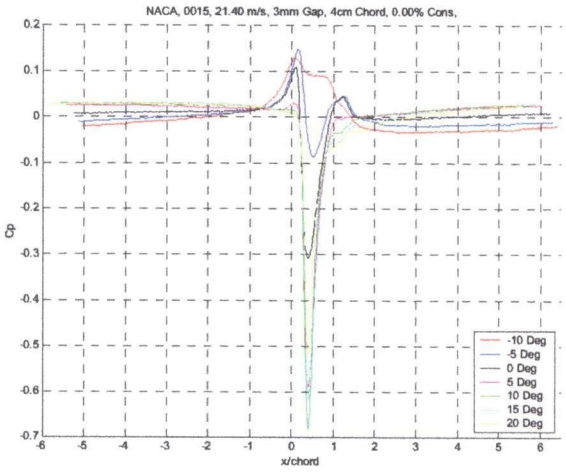
NACA, 0015, 21.40 m/s, 3mm Gap, 4cm Chord, 0.00% Cons,
Cp
x/chord
-10 Deg
-5 Deg
0 Deg
5 Deg
10 Deg
15 Deg
20 Deg

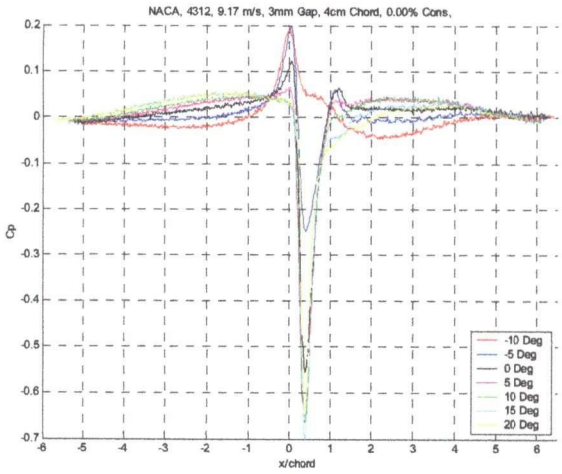
NACA, 4312, 9.17 m/s, 3mm Gap, 4cm Chord, 0.00% Cons,
Cp
x/chord
-10 Deg
-5 Deg
0 Deg
5 Deg
10 Deg
15 Deg
20 Deg

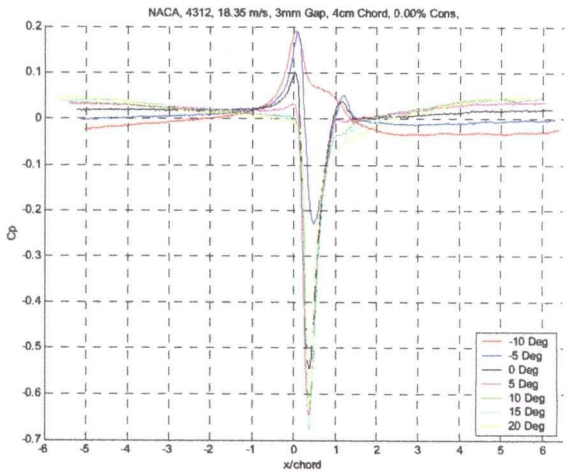
NACA, 4312, 18.35 m/s, 3mm Gap, 4cm Chord, 0.00% Cons,
Cp
x/chord
-10 Deg
-5 Deg
0 Deg
5 Deg
10 Deg
15 Deg
20 Deg

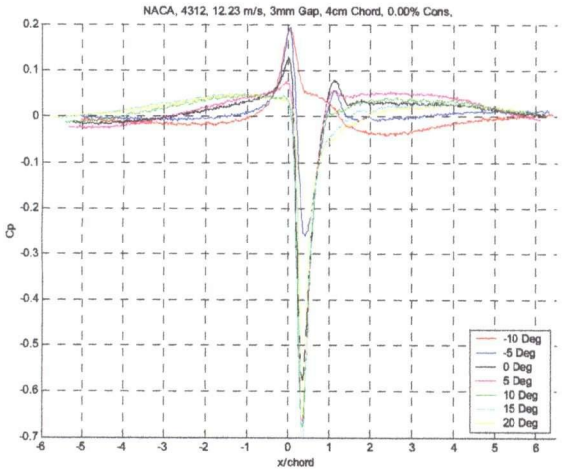
NACA, 4312, 12.23 m/s, 3mm Gap, 4cm Chord, 0.00% Cons,
Cp
x/chord
-10 Deg
-5 Deg
0 Deg
5 Deg
10 Deg
15 Deg
20 Deg

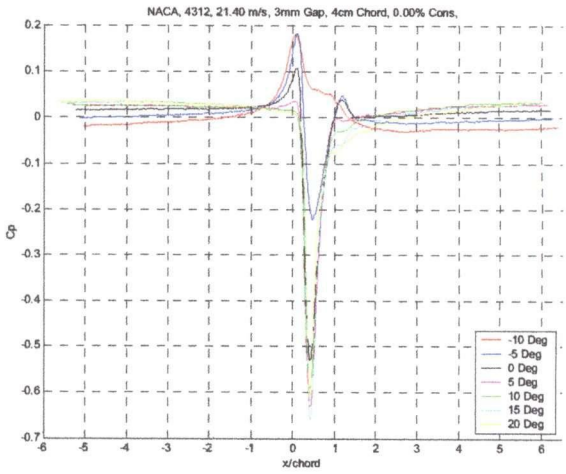
NACA, 4312, 21.40 m/s, 3mm Gap, 4cm Chord, 0.00% Cons,
Cp
x/chord
-10 Deg
-5 Deg
0 Deg
5 Deg
10 Deg
15 Deg
20 Deg

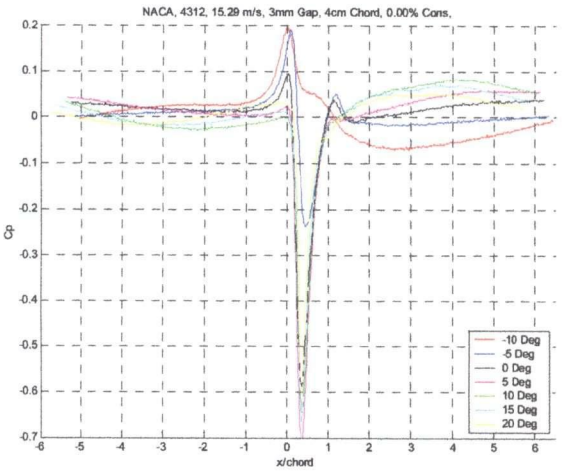
NACA, 4312, 15.29 m/s, 3mm Gap, 4cm Chord, 0.00% Cons,
Cp
x/chord
-10 Deg
-5 Deg
0 Deg
5 Deg
10 Deg
15 Deg
20 Deg